Numerical modelling of sedimentation in Trailing Suction Hopper Dredgers

B.F. Sloof

Delft University of Technology

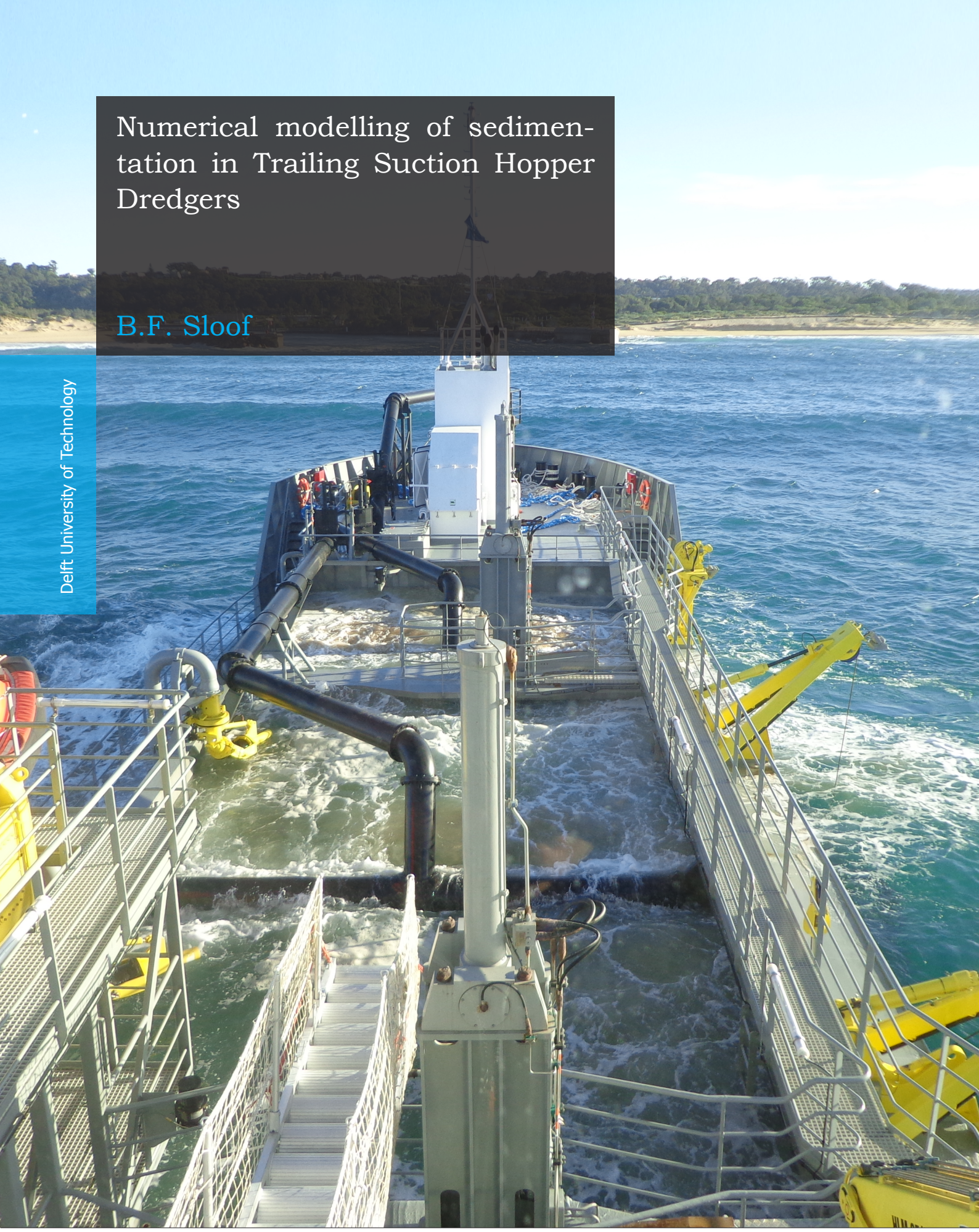

TU Delft Delft University of Technology

DAMEN

Numerical modelling of sedimentation in Trailing Suction Hopper Dredgers

by

B.F. Sloof

in partial fulfillment of the requirements for the degree of

Master of Science

in Offshore and Dredging Engineering

at the Delft University of Technology,

to be defended publicly on Tuesday December 12, 2017 at 9:30 AM.

Supervisors:	Dr. ir. G.H. Keetels,	TU Delft
	Ir. M.O. Winkelman,	Damen Dredging Equipment
Thesis committee:	Prof. dr. ir. C. van Rhee,	TU Delft
	Dr. ir. S.A. Miedema,	TU Delft
	Dr.ir. H.J. de Koning Gans,	TU Delft
	Dr. ir. R.J. Labeur,	TU Delft

This thesis is confidential and cannot be made public until December 31, 2019.

An electronic version of this thesis will be available at `http://repository.tudelft.nl/`.

TU Delft Delft University of Technology

DAMEN

Contents

1 Introduction **1**

2 Settling and sedimentation **7**
2.1 Terminal settling velocity . . . 7
2.2 Sedimentation and Erosion . . . 10

3 Multiphase flow modelling **15**
3.1 Frame of reference . . . 15
3.2 Euler-Euler . . . 16
3.3 Drift Flux . . . 16
3.4 Mixture centre of mass velocity and mixture flux velocity . . . 18
3.5 Turbulence modelling . . . 18
3.6 Boundary layers . . . 19

4 Hopper Models **23**
4.1 Camp . . . 23
4.2 Vlasblom and Miedema . . . 25
4.3 1DV Model Van Rhee . . . 27
4.4 2DV model Van Rhee . . . 27
4.5 Spearman . . . 28
4.6 Braaksma . . . 30
4.7 Jensen . . . 31
4.8 Konijn . . . 31

5 A New 2DV Model **33**
5.1 Fixing the bed . . . 34
5.2 Wall functions . . . 37
5.2.1 Implementation in driftFluxFoam . . . 39
5.2.2 Effect of particle concentration on the wall-functions . . . 40
5.2.3 Mixture Viscosity . . . 41
5.3 Moving mesh . . . 42
5.4 3D Simulations . . . 45

6 Validation **47**
6.1 Validation of settling . . . 47
6.2 Sedimentation validation . . . 50
6.2.1 The experiments . . . 50
6.2.2 Simulations . . . 50
6.3 Hopper validation . . . 54
6.3.1 Velocity . . . 57
6.3.2 Concentration . . . 59
6.3.3 Overflow loss . . . 61

7 Observations **65**
7.1 Flow Pattern . . . 65
7.2 Eddy viscosity and turbulent diffusion . . . 66
7.3 Top layer . . . 68
7.3.1 Phase 1 . . . 69
7.3.2 Phase 2 . . . 70
7.3.3 Phase 3 . . . 72

8 Layer Model **75**
8.1 Monodisperse Layer Model 75
8.2 Polydisperse Layer Model 80

9 Conclusions and Recommendations **83**
9.1 Conclusions 2DV model 83
9.2 Conclusions Layer Model 83
9.3 Recommendations 2DV model 84
9.4 Recommendations Layer Model 84

Bibliography **85**

Nomenclature **92**

A (U)RANS models **93**

B Relative Viscosity **97**

C Derivation Boundary Conditions **99**

D Implementation Moving Mesh **103**

E Numerical Error Analysis Settling Simulations **105**

F Settling experiments **109**

G Numerical Error Analysis Sedimentation Simulations **117**

H Sedimentation Experiments **121**

I Numerical Error Analysis Hopper Simulations **123**

Acknowledgements **129**

1

Introduction

Damen Dredging Engineering is a yard dedicated to the dredging industry. The yard specializes in the design, manufacture and supply of a wide variety of dredging tools. One of the tools Damen offers is the Trailing Suction Hopper Dredger (TSHD). The TSHD is a dredging ship that has a full sailing capacity and is used to maintain waterways or reclaim land.

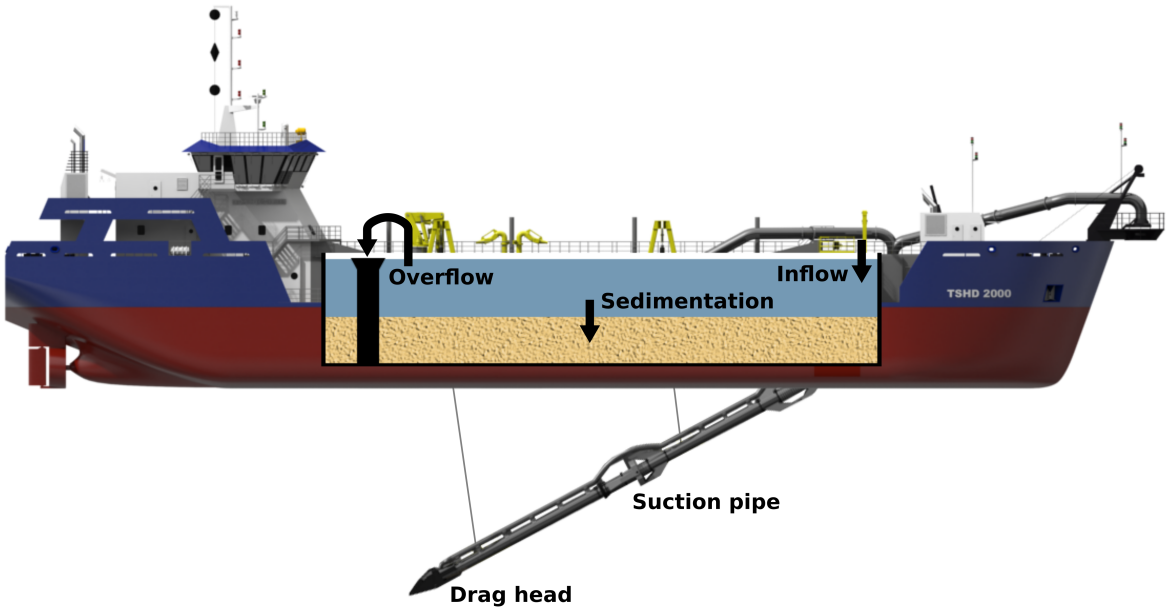

Figure 1.1: Side view of the TSHD 2000 of Damen

From the side of the ship, one or two suction pipes descend to the bottom of the river- or seabed. Due to a low pressure in the pipes, the material at the bed will be sucked inward and discharged in the hopper. In the hopper, the sediment settles on the bottom. The remaining water will leave the hopper via the overflow. Unfortunately, sediment also flows through the overflow. This is called the *overflow loss*. A side view of a Trailing Suction Hopper Dredger is shown in Figure 1.1.

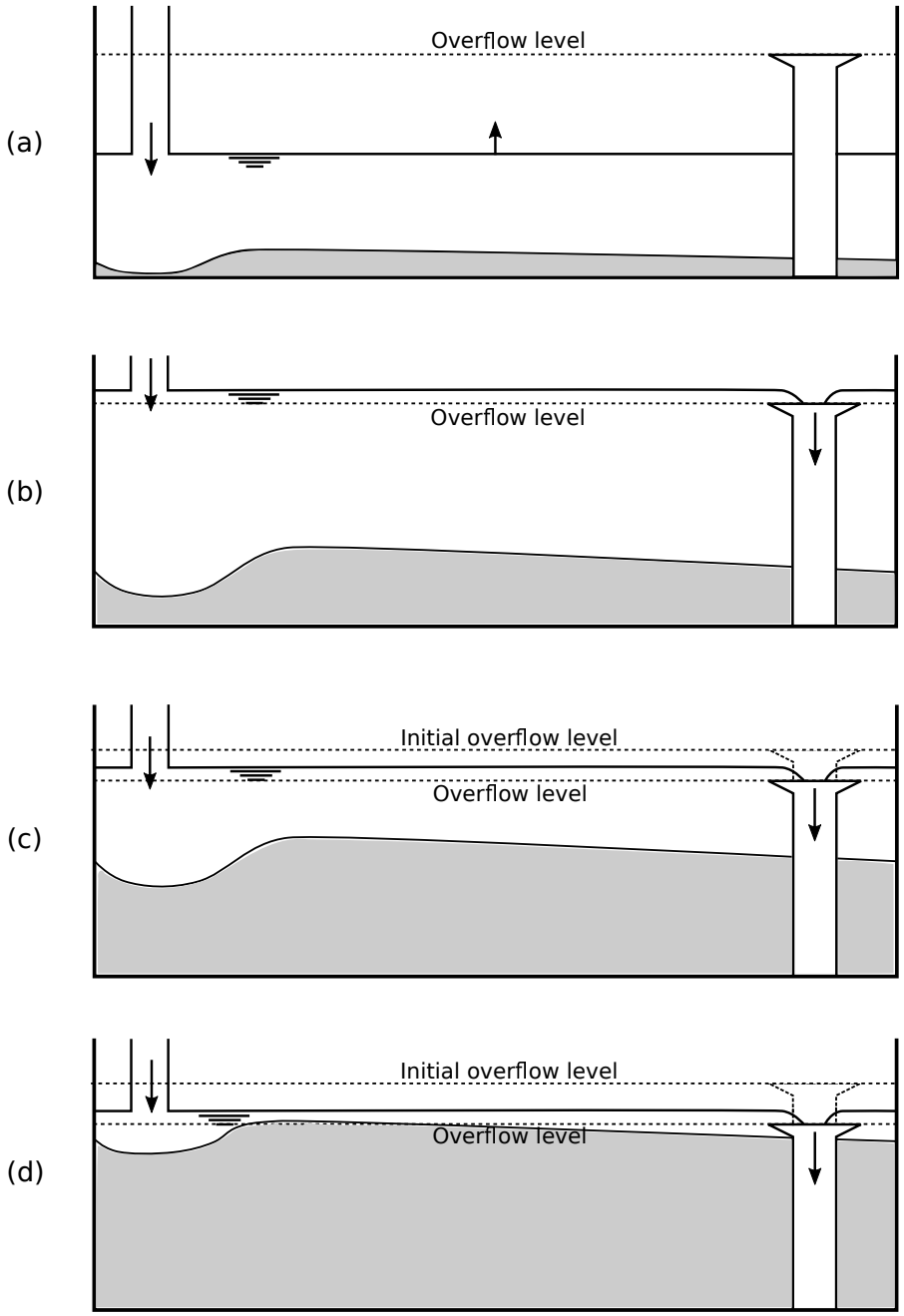

Figure 1.2: (a) Phase 1: filling of hopper. (b) Phase 2: continue loading with minor overflow losses. (c) Phase 3: overflow is lowered. (d) Phase 4: overflow losses increase due to decrease in cross-sectional area above the bed.

The loading process

There are two main methods for loading the hopper. The first system is the *Constant Volume System* (CVS). It has a fixed overflow level, so the effective volume of the hopper is constant. The second system is the *Constant Tonnage System* (CTS). It has an adjustable overflow system. When the content of the hopper reaches the maximum tonnage, the overflow is lowered in order to keep the weight of the material in the hopper constant. Since the overflow level is higher throughout almost the whole cycle, a CTS has lower overflow losses than a CVS. Most TSHDs have a Constant Tonnage System (CTS). Therefore, only the CTS is considered below.

The loading of a CTS can be divided into 4 phases (Miedema[39]):

- Phase 1 (Figure 1.2a): The hopper is filled. The filling process starts with an empty hopper. The

cycle can also be started with a layer of water already in the hopper. This increases the draught, which lowers the pumps. A higher density can be pumped in, resulting in a shorter loading time.

- Phase 2 (Figure 1.2b): Loading is continued. The excess of water flows through the overflow causing minor overflow losses.
- Phase 3 (Figure 1.2c): The maximum draught is reached. The overflow is lowered to keep the total weight in the hopper constant.
- Phase 4 (Figure 1.2d): The overflow is still being lowered. The cross-sectional area of the water above the bed decreases, resulting in high overflow losses.

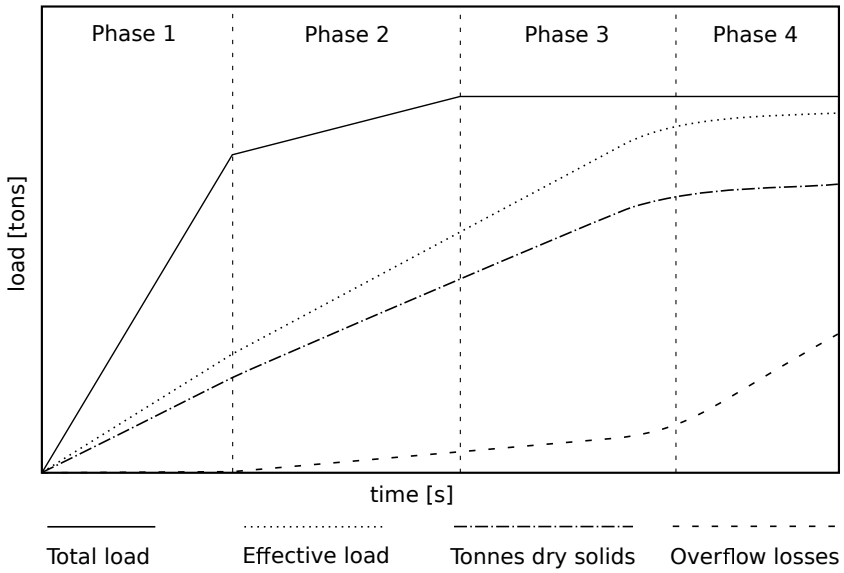

Figure 1.3: A typical loading curve. Source: Miedema[39]

A typical loading curve can be seen in Figure 1.3. The *effective load* is the weight of the bed (including the water in the pores). The *tonnes dry solids* (TDS) is the weight of the particles (excluding the water in the pores). It can be seen that the total load is constant in phases 3 and 4 due to the lowering of the overflow. The overflow losses drastically increase during phase 4.

Flow pattern in the hopper

When the mixture enters the hopper it is denser than its surroundings. The mixture will accelerate towards the bottom (zone 1 in Figure 1.4). This can be called a jet, since it is a stream of fluid being discharged into a surrounding medium. The high velocity and turbulence of the jet creates an erosion

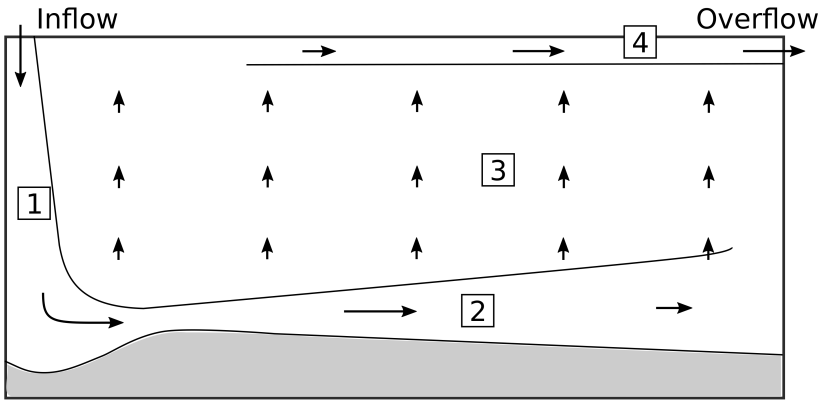

Figure 1.4: Schematic flow field in the hopper derived from experiments. Source: Van Rhee[49]

pit. After leaving the erosion pit, the mixture will flow along the bottom due to its high density (zone 2). This is called a density current. The interaction between the density current and the bed is important. The bed height rises due to sedimentation. The speed with which the bed rises, the sedimentation velocity, depends on the bed shear stress and terminal settling velocity. Above the density current (zone 3), the flow is upwards. Depending on the magnitude of this vertical velocity, the particle diameter, the concentration and turbulent diffusion, a particle will move up or down. Zone 4 is a layer of relatively clean water flowing towards the overflow.

In the end of the loading cycle (phase 4, Figure 1.2d), the top of the density current reaches the water surface. The flow pattern changes compared to figure 1.4. A free water flow (like a river flow) develops and the flow velocity increases. The increased velocity reduces sedimentation and the overflow concentration increases strongly.

Both Van Rhee[49] and Groot[26] observed the processes shown in Figure 1.4.

Objective of this thesis

The performance of such a TSHD is described by its production: the amount of sediment loaded in the hopper per unit time. The overflow loss can easily reach up to 30% of the loaded material, which causes a significant decrease of the production. In addition, the turbidity plume caused by these overflow losses can have a negative environmental impact (Figure 1.5). This turbidity plume reduces light penetration, clogs filter feeders and disperses contaminants which can be attached to the sediment.

Figure 1.5: Turbidity plume of the TSHD 'Queen of the Netherlands'. Source: http://www.abc.net.au/news/2012-11-14/the-dredger-queen-of-the-netherlands/4371312

To stay competitive on the dredging market, Damen is interested in estimating and reducing these overflow losses. A precise estimate of the production and overflow losses is needed to give assurance to the customer. Being able to model these parameters also gives the opportunity to optimize the geometry of the hoppers.
Different models to estimate the amount of material lost overboard exist. All these models have their pros and cons. The analytical model of Miedema[39] gives a quick and good estimate of the overflow losses, but gives no insight about the flow inside the hopper. The model of Van Rhee[49] is able to accurately simulate the flow inside the hopper, but has large computation times. The model of this thesis gives a good estimate of the overflow losses, gives insight in the flow inside the hopper and has an acceptable computation time.

Approach

First, the literary background is described in Chapters 2 to 4. Settling and sedimentation are two important processes and are described in Chapter 2. Chapter 3 gives a general description of the numerical

modelling of suspended sediment. An overview of the most important hopper models can be found in Chapter 4.
Inspired by the 2DV-model of Van Rhee[49], a 2DV-model was made in OpenFOAM. To model the sedimentation in OpenFOAM, some challenges had to be faced. The solution to these problems can be found in Chapter 5.
The model is validated in Chapter 6. The closed flume experiments of Van Rhee[49] have been used to demonstrate that sedimentation is simulated accurately. By comparing hopper simulations with the hopper experiments of Van Rhee[49], it was shown that the flow in the hopper was also simulated accurately. The computed overflow losses are, however, on the low side. The current version of OpenFOAM can calculate with only one particle fraction. In reality, the smaller fractions of the Particle Size Distribution are pushed upwards, causing the overflow losses to be higher.
The 2DV-model gave a deeper insight into the phenomena in the hopper. It was possible to derive several equations which describe the flow in the hopper. These equations can be found in Chapter 7. With these new formulas, a simple phenomenological model was developed, which was named the 'Layer Model'. This model is described and validated in Chapter 8.

2

Settling and sedimentation

Settling and sedimentation are two important processes in the hopper and are described in this chapter. To avoid confusion, it is important to have clear definitions:

- Settling velocity: the velocity with which a particle moves downward in a mixture, with a mixture velocity of zero. This will be dealt with in more detail in Paragraph 2.1.
- Sedimentation velocity: the velocity with which the bed rises. This will be dealt with in more detail in Paragraph 2.2.

2.1. Terminal settling velocity

The settling velocity is an important parameter for hopper flow. However, finding a good formulation of the settling velocity is difficult.
The settling velocity of a single grain in a quiescent surrounding fluid, the *terminal settling velocity*, can be obtained by using the balance of gravity and drag. Van Rhee[49] derives the following formula:

$$w_0 = -\sqrt{\frac{4g\Delta D\Psi}{3C_D}} \tag{2.1}$$

In which D is the sieve diameter of a particle. Δ is the specific density and is defined as $(\rho_s - \rho_w)/\rho_w$. Ψ is the shape factor, which is 1 for perfect spheres and approximately 0.7 for natural grains.

The C_D in Equation 2.2 depends on the Reynolds Particle Number:

$$Re_p = \frac{w_0 D}{\nu} \tag{2.2}$$

For perfect spheres the following empirical relations for C_D are found:

$$\begin{aligned} Re_p \leq 1 \quad &\rightarrow \quad C_D = \tfrac{24}{Re_p} \\ 1 < Re_p < 2000 \quad &\rightarrow \quad C_D = \tfrac{24}{Re_p} + \tfrac{3}{\sqrt{Re_p}} + 0.34 \\ Re_p \geq 2000 \quad &\rightarrow \quad C_D = 0.4 \end{aligned} \tag{2.3}$$

The formula of C_D for the laminar region and the turbulent region can be substituted into Equation 2.2. This gives for the laminar (or Stokes) region:

$$w_0 = -\frac{\Psi\Delta g D^2}{18\nu} \tag{2.4}$$

And for the turbulent region this gives:

$$w_0 = -1.8\sqrt{\Psi \Delta g D} \tag{2.5}$$

The transition regime has to be solved iteratively.

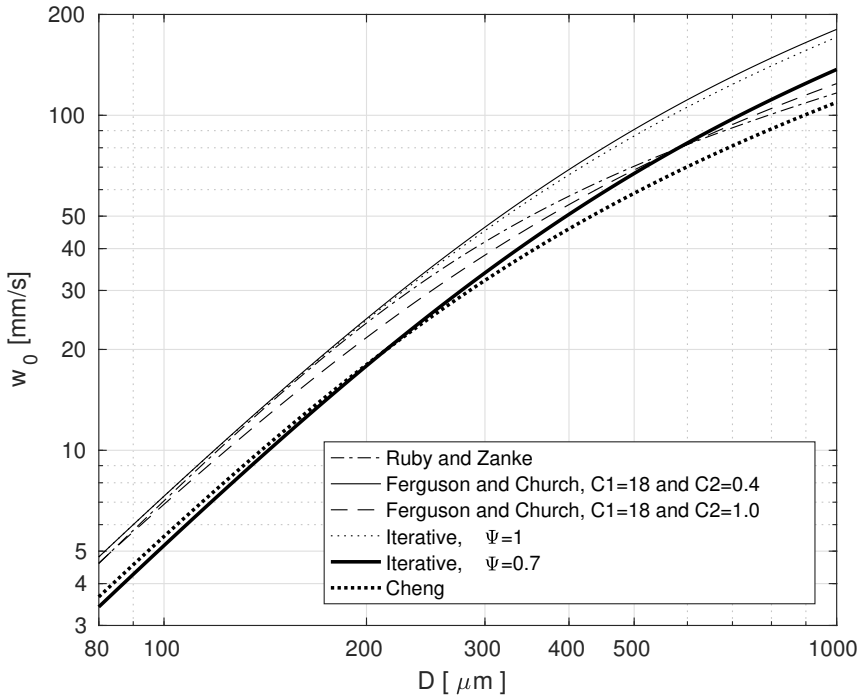

Figure 2.1: Grain diameter versus terminal settling velocity with $\nu = 1.11 \cdot 10^{-6}$ m^2/s

Cheng[16] compared several experimental studies and made a fit which can be used explicitly over the whole range of diameters:

$$\frac{w_0 dD}{\nu} = -\left(\sqrt{25 + 1.2D_*^2} - 5\right)^{1.5} \tag{2.6}$$

In which D_* is the Bonneville parameter, which is a measure for the net gravity versus the viscous forces:

$$D_* = D \sqrt[3]{\frac{\Delta g}{\nu^2}} \tag{2.7}$$

Ferguson and Church[21] also compared different experimental studies and added some experiments of their own. After fitting the data, they arrived at the following empirical formula:

$$w_0 = -\frac{\Delta g D^2}{C_1 \nu + (0.75 C_2 \Delta g D^3)^{0.5}} \tag{2.8}$$

This formula is valid for all regimes. For perfectly round particles the $C_1 = 18$ and $C_2 = 0.4$. For natural grains, Ferguson and Church advise $C_1 = 18$ and $C_2 = 1.0$ when the sieve diameter is used, and $C_1 = 20$ and $C_2 = 1.1$ when the nominal diameter is used.

Another emperical relation is the relation of Ruby and Zanke:

$$w_0 = -\frac{10\nu}{D}\left(\sqrt{1 + \frac{\Delta g D^3}{100\nu^2}} - 1\right) \tag{2.9}$$

The equations described above are plotted in Figure 2.1. It can be concluded that it is hard to estimate the settling velocity. Each excavation site has its own type of sand with its own shape. This gives large variation is settling velocities. The estimation of the settling velocity will probably be the highest contribution to inaccuracy of the model. As can be seen in Figure 2.1, particles with the same diameter but different grain shapes can easily differ 20% in settling velocity. Still, an equation needs to be chosen, which is done in Chapter 6.

Hindered Settling

For an increased volume concentration, the settling velocity decreases. This so called hindered settling is caused by the return flow created by the settling particles, the increased mixture density which reduces the submerged weight, the change in drag coefficient and particle-particle collisions. The hindered settling velocity can be described by the relation of Richardson and Zaki[47]:

$$w_s = w_0(1-\alpha)^n \tag{2.10}$$

Based on experiments Richardson and Zaki found values for n:

$$\begin{aligned} Re_p \leq 0.11 \quad &\rightarrow \quad n = 4.65 \\ 0.11 < Re_p < 1.4 \quad &\rightarrow \quad n = 4.35Re_p^{-0.03} \\ 1.4 < Re_p < 500 \quad &\rightarrow \quad n = 4.45Re_p^{-0.1} \\ Re_p \geq 500 \quad &\rightarrow \quad n = 2.39 \end{aligned} \tag{2.11}$$

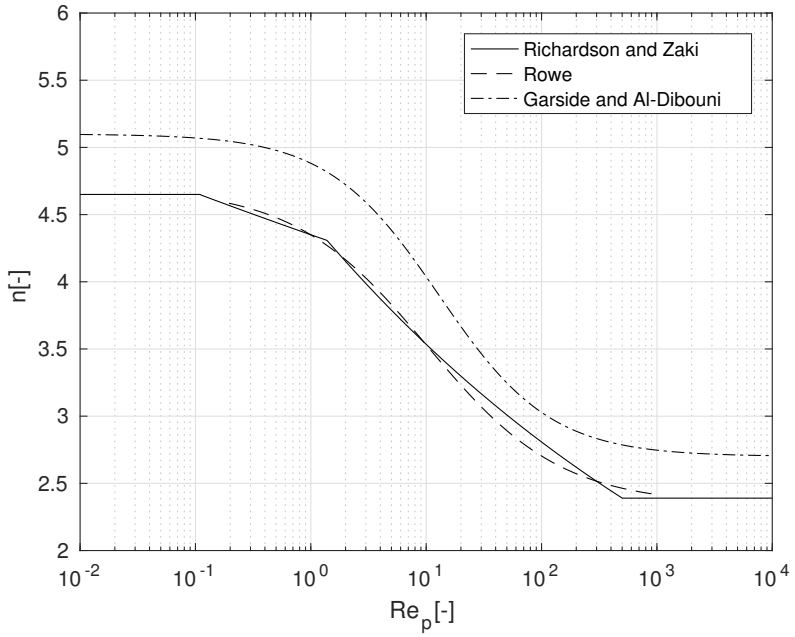

Figure 2.2: Reynolds Particle Number versus the exponent for hindered settling

Two more convenient relations are the relations of Rowe and Garside & Al-Dibouni:

$$n = \frac{a + bRe_p^{\alpha}}{1 + cRe_p^{\alpha}} \tag{2.12}$$

The relation of Rowe has a smaller range for Re_p than Garside & Al-Dibouni and Richardson & Zaki. For this thesis, this is not a problem. For particles of D=60μm the Re_p is approximately 0.2 and for D=1000μm the Re_p is approximately 100.

Both Richardson & Zaki and Garside & Al-Dibouni developed their equations by doing experiments with monodisperse perfect spheres. It appears that the shape of the particles has influence on the hindered

Table 2.1: Constants hindered settling

Author	Re_p	Concentration	a	b	c	α
Richardson & Zaki	$0.000185 < Re_p < 7150$	$0.05 < \alpha < 0.65$	-	-	-	-
Garside & Al-Dib.	$0.001 < Re_p < 3 \cdot 10^4$	$0.04 < \alpha < 0.55$	5.1	0.27	0.1	0.9
Rowe	$0.2 < Re_p < 1 \cdot 10^3$	$0.04 < \alpha < 0.55$	4.7	0.41	0.175	0.75

settling effect. Baldock[3] and Pal[41] found that for natural sand the exponent is slightly higher than Richardson & Zaki.
It can be concluded that the determination of the hindered settling effect is inaccurate. With a typical concentration in the hopper of 20% and an average difference between Garside and Rowe of 0.5, the inaccuracy can be estimated: $(1-0.2)^{0.5} = 0.89$. This means the order of inaccuracy is 10%.

One of the equations described above is selected in Chapter 6.

Influence of a turbulent environment on the settling velocity of a particle
All of the relations above are derived from experiments where the amount of turbulence is low, e.g. a column in which the sand settles. In the hopper, the turbulent energy is much higher. The presence of turbulence in the hopper can influence the terminal settling velocity. Aliseda[1] and Wang & Maxey[62] demonstrate that the terminal settling velocity can increase up to 50% if $St \approx 1$. The Stokes number is defined as a ratio between the particle relaxation time and a turbulent time scale. For the turbulent time scale Aliseda and Wang & Maxey use the Kolmogorov time scale:

$$St = \frac{\tau_p}{\tau_k} \tag{2.13}$$

The particle relaxation time τ_p is the time a particle needs to reach the terminal settling velocity:

$$\tau_p \approx \frac{\rho_s D^2}{18 \rho_w \nu_w} \tag{2.14}$$

For particles of 125 μm the relaxation time is 0.0023 s.
The Kolmogorov scales are the smallest scales in turbulent flow. The Kolmogorov time scale τ_k can be calculated with:

$$\tau_k = \left(\frac{\nu_w}{\epsilon}\right)^{\frac{1}{4}} \tag{2.15}$$

In which ϵ is the turbulent dissipation rate which is in the order of 10^{-4} m^2/s^3 in the hopper (taken from simulations). The Kolmogorov time scale is then in the order of 10^{-1} s, which means $St \ll 1$. The turbulence in the hopper has no influence on the the settling velocity.

2.2. Sedimentation and Erosion

Shields did research towards the initiation of motion of particles. The initiation of motion is the moment at which particles at the bed start to move. This occurs when the driving forces (drag and lift) are higher than the resisting force (gravity). A non-dimensional ratio for the driving forces over the resisting forces is the Shields parameter:

$$\theta = \frac{\tau}{(\rho_s - \rho_w) g D} \tag{2.16}$$

For D the D_{50} is used. τ is the bed shear stress, ρ_s is the density of the particles and ρ_w is the water density.

When the Shields parameter is higher than the critical Shields value θ_{cr} the particles start to move. The critical Shields value can be read from the Shields curve or calculated by one of the several fits. Several relations for the critical Shields value exist. In this thesis, Brownlie[11] is used:

$$\theta_{cr} = 0.22 D_*^{-0.9} + 0.06 e^{-17.77 D_*^{-0.9}} \tag{2.17}$$

D_* is the Bonneville parameter calculated with Equation 2.7. In reality, the initiation of motion is not a single Shields value, but more a regime or band. The fit of Brownlie is the average of this regime.

The critical Shields value changes when the bed is under a slope:

$$\theta'_{cr} = \theta_{cr} \frac{\sin(\phi - \beta)}{\sin(\phi)} \tag{2.18}$$

θ_{cr} is the critical Shields value calculated with Equation 2.17. β is the slope angle and ϕ is the angle of internal friction in the hopper. The slope angle is positive when the mixture is running down the slope (Figure 2.3).

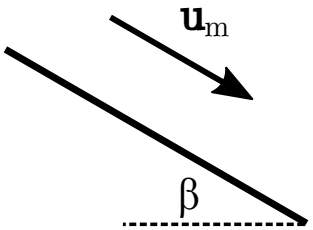

Figure 2.3: Positive slope angle.

Many have used the difference between the θ and θ_{cr} to determine the amount of eroded material. Van Rijn[48] developed the following empirical relation for the so called *pickup flux*:

$$\Phi_p = \frac{E}{\rho_s \sqrt{g \Delta D}} = 0.00033 D_*^{0.3} \left(\frac{\theta - \theta_{cr}}{\theta_{cr}} \right) \tag{2.19}$$

In which Φ_p is the pickup flux[-] and ν is the kinematic viscosity of the ambient fluid[m^2/s]. E is the erosion flux[$kgm^{-2}s^{-1}$] and is a very convenient parameter since it is the amount of material being eroded per second. In practice, erosion is a combination of a sedimentation flux and an erosion flux. The sedimentation flux can be calculated with:

$$S = -\rho_s \alpha_b w_s \tag{2.20}$$

Where α_b is the near bed concentration and w_s is the hindered settling velocity (Equation 2.10). Since $w_s < 0$, S is positive.

When the erosion flux E is higher than the sedimentation flux S, there is erosion. When the Sedimentation flux S is higher than the erosion flux E, there is sedimentation. From the mass balance it follows:

$$v_{sed} = \frac{S - E}{\rho_s (1 - n_0 - \alpha_b)} \tag{2.21}$$

Where v_{sed} is the sedimentation velocity. $v_{sed} > 0$ in case of sedimentation and $v_{sed} < 0$ in case of erosion. The porosity n_0 is defined as $n_0 = 1 - \alpha_{bed}$ in which α_{bed} is the bed concentration.

The pickup function of Van Rijn is, however, based on experiments with dilute flow. It can be expected that particles are less easily picked up when the near bed concentration is high, which is the case in the hopper. Van Rhee[49] executed closed flume experiments to determine the pickup flux under high near bed concentration. These experiments will also be used in Chapter 6 to validate the model.

Figure 2.4 shows the flow loop and Figure 2.5 shows the measurement section. Every experiment started by pumping a concentrated mixture at a higher velocity than the deposition velocity through the measurement section. The deposition velocity is the velocity at which a stationary bed starts forming in a pipe, so at the beginning of every experiment no stationary bed was present in the measurement section. By suddenly, partially closing the butterfly valve, the velocity in the measurement section decreased and the flow rate in the shunt pipeline increased. Due to this decrease in velocity, sedimentation started to occur.

All conductivity probes were placed at different vertical position from the bottom (Figure 2.5b). By measuring the time difference of the passing of the bed between probes, the sedimentation velocity was calculated. The time difference for both probes 1 and 3 and probes 2 and 4 was measured.

Van Rhee noted that the sedimentation velocities between probes 1 and 3 were a bit lower than the sedimentation velocity between probes 2 and 4, since the measurements with probes 1 and 3 were still influenced by the decreasing flow velocity. Therefore, Van Rhee only used probes 2 and 4.

Table 2.2: Height of the conductivity probes above the bottom

probe	z[mm]
1	5
2	10
3	15
4	20

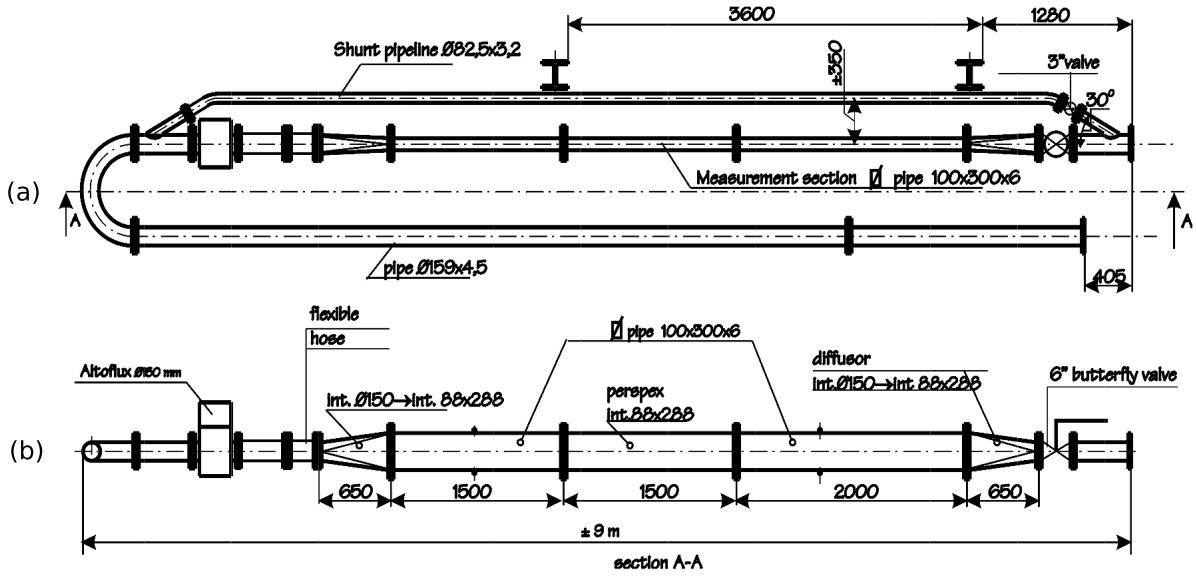

Figure 2.4: (a) Top view of the test arrangement. (b) Side view of the test arrangement in which the mixture flows from right to left. Source: Van Rhee[49]

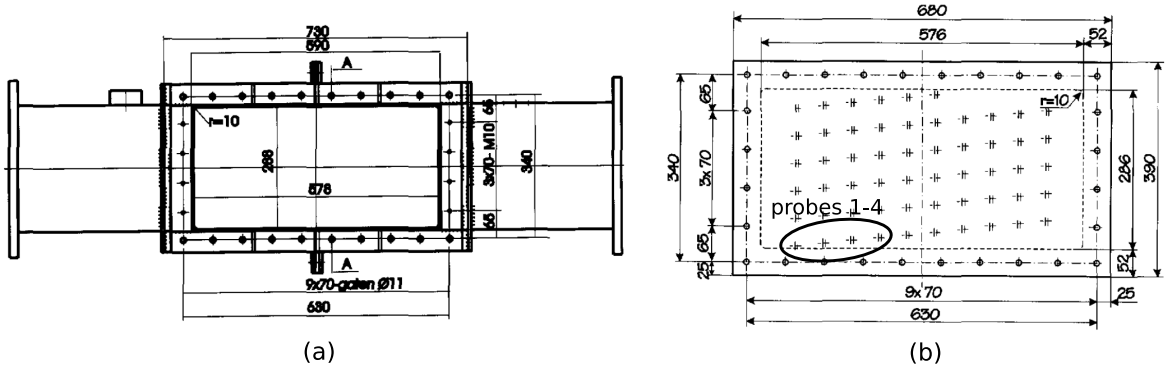

Figure 2.5: (a) Side view of the measurement section. (b) Close-up of the arrangement of the conductivity probes (side view). Source: Van Rhee[49]

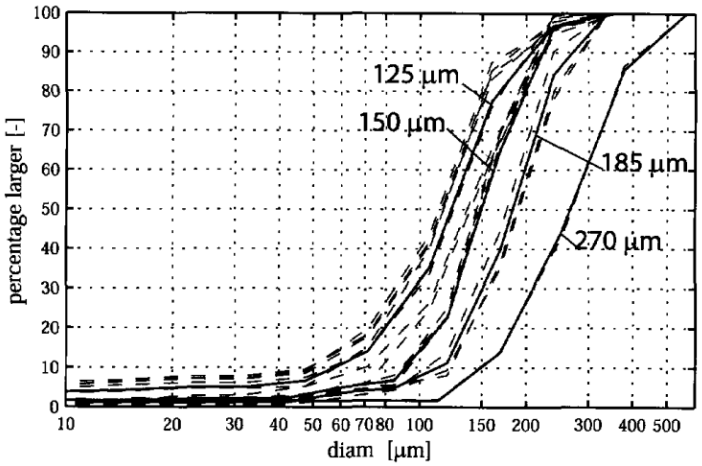

Figure 2.6: Particle Size Distributions of the sand used in the experiments. Source: Van Rhee[49]

To test the influence of the initial velocity, experiments were done for both low and high initial velocities. The low and high velocities before partially closing the valve were respectively 2.7 and 3.7 m/s. An overview of the experiments is shown in Appendix H. In Figure 2.6 the *Particle Size Distributions* (PSDs) of the different sands are shown.

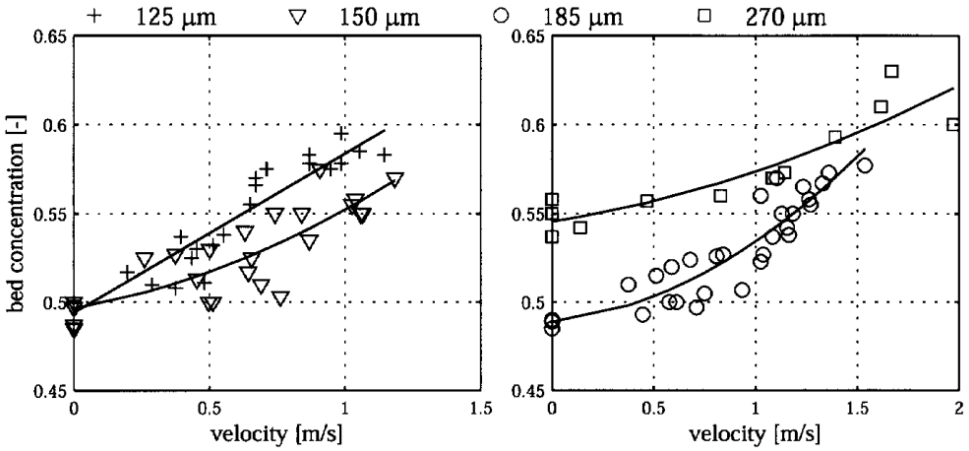

Figure 2.7: Bed concentration versus velocity, D_{50} = 125, 150, 185, 270 μm. Source: Van Rhee[49]

To determine the pickup flux, Van Rhee needed to know the porosity. It appeared that the packing of the grains depended on the flow velocity at which sedimentation occurred (Figure 2.7). For the sand with $D_{50} = 125\mu m$, the following fit could be made with reasonable accuracy:

$$\alpha_{bed} = 0.495 + 0.085U \tag{2.22}$$

In which U is the average velocity in the rectangular tube. Notice that this relation is only valid for this specific PSD and for velocities up to 1.25 m.

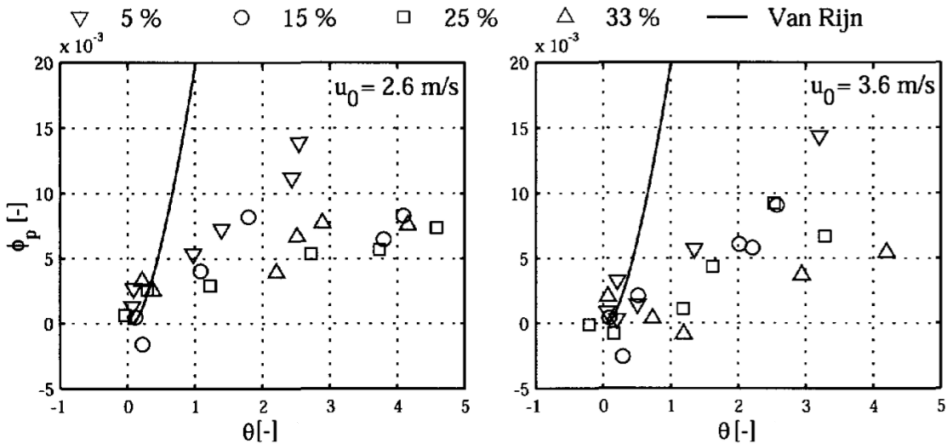

Figure 2.8: Small selection of the measurements of Van Rhee (with high near bed concentration) compared to the pickup function of Van Rijn (Equation 2.19), D_{50} = 125μm. Source: Van Rhee[49]

By estimating the settling flux (Equation 2.20), the pickup flux was obtained. A small selection of the measurements is shown in Figure 2.8. A large difference between the pickup function of Van Rijn and the measurements can be seen. Figure 2.8 clearly shows the influence of the near bed concentration. From the results in Figure 2.8 a fit for the pickup flux can be developed. Van Rhee has been improving these fits over the years. In a recent article about breaching, Van Rhee[51] gives his latest version:

$$\Phi_p = A\frac{1 - n_0 - \alpha_b}{1 - n_0}\frac{\theta}{\theta'_{cr}} \tag{2.23}$$

In which A is 0.000616 and θ'_{cr} can be calculated with Equation 2.18.

3

Multiphase flow modelling

Before the different hopper models are explained (Chapter 4), it is important to get some general understanding of multiphase flow modelling. Multiphase flow is the flow of materials with different states or phases, i.e. gas, liquid or solid. This thesis is about the multiphase flow which falls into the category of solid-liquid flow, also called *suspended sediment transport*. This chapter gives an overview of how multiphase flow can be modelled.

3.1. Frame of reference

The numerical modelling of suspended sediment can be divided in two types of modelling: Lagrangian and Eulerian. The difference between these two types lies in the choice of reference frame.

Lagrangian
With Lagrangian modelling the reference frame is following the individual particles. The trajectory of every particle is described by Newton's second law. This means the trajectory of every particle can be determined. The advantage of this approach is its accuracy. The influence of the particle on the surrounding liquid and the particle-particle interactions can be calculated accurately. A disadvantage is the calculation effort needed when the amount of particles is big. Therefore, this approach is mainly used when particles are relatively big compared to the fluid domain.

Eulerian
In the Eulerian approach the reference frame is chosen to be fixed. To calculate the velocity of every phase, the continuity and momentum equation are solved for each phase. This can only be done if the characteristics of the particles can be described as a continuum. This is only possible for small particles. It can be questioned if continuum holds for coarse sand or gravel. To simulate gravel the Lagrangian method could be needed. Luckily, we know that coarse sand or gravel directly settles on the bed. To calculate the overflow losses, particle diameters from approximately 70 to 400 μm are of interest. Particles of this size are small enough to simulate with an Eulerian approach.

Further, the Eulerian approach can be subdivided into different types: Euler-Euler and Drift Flux. In the Euler-Euler approach, every fraction has its own continuity and momentum equation. With a Drift Flux model, the mixture is considered as a whole instead of several separate phases. Hence, only one momentum equation is solved with Drift Flux: the momentum equation of the mixture.

3.2. Euler-Euler

Every fraction is denoted by its value of k. Then it follows:

$$\alpha_k = \frac{V_k}{V_0} \tag{3.1}$$

Here α_k is the concentration of fraction k. V_k is the volume of fraction k and V_0 is the total volume. If the concentrations of the different fractions are summed we get:

$$\sum_{k=1}^{N} \alpha_k = 1 \tag{3.2}$$

In the Euler-Euler approach, every fraction has its own continuity and momentum equation:

$$\frac{\partial \alpha_k \rho_k}{\partial t} + \nabla \cdot \alpha_k \rho_k \mathbf{u}_k = 0 \tag{3.3}$$

$$\frac{\partial \alpha_k \rho_k \mathbf{u}_k}{\partial t} + \nabla \cdot (\alpha_k \rho_k \mathbf{u}_k \mathbf{u}_k) = -\nabla \alpha_k p_k + \nabla \cdot \left(\alpha_k \mathbf{T}_k + \alpha_k \mathbf{T}_k^t\right) + \alpha_k \rho_k \mathbf{g} + \alpha_k \mathbf{m}_k \tag{3.4}$$

$\mathbf{T}_k$ and $\mathbf{T}_k^t$ are the contributions of the viscous and turbulent stresses, respectively. $\mathbf{T}_k$ is expressed as:

$$\mathbf{T}_k = \mu_m \left(\nabla \mathbf{u}_k + \nabla \mathbf{u}_k^T - \frac{2}{3}(\nabla \cdot \mathbf{u}_k)\mathbf{I}\right) \tag{3.5}$$

Normally for incompressible flow, the third term is omitted, but since $\nabla \cdot \mathbf{u}_k \neq 0$ this is not possible for suspended sediment transport. The calculation of $\mathbf{T}_k^t$ depends on the turbulence modelling.

$\mathbf{m}_k$ represents the momentum transfer between the phases. The challenge with Euler-Euler is the determination of this momentum transfer. Incorrect calculation of the momentum transfer easily leads to numerical instabilities. When correctly used, an Euler-Euler approach is more accurate than the Drift Flux.

3.3. Drift Flux

With a Drift Flux model, the mixture is considered as a whole instead of several separate phases. The continuity equation of the mixture is obtained, by adding the continuity equations of the different phases.

$$\frac{\partial \rho_m}{\partial t} + \nabla \cdot \rho_m \mathbf{u}_m = 0 \tag{3.6}$$

The mixture density can be calculated with:

$$\rho_m = \sum_{k=1}^{N} \alpha_k \rho_k \tag{3.7}$$

Also the mixture momentum equation is obtained by adding the the momentum equations of the different phases:

$$\frac{\partial \rho_m \mathbf{u}_m}{\partial t} + \nabla \cdot (\rho_m \mathbf{u}_m \mathbf{u}_m) = -\nabla p_m + \nabla \cdot \left(\mathbf{T}_m + \mathbf{T}_m^t - \sum_{k=1}^{N} \alpha_k \rho_k \mathbf{u}_{km} \mathbf{u}_{km}\right) + \rho_m \mathbf{g} \tag{3.8}$$

For the derivation of Equations 3.6 and 3.8, the reader is directed to Appendix A of Brennan[9]. From adding the momentum equations of the different fractions, it also follows that:

$$\mathbf{u}_m = \frac{\sum_{k=1}^{N} \alpha_k \rho_k \mathbf{u}_k}{\rho_m} \tag{3.9}$$

This is called the *mixture centre of mass velocity*.

When the different momentum equations are added the term $\alpha_k \mathbf{m}_k$ cancels out. Every force of each phase exerts an opposite force to another phase, so $\sum_{k=1}^{N} \alpha_k \mathbf{m}_k = 0$. This is very convenient and makes Drift Flux easier to apply than Euler Euler.

$\mathbf{T}_m$ and $\mathbf{T}_m^t$, again, are the contribution of the viscous and turbulent stresses, respectively. $\mathbf{T}_m$ is calculated as follows:

$$\mathbf{T}_m = \mu_m \left(\nabla \mathbf{u}_m + \nabla \mathbf{u}_m^T - \frac{2}{3} (\nabla \cdot \mathbf{u}_m) \mathbf{I} \right) \tag{3.10}$$

The concentration of the different fraction are determined with the advection-diffusion equation:

$$\frac{\partial \alpha_k}{\partial t} + \nabla \cdot (\alpha_k \mathbf{u}_k) = \nabla \cdot (\Gamma_t \nabla \alpha_k) \tag{3.11}$$

In which Γ_t is the turbulent diffusion coefficient and $\mathbf{u}_k$ the fraction velocity. Goeree[25] derived a formula for the fraction velocity:

$$\mathbf{u}_k = \mathbf{u}_m + \mathbf{u}_{k,m} = \mathbf{u}_m + \mathbf{u}_{k,r} - \sum_{k=1}^{N} c_k \mathbf{u}_{k,r} \tag{3.12}$$

The mass fraction, c_k, can be calculated with:

$$c_k = \frac{\rho_k \alpha_k}{\rho_m} \tag{3.13}$$

The slip velocity, $\mathbf{u}_{kr}$, is the velocity of a fraction compared to the fluid phase:

$$\mathbf{u}_{k,r} = \mathbf{u}_k - \mathbf{u}_f \tag{3.14}$$

In horizontal direction, this is assumed to be zero. In vertical direction it is:

$$w_{k,r} = w_{k,0} \, (1 - \alpha_t)^{n_k - 1} \tag{3.15}$$

Note that $w_{0,k}$ is negative.

The Drift Flux approach is valid when $St \ll 1$. For Stokes values much smaller than 1, the particles response time is less than the characteristic time of the flow, i.e. those particles simply follow the flow. A Stokes number much greater than 1 describes particles that remain unaffected by the fluid velocity change and continue their original trajectory. The Stokes number is calculated as follows:

$$St = \frac{\tau_p}{t_{flow}} \tag{3.16}$$

Notice that this Stokes number is slightly different than the Stokes number of Equation 2.13. The particle relaxation time τ_p is the time a particle needs to reach the terminal settling velocity and can be calculated with Equation 2.14. The characteristic time of the flow t_{flow} can be estimated by dividing a length scale over a velocity scale. In the middle of the domain this is:

$$t_{flow} = O\left(\frac{z}{U}\right) \tag{3.17}$$

In which z is the distance to the wall and U the velocity of the mixture. Close to the wall t_{flow} can be estimated with:

$$t_{flow} = O\left(\frac{z}{u_*}\right) \tag{3.18}$$

In which z is again the distance to the wall and u_* the shear velocity velocity: $\sqrt{\tau/\rho}$.

3.4. Mixture centre of mass velocity and mixture flux velocity

For the derivation of the pressure equation, the continuity equation is needed. The correct continuity equation for the *mixture centre of mass velocity* $\mathbf{u}_m$ is Equation 3.6, which means:

$$\nabla \cdot \mathbf{u}_m \neq 0 \tag{3.19}$$

However, very often, $\nabla \cdot \mathbf{u} = 0$ is still assumed. When $\nabla \cdot \mathbf{u} = 0$ is assumed, not the *mixture centre of mass velocity*, but the *mixture flux velocity* is calculated:

$$\mathbf{j}_m = \sum_{k=1}^{N} \alpha_k \mathbf{u}_k \tag{3.20}$$

For $\mathbf{j}_m$ indeed the following continuity equation is valid:

$$\nabla \cdot \mathbf{j}_m = 0 \tag{3.21}$$

Although, the results between usage of $\mathbf{j}_m$ and $\mathbf{u}_m$ do not differ that much, it is incorrect to use $\mathbf{j}_m$. Furthermore with $\mathbf{j}_m$, Equation 3.12 cannot be used, since $\mathbf{u}_m$ is unknown. Instead, the following equation for the fraction velocity needs to be used:

$$\mathbf{u}_k = \mathbf{j}_m + \mathbf{u}_{k,j} = \mathbf{j}_m + \mathbf{u}_{k,r} - \sum_{k=1}^{N} \alpha_k \mathbf{u}_{k,r} \tag{3.22}$$

The slip velocity, $\mathbf{u}_{kr}$, can still be calculated with Equation 3.15.

3.5. Turbulence modelling

The starting point for turbulence modelling is separating the velocity into an averaged velocity and velocity fluctuation:

$$\mathbf{u} = \overline{\mathbf{u}} + \mathbf{u}' \tag{3.23}$$

This filtering is a spatial filtering for LES, a time filtering for RANS and an ensemble filtering for URANS. By substituting Equation 3.23 into the Navier-Stokes equation (Equations 3.4 and 3.8) and doing some derivations, it can be found that:

$$\mathbf{T}^t = -\rho \overline{\mathbf{u}'\mathbf{u}'} \tag{3.24}$$

Since its effect on the mean flow is like that of a stress term, this term is known as the Reynolds stress. Momentum is transported across the fluid by the eddies. When a velocity gradient is present in the mean flow, faster moving layers will be decelerated and slower layers will be accelerated due to this transport of momentum.

To obtain equations containing only the mean velocity and pressure, we need to close the momentum equations by modelling the Reynolds stress term. This is called the closure problem. Boussinesq was the first to attack the closure problem, by introducing the concept of eddy viscosity. The relation he proposed is called the Boussinesq hypothesis:

$$-\rho \overline{\mathbf{u}'\mathbf{u}'} = \mu_t \left(\nabla \mathbf{u} + \nabla \mathbf{u}^T \right) - \frac{2}{3} \left(\mu_t \nabla \cdot \mathbf{u} + \rho k \right) \mathbf{I} \tag{3.25}$$

In which k is the turbulent kinetic energy and is defined by $k = \frac{1}{2}(\overline{u'^2} + \overline{v'^2} + \overline{w'^2})$. The calculation of this eddy viscosity μ_t depends on the type of turbulence modelling. The various types of turbulence modelling can be divided into four main groups:

Direct Numerical Simulation (DNS)
With DNS, actually, no turbulence is modelled, so $\mathbf{T}^t$ and μ_t are zero. This means all turbulent scales must be resolved down to the Kolmogorov scale. At the Kolmogorov scale, viscosity dominates and the turbulent kinetic energy is dissipated into heat. A very fine mesh is needed to simulate these small scales. For this reason, DNS is only used for the purpose of research.

Large Eddy Simulation (LES)
With LES, only the large eddies are resolved. The smaller scales need to be modelled and are represented by an additional stress, which is called the Sub-Grid-Scale (SGS) stress. In deriving the SGS turbulence models, a spatial filtering in the order of the grid size is applied on the Navier-Stokes equations. A model which is frequently used nowadays is the Wall Adapting Local Eddy (WALE) viscosity model. The eddy viscosity, obtained with the SGS model, can be substituted in Equation 3.25.

Reynolds Averaged Navier-Stokes (RANS)
In RANS, all turbulent scales, large and small, are modelled by filtering over time. Again, a model is needed for the turbulent scales. Contrary to DNS and LES, where simulation needs to be done in 3D, simulating in 2D is also possible with RANS. The most basic turbulence model is Prandtl's mixing length model. In the Prandtl's mixing length model, the spatial variation of the mixing length is assumed to be known beforehand.
If the spatial variation of the mixing length is unknown, a more advanced method is required. The two-equation turbulence models are frequently used. These models consist of two additional transport equations. The first equation is for the turbulent kinetic energy k. The second equation is for the dissipation rate ϵ or the specific dissipation rate ω. The dissipation rate ϵ is the rate at which the turbulent kinetic energy dissipates into heat. The specific dissipation rate ω is defined as ϵ/k. An overview of the different two-equation models can be seen in appendix A.

Unsteady Reynolds Averaged Navier-Stokes (URANS)
There are some flows for which the mean flow contains slow variations with time that are not turbulent in nature. Equation 3.23 can then be written as:

$$\mathbf{u}(x,t) = \overline{\mathbf{u}}(x,t) + \mathbf{u}'(x,t) \tag{3.26}$$

Where:

$$\overline{\mathbf{u}}(x,t) = \frac{1}{T}\int_t^{t+T} \mathbf{u}(x,t)dt \quad \text{and} \quad T_1 \ll T \ll T_2 \tag{3.27}$$

The mean velocity $\overline{\mathbf{u}}(x,t)$ varies over time. This method is only valid if the period of the slow variations T_2 differs several orders of magnitude compared to the time period of the turbulent variations T_1. In that case, the RANS-equations can be used to calculate the Reynolds stress term. Numerically, the difference between RANS and URANS lies in how the pressure equation is solved.

3.6. Boundary layers

A lot of research has been done regarding the flow close to the wall, e.g. Chieng & Launder[17], Patel, Rodi & Scheuerer[43], Cebeci & Smith[14]. To describe the flow near the wall, a certain division in regions is used:

- Inner layer:
  - Viscous region
  - Buffer region
  - Log-law or inertial region
- Defect layer

Boundary conditions for k, ϵ, ω and μ_t need to be applied to model the flow in these layers.
The viscous region is the area with an $y+$ smaller than 5. In the viscous region the following relation can be found:

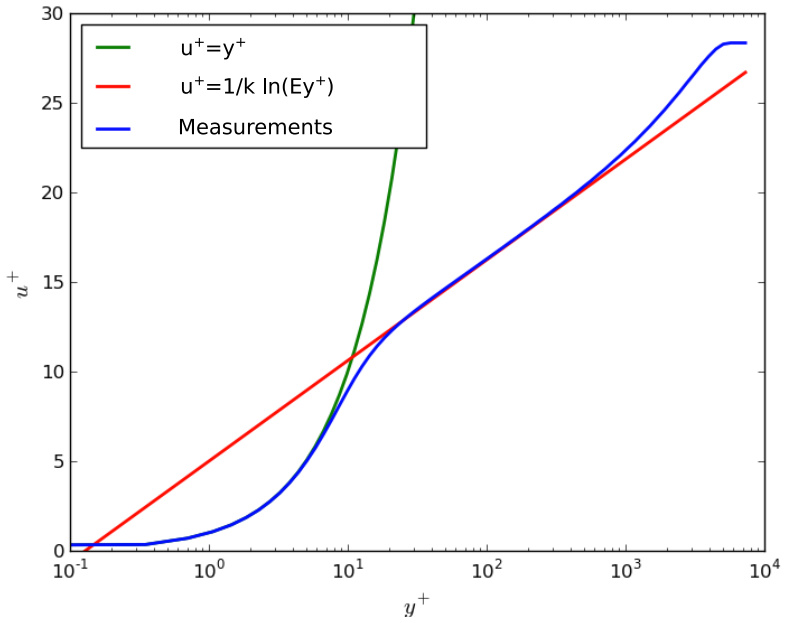

Figure 3.1: Velocities near the wall. Source: https://github.com/su2code/SU2/wiki/Turbulent-Flat-Plate

$$u_+ = y_+ \tag{3.28}$$

In which u_+ and y_+ are the non-dimensional velocity and distance:

$$u_+ = \frac{u}{u_*} \tag{3.29}$$

$$y_+ = \frac{u_* y}{\nu} \tag{3.30}$$

$$u_* = \sqrt{\frac{\tau}{\rho}} \tag{3.31}$$

The log-law region is the region with approximately $30 < y_+ < 100$. The upper limit depends on the Bulk Reynolds number, but an y_+ of 100 is often chosen as the upper limit. For the log-law region, another relation is valid:

$$u_+ = \frac{1}{\kappa} \ln (y_+) + B - \Delta B \tag{3.32}$$

κ is 0.40 and B is experimentally found to be between 4.9 and 5.7 for smooth walls. ΔB is the influence of the wall roughness. This formula is often written in the following form:

$$u_+ = \frac{1}{\kappa} \ln (E y_+) - \Delta B \tag{3.33}$$

E is then between 7.0 and 9.8. A lot of a CFD-packages use a value of 9.8.

For walls with a dimensionless roughness k_s^+ above 90, ΔB is:

$$\Delta B = \frac{1}{\kappa} \ln \frac{k_s u_*}{\nu} - 3.3 = \frac{1}{\kappa} \ln k_s^+ - 3.3 \tag{3.34}$$

Substituting this in Equation 3.33 gives:

$$u_+ = \frac{1}{\kappa} \ln (E y_+) - \frac{1}{\kappa} \ln (k_s^+) + 3.3 \tag{3.35}$$

$$u_+ = \frac{1}{\kappa} \ln \frac{E y_+}{k_s^+} - \frac{1}{\kappa} \ln e^{-3.3\kappa} \tag{3.36}$$

$$u_+ = \frac{1}{\kappa} \ln \frac{E y_+}{e^{-3.3\kappa} k_s^+} \tag{3.37}$$

$$u_+ = \frac{1}{\kappa} \ln \frac{E y_+}{0.27 k_s^+} \tag{3.38}$$

Most CFD-packages use a formula which looks like:

$$u_+ = \frac{1}{\kappa} \ln \frac{E y_+}{1 + C k_s^+} \tag{3.39}$$

This is a very convenient formulation. For rough walls ($k_s^+ > 90$) $C k_s^+$ is a lot bigger than one. Equation 3.39 then gives the same outcome as Equation 3.38. And for smooth walls (k_s^+=0) Equation 3.39 gives the same outcome as Equation 3.33. Ansys uses a value of C=0.3 (Blocken[7]). With this value of 0.3, one will attain the exact same formula as Van Rhee[49] uses for rough walls:

$$u_+ = \frac{1}{\kappa} \ln \frac{9.8 y_+}{0.3 k_s^+} = \frac{1}{\kappa} \ln \frac{32 y}{k_s} \tag{3.40}$$

To make use of Equation 3.28 is called *low-Reynolds closure*. This name is very misleading. It is called low-Reynolds, because the mathematical formulations are capable to resolve the turbulence flow down to the wall where the flow is laminar (Reynolds number is low). The name 'low-Reynolds' does not refer to the bulk Reynolds number.
Equation 3.28 is valid for $y_+ < 5$. To get an y_+ smaller than 5, the distance between the cell centre of the first cell and the wall needs to be very small. With a low-Reynolds closure, a grading of the cell size near the wall is used. This causes the calculation time of simulations with a low-Reynolds closure to be relatively large.

To make use of a relation in the log-law region (for example Equation 3.33) is called a *high-Reynolds closure*. The High-Reynolds closure is valid for $30 < y_+ < 100$. Therefore, grading near the wall is often not needed, which makes a high-Reynolds closure faster than a low-Reynolds closure. In flows where the existence of wall functions is not established (for instance: unsteady flows and flows where flow separation occurs) a low-Reynolds closure gives more accuracy (Pattijn[44] and Yang & Shih[66]).

4

Hopper Models

In this chapter, all important hopper models are reviewed. Keeping the theory of Chapters 2 and 3 in mind, it will be discussed to which extent each model represents reality.

4.1. Camp

Camp[12] developed his model for the field of wastewater treatment. He assumed a hopper with a horizontal velocity U, which is constant over the height. Camp does not take the hindered settling effect into account, so each particle moves with a straight line as can be seen in Figure 4.1.

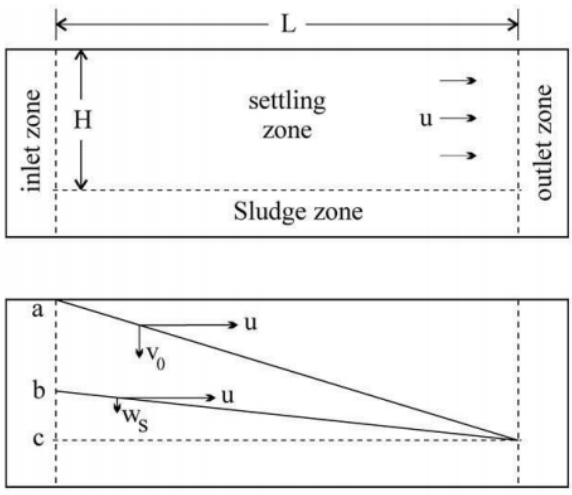

Figure 4.1: Ideal settling basin according to Camp. Source: Van Rhee[49]

v_0 is called the *hopper load parameter:*

$$v_0 = U\frac{H}{L} = \frac{Q}{WL} \tag{4.1}$$

The hopper load parameter is the settling velocity needed to travel from 'point a' (Figure 4.1) to the end of the bed. This means that if a particle fraction has a settling velocity which is bigger than the hopper load ($w_s > v_0$), all particles with this particle diameter will reach the bed independent of the height at which these particles enter the hopper. This is the fraction $1 - p_0$ of the PSD (Figure 4.2).
The particles with $w_s < v_0$ will only settle depending on the height on which they enter the settling zone (fraction $p_0 - p_s$). After doing some derivation, it can be found that the percentage of these particles which reach the bed is $w_s(p)/v_0$.
The smallest particles (fraction p_s) will not settle, because for these particles the horizontal velocity U exceeds the scour velocity. Camp made the conservative consumption that erosion occurs when the fluid friction on the top layer of particles is higher than the static friction with the layer under it:

$$U_s(D) = \sqrt{\frac{8\,(1-n_0)\,\mu\Delta g D}{\lambda}} \tag{4.2}$$

In which λ is the Darcy friction factor. The removal ratio is the percentage of all particles which settle onto the bed, and can be determined by:

$$r_r = 1 - p_0 + \int_{p_s}^{p_0} \frac{w_s(p)}{v_0} dp \tag{4.3}$$

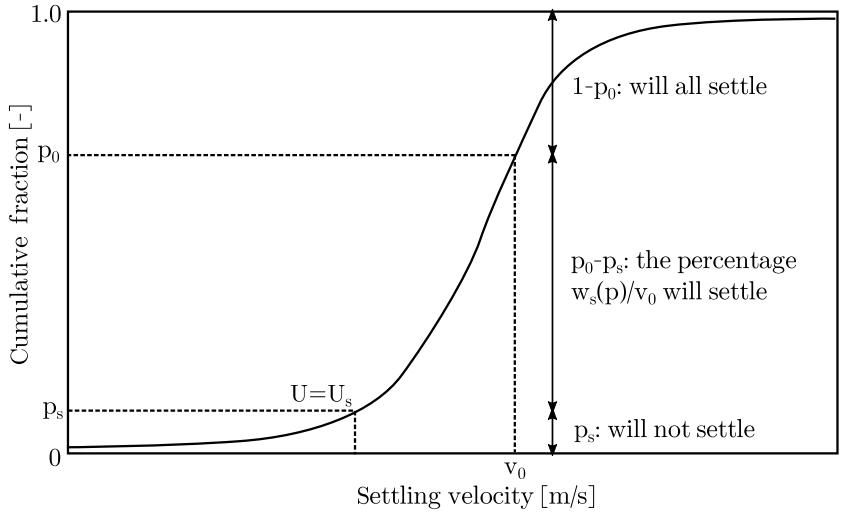

Figure 4.2: Cumulative PSD as function of the settling velocity

Influence of turbulent diffusion
In a later article, which was inspired on the work of Dobbins[20], Camp[13] described the effect of turbulence. By simplifying the advection-diffusion equation (Equation 3.11), Camp arrived at the following equation:

$$U\frac{\partial \alpha}{\partial x} = \Gamma_z \frac{\partial^2 \alpha}{\partial z^2} + w_s \frac{\partial \alpha}{\partial z} \tag{4.4}$$

To arrive at this formula, Camp made the following simplifications:

1. Stationary flow: $\frac{\partial \alpha}{\partial t} = 0$
2. The horizontal velocity U is constant in x- and z-direction. In reality, however, a buoyant jet and density current can be observed.
3. The turbulent diffusion coefficient Γ is constant in x- and z-direction.
4. The vertical mixture velocity is zero, therefore: $w = -w_s$. The hindered settling effect is not taken into account: $w_s \neq f(c)$

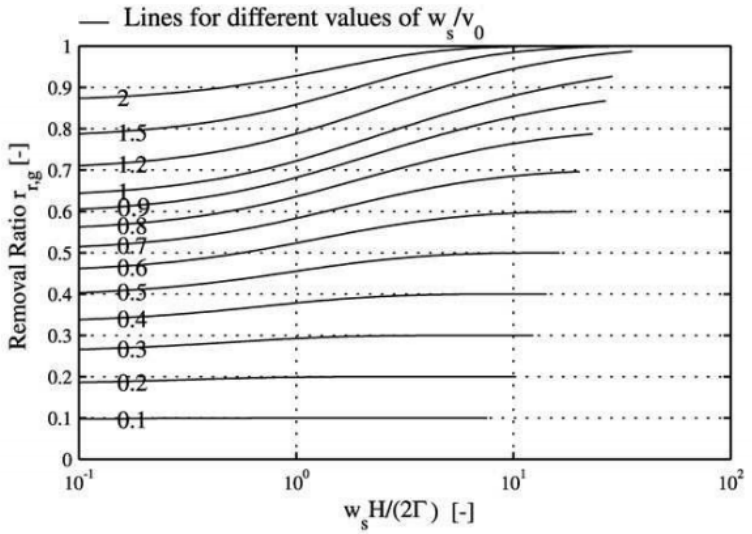

Figure 4.3: Removal rate with the influence of turbulence

An analytical solution of Equation 4.4 was found by separation of variables. Since the analytical solution was cumbersome in usage, Camp presented his results in the form of Figure 4.3. For the turbulent diffusion coefficient, Camp used $\Gamma_t = 0.075Hu_*$ in which u_* and H are the shear velocity and total height above the bed, respectively. The removal ratio can be calculated with:

$$r_r = \int_{p_s}^{1} r_{r,g}(p)\frac{w_s(p)}{v_0}dp \tag{4.5}$$

Next to the assumptions described above to arrive at Equation 4.4, the following assumptions also lead to discrepancies:

1. Pickup cannot be calculated correctly, since the density current is not modelled.
2. The bed doesn't rise or erode.
3. The time effect: particles which enter the hopper and don't settle are assumed to leave the hopper instantly. In reality particles stay for a while in the hopper.

4.2. Vlasblom and Miedema

Vlasblom and Miedema[35] also assumed a uniform flow profile. By fitting the curves in Figure 4.3, new explicit equations for $r_{r,g}$ were developed. The correct version of the formulas can be found in Miedema[37]. For $r_g = w_s/v_0 > 1$ holds:

$$r_{r,g}(p) = 1 - 0.184r_g^{0.88-0.2r_g}\left[1 - \tanh\left(r_g^{-0.13-0.8r_g}\left(\log\left(\frac{w_s(p)}{U}\right) - 0.2614 - 0.5\log\lambda + r_g^{-0.33-0.94r_g}\right)\right)\right] \tag{4.6}$$

In which λ is the Darcy friction factor. For $r_g < 1$ the following fit needs to be used:

$$r_{r,g}(p) = r_g^{-1}\left(1 - 0.184 r_g^{-0.69-0.38 r_g}\left[1 - \tanh\left(r_g^{0.77-0.08 r_g}\left(\log\left(\frac{w_s(p)}{U}\right) - 0.2614 - 0.5\log\lambda + r_g^{1.01-0.18 r_g}\right)\right)\right]\right) \quad (4.7)$$

These formulas are a lot easier to use than the analytical equations of Camp. Over the years Vlasblom and Miedema have been adding features to improve the model of Camp:

1. The rise of the sand bed (Vlasblom & Miedema [35]).
2. Initially, Vlasblom and Miedema used Equation 4.2 to calculate the critical diameter. Later on, they used a method based in Shields (Miedema[37]).
3. Ooijens[40] added the time effect by regarding the hopper as an ideal mixing vessel.
4. An estimation of the thickness of the layer of water above the overflow (Miedema[37]).

A clear advantage of the model of Miedema is its simplicity and low calculation times. On the other hand, this simplicity also gives rise to some inaccuracy or effects which are not incorporated:

1. Since the density current at the bottom is not modelled, the pickup flux cannot be correctly accounted for.
2. Due to the wrongly assumed velocity pattern, the turbulence may differentiate.
3. The near bed concentration cannot be calculated, so it needs to be estimated.

The model of Miedema can predict the overflow losses quite well as can be seen in 4.4 and 4.9. At the beginning of the loading cycle, though, the overflow concentration is too high and at the end it is too low. This is due to the uniform velocity profile, which has low velocities at the beginning of the cycle and higher velocities towards the end.

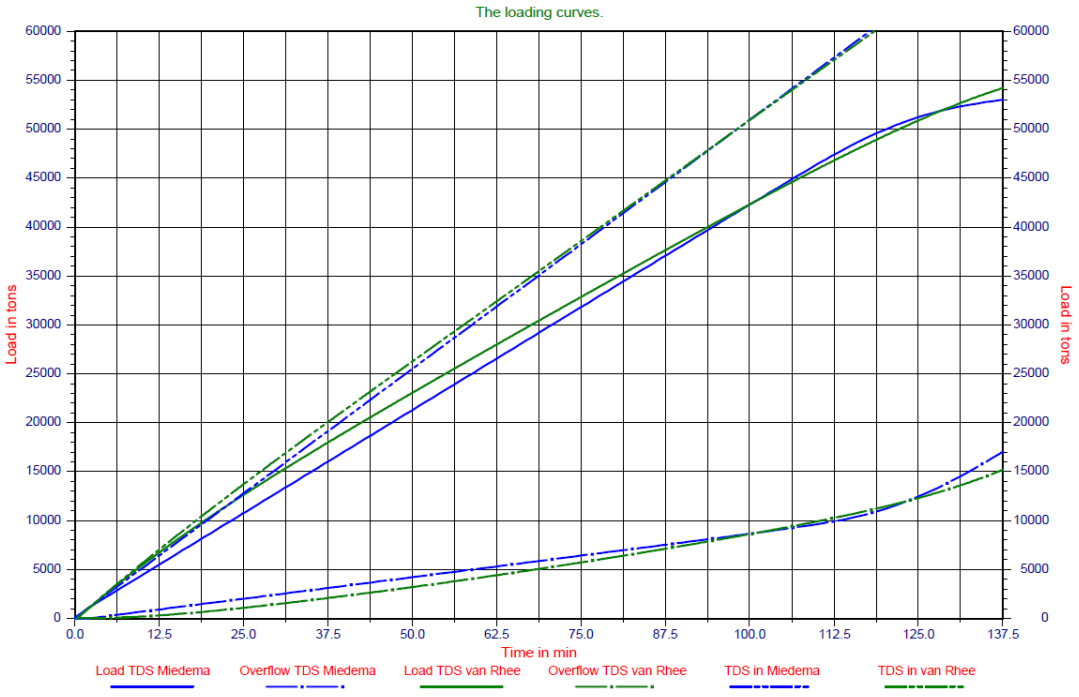

Figure 4.4: Comparison of the models of Van Rhee and Miedema. Source: Miedema[36]

4.3. 1DV Model Van Rhee

Van Rhee[49] models the hopper as in Figure 4.5. In this model, the following simplifications are made:

1. The sand is uniformly distributed over the whole surface of the hopper.
2. The inflow concentration and discharge which enter zone 2 are assumed to be the same as at the inflow of the hopper.
3. All quantities are assumed to be uniformly distributed over the length of the hopper.
4. In reality there is a bed shear stress caused by the density current. This can reduce the sedimentation velocity. With this 1DV model, this effect is not simulated. This is an important simplification as will be seen later on.

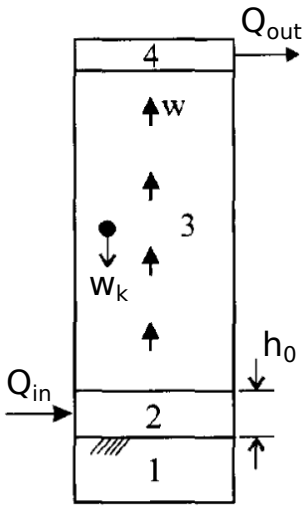

Figure 4.5: 1DV model. Source: Van Rhee[49]

The transport of sediment in zone 3 is calculated with the one-dimensional advection-diffusion equation:

$$\frac{\partial \alpha_k}{\partial t} = -\frac{\partial (\alpha_k w_k)}{\partial z} + \frac{\partial}{\partial z}\left(\Gamma_t \frac{\partial \alpha_k}{\partial z}\right) + \delta_{s,k} \tag{4.8}$$

In which $\delta_{s,k}$ is the source term at the inlet and outlet. The vertical fraction velocity w_k is the vertical component of Equation 3.22. The vertical flux velocity j_z, which is needed in Equation 3.22, is calculated with Q_{in}/A.
The turbulent diffusion coefficient Γ_t is assumed to be related to the eddy viscosity:

$$\Gamma_t = \frac{\nu_t}{\sigma} \tag{4.9}$$

For the Schmidt number σ a value of one was used. The eddy viscosity was assumed to be constant over the height and was determined with Prandtl's Mixing Length Model:

$$\nu_t = \ell_m^2 \left|\frac{\partial u}{\partial z}\right| \tag{4.10}$$

In which ℓ_m is the mixing length. The calculation of the mixing length was based on Rodi[53]. Rodi proposes $\ell_m = 0.09 h_0$ for density currents, in which h_0 is the height of the density current.
Van Rhee investigated the influence of the diffusion coefficient. A factor ten difference in diffusion had only a minor effect.

On model scale, the cumulative overflow losses were predicted well. However, compared to a prototype scale test with the TSHD 'Cornelia', the 1DV model underpredicted the overflow losses by a factor 5. Van Rhee gives an explanation for this. During the model tests, the influence of the bed shear stress on the sedimentation was negligible. At prototype scale, the influence of the bed shear stress has become significant due to scale effects.

4.4. 2DV model Van Rhee

Van Rhee[49] also developed a 2D model. An example of a simulation can be seen in Figure 4.6. It can be seen that the density current is simulated. Therefore, the pickup flux can be calculated correctly, which results in a higher accuracy compared to other models. Comparison between model and measurements show very good resemblance. Differences between measured an simulated overflow losses are small. The velocity profiles are similar and show the same behaviour over time.

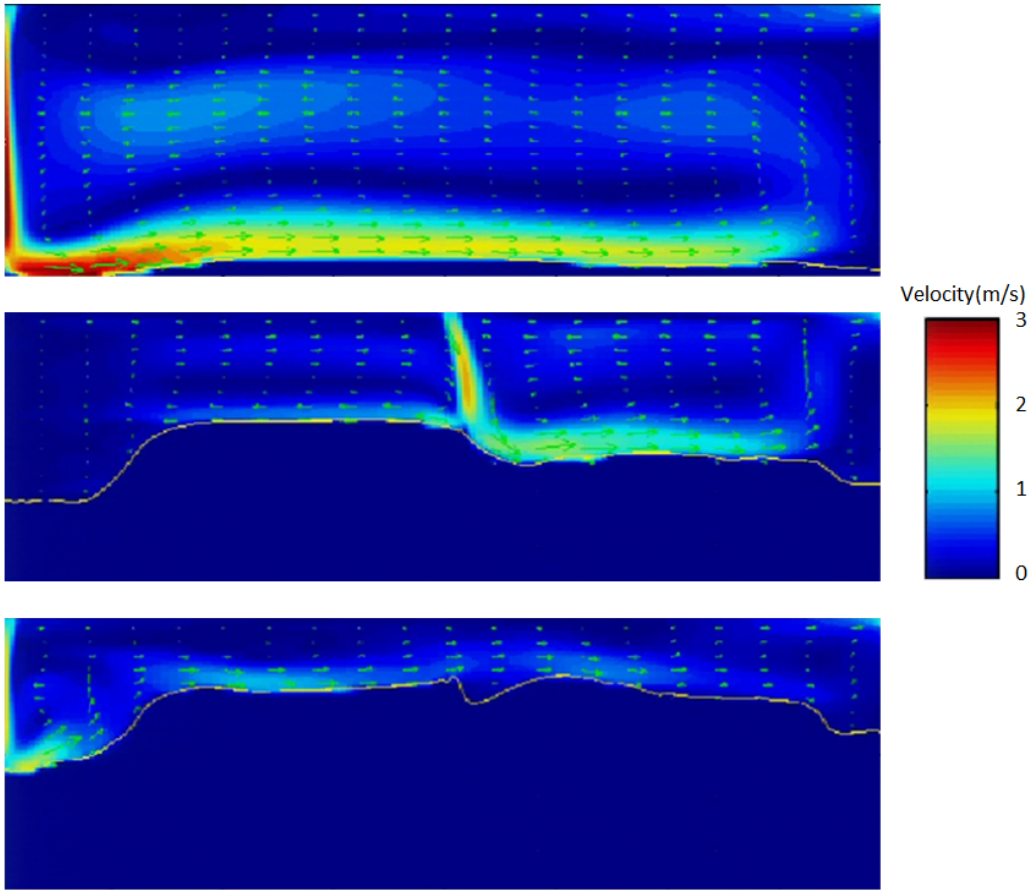

Figure 4.6: Velocities in a hopper at three time steps simulated with the 2DV model of Van Rhee. Source: https://ocw.tudelft.nl/courses/dredging-processes/?view=lectures

Van Rhee noted that the velocity in the jet and density current are higher than in the measurements. This leads to higher entrainment and hence more dilution of the inflowing mixture. The concentration of the density current above the bed is therefore lower. This higher velocity in the jet is caused by the choice of turbulence model. Air entrainment can also play a role.
The simulations of this model give a lot of insight into the processes inside the hopper.

4.5. Spearman

The 1DV model of Spearman[59] looks very similar to the 1DV model of Van Rhee. The hopper is divided into 20 cells which are layered on top of each other. Just like Van Rhee, he assumes that the sediment influx is uniformly distributed over the bottom of the hopper. The vertical transport is described with Equation 4.8.

The difference between the models is the outflow. In the model of Van Rhee (Figure 4.5) there is only outflow at the top. Spearman assumes that sediment from every layer flows into the overflow. In his model there is horizontal flow in the whole hopper. When the mixture arrives at the end of the hopper, everything moves up and goes through the overflow.

To calculate the horizontal velocity first the pressure gradient is calculated. Every layer is assumed to

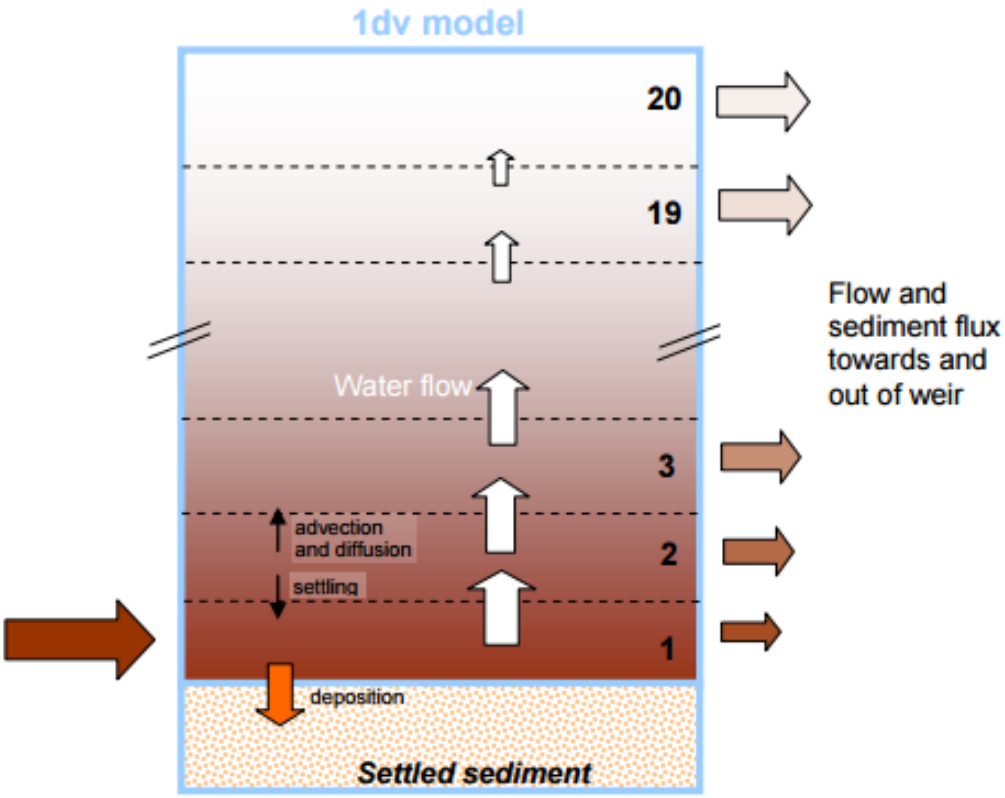

Figure 4.7: 1DV Model of Spearman[59]

have the same value of the pressure gradient:

$$\frac{1}{\rho}\frac{\partial p}{\partial x} = -\frac{\tau_b}{\rho h_{water}} + \frac{U(t) - U_0(t)}{T_{rel}} \tag{4.11}$$

ρ is the water density
τ_b is the shear stress imparted on the bed
h_{water} is the water depth
U is the mean horizontal velocity during the last time-step
U_0 is the desired mean velocity which is $Q/(W * H)$
T_{rel} is the relaxation time. For this value twice the time step is used.

Next, this value is used to compute the velocities with the one-dimensional equation for horizontal momentum:

$$\frac{\partial u}{\partial t} + \frac{1}{\rho}\frac{\partial p}{\partial x} = \frac{\partial}{\partial z}\left((\nu_m + \nu_t)\frac{\partial u}{\partial z}\right) \tag{4.12}$$

ν_m and ν_e are the mixture viscosity and eddy viscosity, respectively. The shape of the velocity profile can be seen in Figure 4.7. With these horizontal velocities, the outflow is calculated.

Since Spearman's model has a horizontal velocity, a bed shear could be calculated. However, Spearman doesn't model the density current causing the pickup flux to be lower.

The 1DV of Van Rhee was not able to predict overflow losses at prototype scale. On the contrary, comparing the 1DV model of Spearman with measurements of the TSHD the 'Oranje', it was shown that the model is able to predict these overflow losses very well. According to Spearman, at the end of the loading cycle, the density current plunges directly into the overflow causing higher overflow losses. Since sediment from every layer goes into the overflow, the overflow losses for Spearman are higher than the 1DV model of Van Rhee, giving better resemblance at prototype scale.

4.6. Braaksma

The model of Braaksma[8] was designed for the field of System & Control. The future goal of this model is controlling a TSHD. By using this sedimentation model, the ideal trajectory of the pump settings, drag head settings and sailing speed for the next 5 minutes could be calculated. To calculate the ideal trajectory, the calculation speed is a very important. Braaksma accounts for pickup by applying a reduced sedimentation:

$$v_{sed} = R(\theta, \alpha_b) v_{sed,0} \tag{4.13}$$

$v_{sed,0}$ is the sedimentation velocity in absence of a bed shear stress ($E = 0$). The reduction $R(\theta, \alpha_b)$ is estimated with:

$$R(\theta, \alpha_b) = \frac{Q^2}{k_e * h_{water}^2} \tag{4.14}$$

h_{water} is the height of the water above the bed and k_e a constant defined with a least square method. The increase in bed volume can then be calculated with:

$$Q_s = A v_{sed} = A \cdot R(\theta, \alpha_b) \frac{-\alpha_b w_0 (1 - \alpha_b)^n}{1 - n_0 - \alpha_b} \tag{4.15}$$

For the near bed concentration the following formula is used:

$$\alpha_b = \frac{\rho_m - \rho_w}{\rho_s - \rho_w} \tag{4.16}$$

The mixture density ρ_m is determined by assuming a density profile over the height. For this he tested three options: a linear, an exponential and a two layer model. After validation with measurements on a TSHD, the two layer model appeared to be the best. ρ_m is calculated with the total mass of all

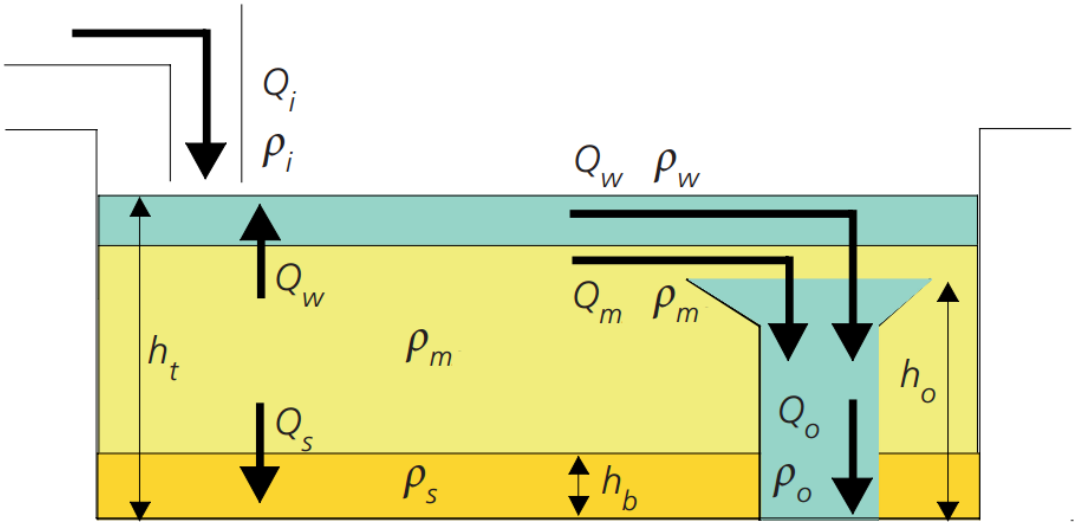

Figure 4.8: Two layer model of Braaksma[8]

the particles in the mixture divided by the mixture volume. ρ_m is assumed to be constant in the layer above the bed.

In the model of Braaksma it is not needed to use a particle diameter as input. During the first dredging cycle on an excavation site the bed height, overflow level, inflow concentration and inflow discharge are measured. Next, the w_0, k_e, ρ_{bed} and n (exponent for hindered settling) are determined with a least squares method. The first loading cycle is modelled with different values of $w_{s,0}$, k_e, ρ_{bed} and n. The values which give the best fit are used in the rest of the loading cycles at that excavation site.

Because Braaksma has the possibility of using a least squares method, a less accurate model can still give reasonable results. In this thesis a least squares method is not possible.

4.7. Jensen

Jensen[22] inspired his model on Braaksma. An improvement on the model of Braaksma is the usage of a PSD. Contrary to Braaksma, Jensen uses only one mixture layer instead of two. The concentration of every particle diameter is assumed to be constant throughout the whole layer. To calculate the sedimentation velocity he uses a non-dimensional variant of:

$$v_{sed} = \frac{-\sum(\alpha_k w_k)}{1 - n_0 - \sum \alpha_k} \tag{4.17}$$

w_k was calculated with $w_{k,0}(1-\sum \alpha_k)^{n_k}$. This is possible, because perfect mixing is assumed. Normally, w_k should be calculated with Equation 3.22.

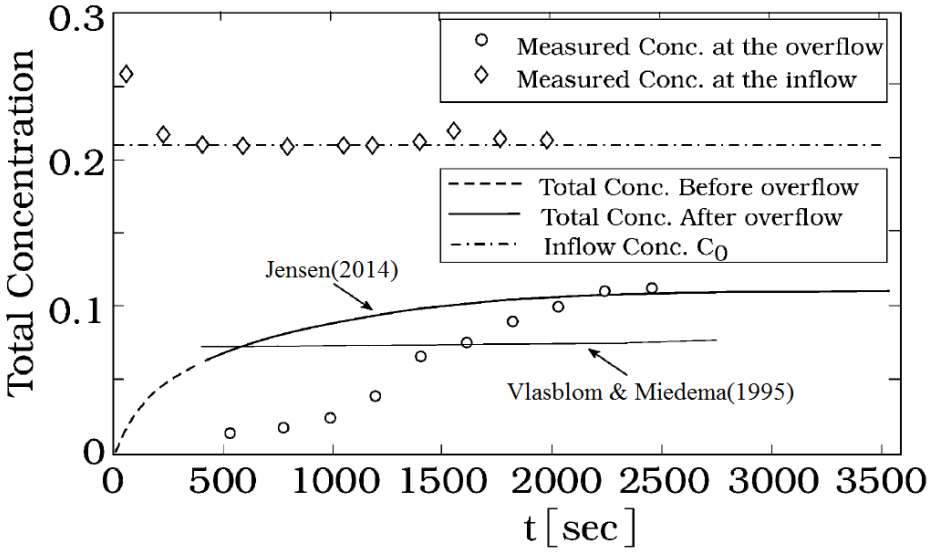

Figure 4.9: Overflow concentration of Test 5 of Van Rhee[49]. Source: Jensen[22]

The overflow losses predicted with this model are too high (Figure 4.9). The concentration of the particles is assumed to be homogeneous, so when the water level reaches the overflow, a high concentration of particles directly leaves the hopper.

4.8. Konijn

Konijn[31] has also developed a 2DV model. Konijn used an Euler-Euler approach. As explained in Paragraph 3.2, a big challenge with Euler-Euler is determining the coupling forces. In his model, the coupling forces were causing instabilities, hence calculation times were huge. To make sure the calculation time was days instead of weeks, Konijn used a hopper of 1 by 5 meter(a mesh of 90 x 350). Figure 4.10 is an example of a simulation.

The physical phenomena in the hopper are not simulated correctly. The first thing that can be seen, is that there is (almost) no entrainment in the inflowing jet. Secondly, the density current disappears very quickly in the model while in the measurements of Van Rhee[49] a density current is present throughout the whole measurement.

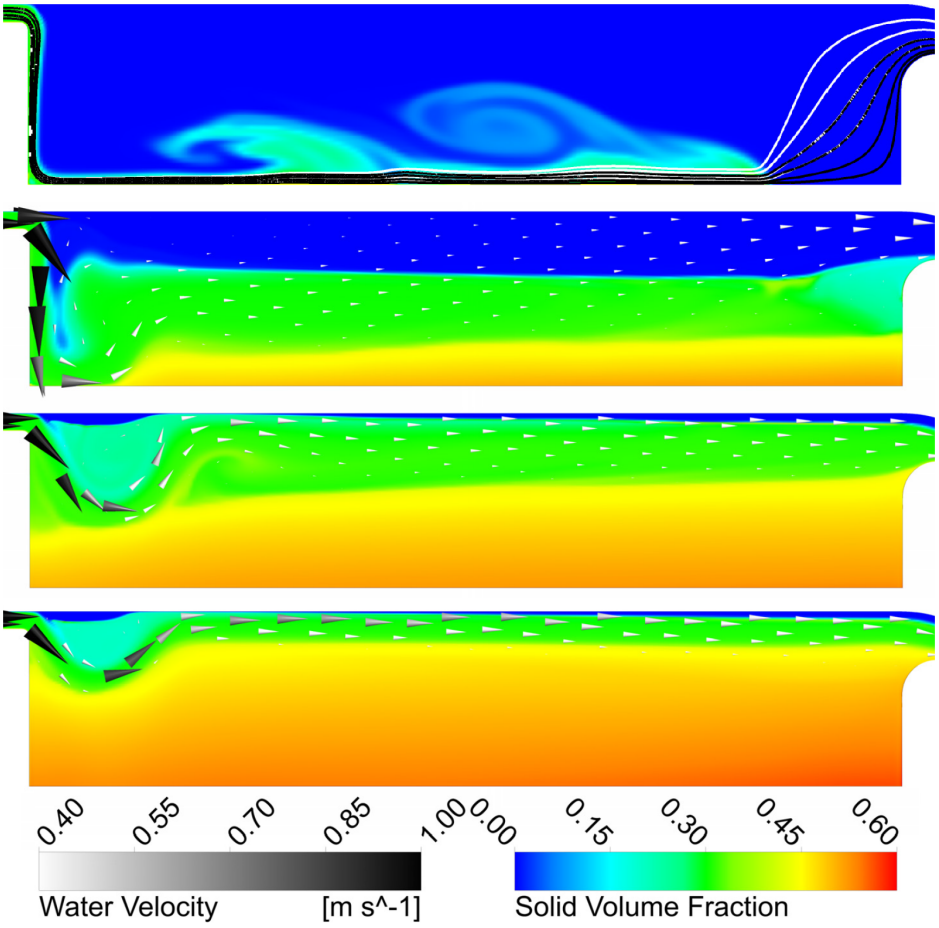

Figure 4.10: Concentration and velocity after 7 s, 39 s, 100 s and 170 s. $d = 200\ \mu m$, $\alpha_i n = 0.3$ and $u_{in} = 1\ m/s$, Konijn[31]

5

A New 2DV Model

Out of the existing models a separation can be made into two groups. First, there are the rather simple models with low calculation time. In this category, the models of Miedema and Spearman have the most potential. The model of Spearman could, for example, be improved by incorporating a density current at the bottom. The velocity at the beginning of the density current could be estimated by the jet model of Yannopoulos[67]. In the rest of the density current, the velocity could be modelled with the theory of Parker[42]. With these velocities, the correct bed shear stress and sedimentation velocities can be calculated at every position along the x-axis. This would give a rather simple model with a low calculation time.

The second category are the more heavy 2DV models. A model could be made with a CFD-package like `OpenFOAM`. `OpenFOAM` is an open-source code. This gives the opportunity to easily add features. 2DV-modelling has several advantages. The first advantage is the accurate physical modelling. Each individual process can be modelled in great detail. Secondly, all processes have a high influence on each other. The effects of all the processes can only be integrated with a 2DV model. Thirdly, it gives the possibility to model the geometry of the hopper in great detail. When the model is able to simulate in 3D, it even gives the opportunity to investigate the influence of different inlet and overflow configurations.

> If something is written in these `thin letters`, it is a name in `OpenFOAM`, e.g. the name of a solver, function or turbulence model.

A clear downside of a 2DV model is the calculation time. One of the design constraints is a calculation time of maximum 10 minutes. A way to work around this problem is to let the 2D model do a great amount of calculations with different hopper geometries and inlet properties. Once the loading time of a certain hopper needs to be known, the calculation is done by doing an interpolation in the already generated database. It was decided to go for this second approach.

As explained in Paragraph 3.3, the Stokes number should be much smaller than 1 for the Drift Flux Approach to be valid. For particles of 125 μm the particle relaxation time τ_p is in the order of milliseconds. The characteristic time of the flow t_{flow} in the middle of the hopper is in the order of seconds. This means the Stokes Number in the middle of the hopper is much smaller than 1.
Near the bed, $u_* \approx 0.005\ m/s$ and $z = 0.01875\ m$ (distance from the cell centre to the wall) as will be seen later on in Chapter 7. This means that the characteristic time of the flow t_{flow} at the bed is also in order of seconds, which results in $St \ll 1$. It can be concluded that the Drift Flux approach is valid for hopper modelling.
In that case, Drift Flux is preferred over Euler-Euler due to the complexity of Euler-Euler. Stability is an issue when multiple particle fractions are modelled with Euler-Euler. A lot of effort would be needed to develop a stable Euler-Euler model.

Since LES is only able to operate in three dimensions and gives rather large calculation times, URANS-modelling is chosen. In `OpenFOAM`, the model `buoyantKEpsilon` is used. More information on the different (U)RANS-models can be found in Appendix A.

The calculation time is a constraint, so high-Reynolds closure is preferred for the handling of the near-wall region.

The `driftFluxFoam` solver is able to simulate flow of the mixture, but the modelling of a bed is not yet incorporated. In this thesis, several features were added to model the bed. In Paragraph 5.1, it is described how the bed is fixed. The implementation of wall functions and pickup at the bed are explained in Paragraph 5.2. A custom made, moving mesh was developed during this thesis which is explained in Paragraph 5.3. In Paragraph 5.4, it is described how the model was expanded from 2D to 3D.

5.1. Fixing the bed

The `driftFluxFoam` solver contains a function which is called `MULES`. `MULES` means *Multidimensional Universal Limiter for Explicit Solutions* and is explained in the Ph.D. Thesis of Márquez Damián[33]. `MULES` makes sure the concentration of the particles doesn't exceed a maximum concentration: α_{max}. By default, this is a concentration of 100%. `MULES` achieves this by making a correction after the advection-diffusion equation is solved. If the concentration in a certain cell exceeds α_{max}, `MULES` limits the fluxes going into that cell. In that way the concentration of that cell exactly becomes α_{max}.

The default setting of $\alpha_{max} = 100\%$ can easily be adjusted to the maximum concentration in the hopper. Due to sedimentation, a layer with a concentration of α_{max} is now formed. This layer still behaves as a fluid and cannot be considered to be a bed, since this layer of α_{max} easily starts to flow.

`driftFluxFoam` is inspired on the work of Goeree[24]. To fix the bed, Goeree increases the viscosity in the bed with a Bingham plastic model:

$$\mu_{Bp} = \mu_m + \frac{\tau_y}{\frac{1}{2}\sqrt{I_2} + \epsilon} \tag{5.1}$$

Where ϵ is a very small number to prevent the denominator to go to zero. I_2 is the second invariant of the deformation tensor (which is a scalar):

$$I_2 = \sqrt{\mathbf{S}:\mathbf{S}} \tag{5.2}$$

And the deformation tensor $\mathbf{S}$ is:

$$\mathbf{S} = \frac{1}{2}\left(\nabla \mathbf{u}_m + \nabla \mathbf{u}_m^T\right) \tag{5.3}$$

The yield stress τ_y is calculated by Goeree with:

$$\tau_y = \tau_{y,max}\left(\frac{\alpha}{\alpha_{max}}\right)^{\beta} \tag{5.4}$$

With β is 400. This gives a yield stress of zero for $\alpha < \alpha_{max}$ and a yield stress of $\tau_{y,max}$ for $\alpha = \alpha_{max}$. `driftFluxFoam` uses something very similar:

$$\tau_y = \tau_{y,max}\left(10^{c(\alpha-\alpha_{max})} - 10^{-c\alpha_{max}}\right) \tag{5.5}$$

This principle can be used to fixate the bed. The problem, however, is that the viscosity is an semi-implicit term in the momentum equation. To reach stability a very small time step is needed.

Instead of the method of Goeree, the bed was fixed with the *Volume Penalization Method* of Angot[2]. Since this method can be implemented implicitly, no instability problems occurred. At the right side of the momentum equation (Equation 3.8), a so called penalty term was added:

$$-C_{penalty} H \mathbf{u}_m \tag{5.6}$$

H is a volScalarField with a value one at the bed and a value zero where there is no bed. The penalty term has therefore only influence in the bed. $C_{penalty}$ is a big number, in this case 10^{12}. Physically, the penalty term could be seen as a very big force which always acts in the opposite direction of $\mathbf{u}_m$. This big force always causes the velocity in the bed to be close to zero. Making the velocity in the bed zero is not enough. When the velocity at the centre of the bed cells is zero, there can still be velocity-fluxes and concentration-fluxes over the bed-interface. The concentration-flux needs to be zero. The velocity-flux needs to be as small as possible.

Making the concentration-flux zero
The concentration is calculated in two steps. First, the advection is calculated. The advection at the bed is made zero by multiplying the velocity-flux at the bed interface by zero in the advection-equation. Second, the diffusion is calculated. The diffusion-flux over the bed-interface can easily be stopped by making the diffusion-coefficient at the bed interface zero.

Limit the velocity-flux
Limiting the velocity-fluxes at the bed-interface is more complicated. To explain how this is done, it needs to be explained how the velocity-fluxes are calculated.

The derivation is started with a semi-discretised form of the momentum equation (Equation 3.8):

$$a_p \mathbf{u}_p = H(\mathbf{u}) - \nabla p \tag{5.7}$$

In which a_p are the terms on the diagonal of the FvMatrix of the momentum equation. $\mathbf{u}_p$ is the velocity in the cell centre which is assumed to be the average velocity in the cell:

$$\mathbf{u}_p = \frac{1}{V}\int_V \mathbf{u} dV \tag{5.8}$$

The term $H(\mathbf{u})$ in Equation 5.7 is defined as:

$$H(\mathbf{u}) = -\sum_n a_n \mathbf{u}_n + \frac{\mathbf{u}_p^0}{\Delta t} \tag{5.9}$$

The first term represents the matrix coefficients of the neighbouring cells multiplied by their velocity. The second part contains the unsteady term and all the sources except the pressure gradient. Equation 5.7 can be rewritten to:

$$\mathbf{u}_p = \frac{H(\mathbf{u})}{a_p} - \frac{\nabla p}{a_p} \tag{5.10}$$

To arrive at Equation 5.11, Equation 5.10 has to be substituted in the continuity equation ($\nabla \cdot \mathbf{u} = 0$):

$$\nabla \cdot \left(\frac{1}{a_p}\nabla p\right) = \nabla \cdot \left(\frac{H(\mathbf{u})}{a_p}\right) \tag{5.11}$$

Note however that $\nabla \cdot \mathbf{u} \neq 0$. As mentioned in section 3.4, this is done wrong in `driftFluxFoam`. To do this derivation correctly, Equation 3.6 should be used. This means that the term $\frac{\partial \rho_m}{\partial t}$ should be added at the RHS. Since this is not done, `driftFluxFoam` actually calculates the *mixture flux velocity* instead of the *mixture centre of mass velocity*. `settlingFoam` does take this derivative of the density into account. By copy-pasting pieces of code from `settlingFoam`, the pressure equation of `driftFluxFoam` can easily be corrected, but for the sake of saving time this is not done during this thesis. Furthermore, ignoring this density term probably gives more stability.

Equation 5.11 can be discretized into:

$$\nabla \cdot \left(\frac{1}{a_p} \nabla p \right) = \sum_f \mathbf{S}_f \left(\frac{H(\mathbf{u})}{a_p} \right)_f \tag{5.12}$$

In which $\mathbf{S}_f$ is the surface vector. Instead of p, `driftFluxFoam` uses the dynamic pressure, which is defined as:

$$p_{rgh} = p - \rho_m g h \tag{5.13}$$

In which h is the vertical distance relative to a fixed reference point.

Substituting Equation 5.13 in Equation 5.14 gives:

$$\nabla \cdot \left(\frac{1}{a_p} \nabla (p_{rgh} + \rho g h) \right) = \sum_f \mathbf{S}_f \left(\frac{H(\mathbf{u})}{a_p} \right)_f \tag{5.14}$$

$$\nabla \cdot \left(\frac{1}{a_p} \nabla p_{rgh} \right) = \sum_f \mathbf{S}_f \left(\frac{H(\mathbf{u})}{a_p} \right)_f + \sum_f \mathbf{S}_f \frac{(-gh\nabla\rho)_f}{(a_p)_f} \tag{5.15}$$

The equation above is the pressure equation which can be found in `driftFluxFoam`. The term $\mathbf{S}_f \left(\frac{H(\mathbf{u})}{a_p} \right)_f$ is called ϕ_{HbyA} and the term $\mathbf{S}_f \frac{(-gh\nabla\rho)_f}{(a_p)_f}$ is called ϕ_g in `driftFluxFoam`.

When Equation 5.15 is solved, the pressure-corrected velocities and fluxes can be calculated. The velocity on the face is obtained by interpolating Equation 5.10:

$$\mathbf{u}_f = \left(\frac{H(\mathbf{u})}{a_p} \right)_f - \frac{(\nabla p)_f}{(a_p)_f} = \left(\frac{H(\mathbf{u})}{a_p} \right)_f + \frac{(-gh\nabla\rho)_f}{(a_p)_f} - \frac{(\nabla p_{rgh})_f}{(a_p)_f} \tag{5.16}$$

$$\phi = \mathbf{S}_f \cdot \mathbf{u}_f = \mathbf{S}_f \cdot \left(\frac{H(\mathbf{u})}{a_p} \right)_f + \mathbf{S}_f \cdot \frac{(-gh\nabla\rho)_f}{(a_p)_f} - \mathbf{S}_f \cdot \frac{(\nabla p_{rgh})_f}{(a_p)_f} \tag{5.17}$$

$$\phi = \phi_{HbyA} + \phi_g - \phi_{p_{rgh}} \tag{5.18}$$

ϕ is the velocity-flux over a face. To calculate the fluxes and solve the pressure equation, `driftFluxFoam` uses the following order:

1. $H(\mathbf{u})$ is calculated with Equation 5.9.
2. ϕ_{HbyA} and ϕ_g are calculated: $\phi_{HbyA} = \mathbf{S}_f \left(\frac{H(\mathbf{u})}{a_p} \right)_f$ and $\phi_g = \mathbf{S}_f \frac{(-gh\nabla\rho)_f}{(a_p)_f}$.
3. The pressure equation is solved (Equation 5.15), which gives p_{rgh}.
4. The fluxes are calculated with Equation 5.17.
5. $\mathbf{u}_p$ is calculated with Equation 5.10. The term $\frac{\nabla p}{a_p}$ is calculated with the function `reconstruct`.

The velocity flux should be as small as possible at the bed interface. To make ϕ_{HbyA} zero, different options were tried. At the boundaries of the mesh, this is done with a `fixedFluxPressure` or `fixedFluxExtrapolatedPressure`. These boundary conditions were also applied at the bed interface, but both gave stability problems. Simply multiplying ϕ_{HbyA} at the bed by zero appeared to be the most stable solution. Both ϕ_g and $\phi_{p_{rgh}}$ were left untouched. ϕ_g is small and $\phi_{p_{rgh}}$ is needed for continuity.

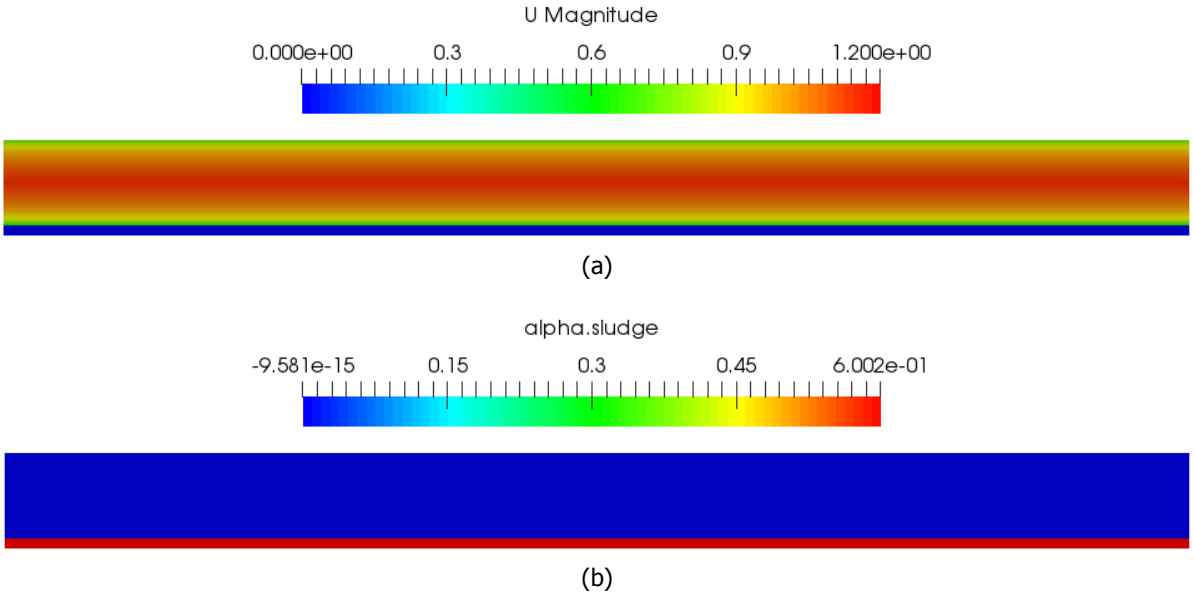

Figure 5.1: Simulation of the bed at t=20s with in (a) the velocity and in (b) the concentration.

In Figures 5.1a and 5.1b, a simulation is shown which demonstrates that the bed is fixated. The grid is a 2D channel of 0.324 x 4.0 m. At the bottom, a bed with a height of 0.036 m is placed. At the left, water without particles is flowing into the tube with an average velocity of $1.0\ m/s$. As can be seen in Figure 5.1b, the bed stays nicely in its place. Exactly the same results can be seen for higher velocities. The velocity of the top cells in the bed is $1.235 * 10^{-8} m/s$. This is a very low velocity which shows that $C_{penalty}$ can be made lower if such a large value appears to increase the simulation time.

5.2. Wall functions

In this paragraph, two types of simulations are compared. The first simulation is again a 2D representation of a channel with dimensions 0.288 x 4.0 m (Figure 5.2a). The water at the inlet has a velocity

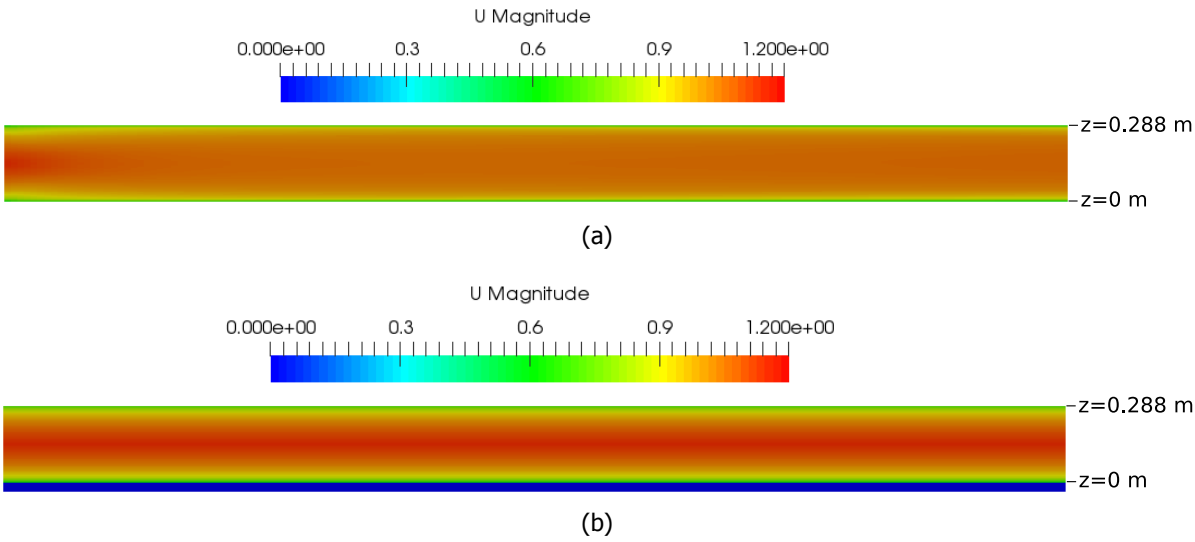

Figure 5.2: (a) Simulation with wall at the bottom. (b) Simulation with a bed without boundary conditions at the bed surface.

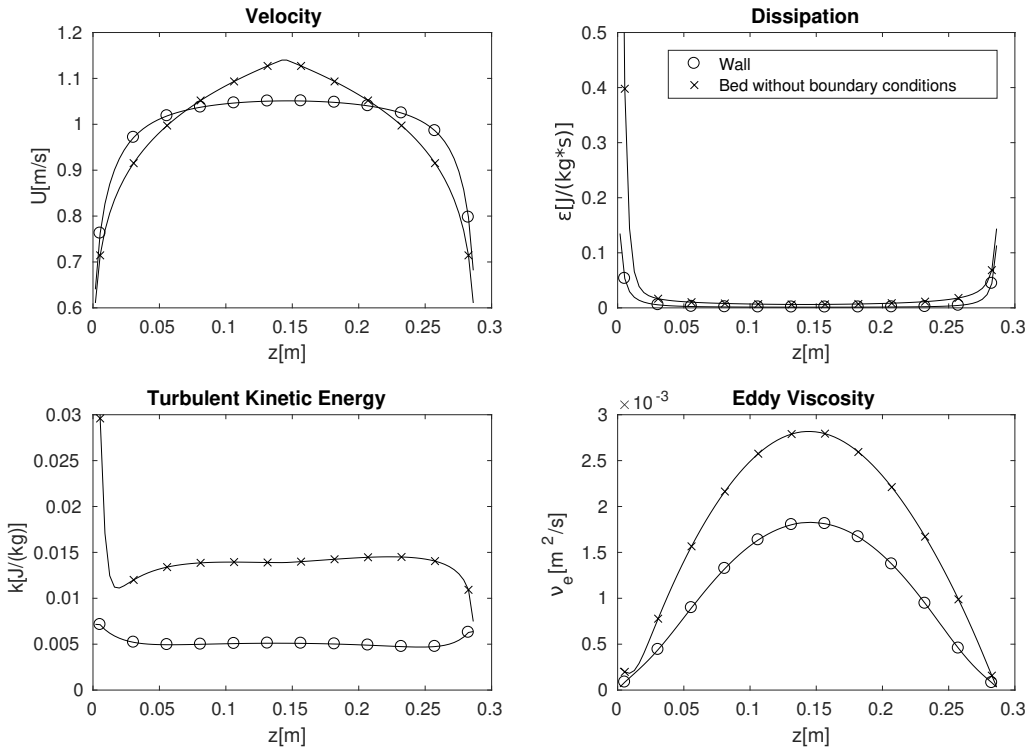

Figure 5.3: Verification of the code. Simulation with a wall and simulation with a bed (x = 3.5 m).

of 1 m/s and a solid concentration of 0%. The wall at the top has approximately the roughness of steel, which is 0.05 mm. The wall at the bottom has the roughness of sand with $D_{50} = 125\mu m$, which is approximately $2.5 \cdot D_{50} = 0.3125mm$.

The second simulation is similar to the first. The wall at the bottom is replaced by a bed with $D_{50} = 125\mu m$ (see Figure 5.2b). In the bed, the k and ϵ are set to nearly zero (10^{-8}). Obviously, these two simulations should give exactly the same results. Without applying boundary conditions for k, ϵ and ν_e at the bed this not the case as can be seen in Figure 5.3. It is clear that boundary conditions need to be applied.

For a high-Reynolds closure with k-ϵ, the following boundary conditions are mainly used in `OpenFOAM`:

- **`kqRWallFunction`**
  This is a simple wrapper around the zero-gradient condition.
- **`epsilonWallFunction`**
  This boundary condition calculates the ϵ:

$$\epsilon = \frac{c_\mu^{0.75} k^{1.5}}{\kappa y} \tag{5.19}$$

  To calculate the k correctly at the first grid-cell, the production of turbulent kinetic energy, P, needs to be calculated correctly. `epsilonWallFunction` therefore also does a correction for the production:

$$P = \mu_{eff} \frac{\partial u}{\partial y} \frac{k^{0.5} c_\mu^{0.25}}{\kappa y} \tag{5.20}$$

  In which $\mu_{eff} = \mu_t + \mu_m$ where μ_t is the eddy viscosity and μ_m the mixture viscosity.

- **nutkRoughWallFunction**
  This boundary condition uses:

$$\nu_{eff} = \frac{\nu_w \kappa y_+}{\ln\left(\frac{Ey_+}{1+Ck_s^+}\right)} \tag{5.21}$$

  In which ν_w is viscosity of water. Since this boundary condition is originally designed for a liquid and not for a mixture, it can be questioned if it would be better to use the mixture viscosity instead of the water viscosity. Paragraph 5.2.2 deals with this question.

These boundary conditions are also applied at the bed surface. The derivation of these boundary conditions can be found in Appendix C.

5.2.1. Implementation in driftFluxFoam

The contribution of the shear stress in the momentrum equation, $\nabla \cdot \left(\mathbf{T}_m + \mathbf{T}_m^t\right)$, is calculated in `driftFluxFoam` with the function:

```
fvm::laplacian(rho*turbulence->nuEff(), U)
```

This function calculates the shear stress at every face with:

$$\tau = \mu_{eff}\frac{\partial u}{\partial y} = \mu_{eff}\frac{u_i - u_{i-1}}{\Delta y} \tag{5.22}$$

The velocity in the bed is zero. At the bed interface, τ is calculated by (see Figure 5.4):

$$\tau = \mu_{eff}\frac{u_i - 0}{\Delta y} \tag{5.23}$$

This is incorrect; it should be:

$$\tau = \mu_{eff}\frac{u_i - u_{wall}}{\frac{1}{2}\Delta y} = \mu_{eff}\frac{u_i - 0}{\frac{1}{2}\Delta y} \tag{5.24}$$

This is a difference by a factor 2. To adjust the calculation of the $\frac{\partial U}{\partial y}$, the code behind the `fvm::laplacian` has to be adjusted. This is way too complicated. Weij[63] found an easy workaround for this problem: multiplying Equation 5.21 with a factor 2. Also the implementation of the zero-gradient is based on the ideas of Weij.

The same simulations, described at the beginning of the paragraph, are run again. This time, at the bed, the following boundary conditions are applied: for k a zero-gradient is used; for ϵ Equation 5.19 is used; and for the eddy viscosity Equation 5.21 with a factor 2 is applied. The results are shown in Figure 5.5. As can be seen, the results are almost exactly the same. Only a small difference can be seen for the k. This difference is negligible.

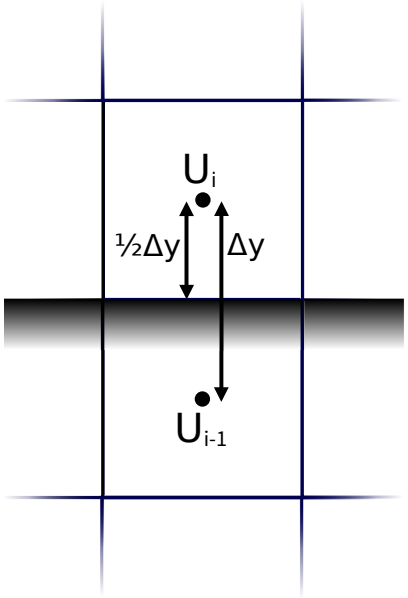

Figure 5.4: Definitions near the wall

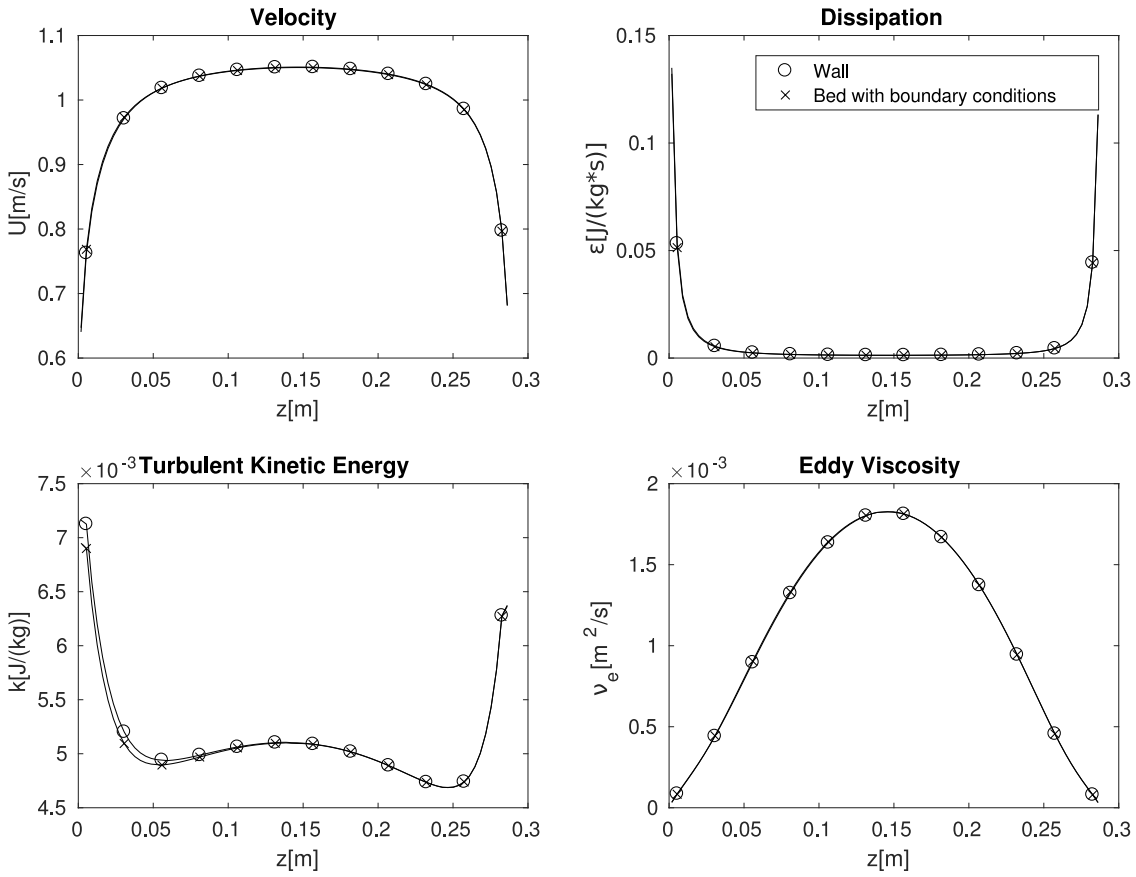

Figure 5.5: Verification of the code. Simulation with a wall and simulation with a bed (x = 3.5 m).

5.2.2. Effect of particle concentration on the wall-functions

Costa[19] and Picano[45] both investigated the effect of neutrally buoyant particles on the flow in the near-wall region. By doing DNS-simulations with concentrations of up to 20%, they showed that the wall-functions change for higher concentrations. Costa used the mixture viscosity calculated with the relation of Eilers (Figure B.1 of Appendix B) for the wall-functions. This gave better resemblance. Despite this improvement, a difference was still observed. Picano fitted the von Karman constant κ and the additive constant B for concentrations up to 20% and a range of $50 < y_+ < 150$.
In the work of Costa and Picano, several effects are not taken into account. By using neutrally buoyant particles in the simulations, there was no influence of the density. Close to the bed in the hopper, a density gradient can be found, meaning turbulence is destructed. To correctly derive the boundary conditions, the buoyancy destruction term has to be added in Equation C.1 (Appendix C).
In addition, they used rather large particles; the channel height divided by the particle diameter was in the range of 5 to 36.
Nevertheless, the method of Costa is used since this is the best available method to take into account the particle concentration. This means that in Equation 5.21, instead of ν_w, the mixture viscosity is used.

To calculate the Shields parameter (Equation 2.16) the shear stress is needed. The shear stress is calculated with Equation 3.31:

$$\tau = \rho u_*^2 \tag{5.25}$$

For the density the mixture density is used.

5.2.3. Mixture Viscosity

A very exact calculation of the viscosity is not that important. In most of the hopper, the eddy viscosity is much higher. Near the bed, however, the concentration of solids is high and the eddy viscosity is low. Near the bed, the calculation of the viscosity might have some influence. For this reason, in this paragraph attention is given to the mixture viscosity.
The dynamic mixture viscosity is calculated with:

$$\mu_m = \mu_f \mu_{rel} \tag{5.26}$$

μ_f is the fluid viscosity. The relative viscosity μ_{rel} is dependent on several variables: concentration, μ_f, particle diameter and shear rate. For small shear rates, numerous relations have been found. An overview is given in Appendix B. In this work, the relation of Thomas[60] is used:

$$\mu_{rel} = 1 + 2.5\alpha + 10.05\alpha^2 + A\left(\exp(B\alpha) - 1\right) \tag{5.27}$$

In which A and B are 0.00273 and 16.6 respectively. The accuracy is $\pm$ 13% at a solids concentration of 50% and particle sizes between 0.099 and 240 μm.

Bagnold[4] investigated the influence of the shear rate on the relative viscosity. With high shear rate, the grain-grain interactions become more important. The importance of grain-grain interactions can be characterized with the Bagnold number:

$$N = \frac{\sqrt{\lambda}\rho_s D^2}{\mu_{fluid}}\dot{\gamma} \tag{5.28}$$

In which the linear concentration λ is calculated:

$$\lambda = \left(\left(\frac{\alpha_{max}}{\alpha}\right)^{1/3} - 1\right)^{-1} \tag{5.29}$$

Bagnold defines three regimes: for $N < 40$ the macro viscous regime (viscous effects are dominant), for $40 < N < 450$ transitional regime and for $N > 450$ the grain inertia regime (there grain collisions are dominant).

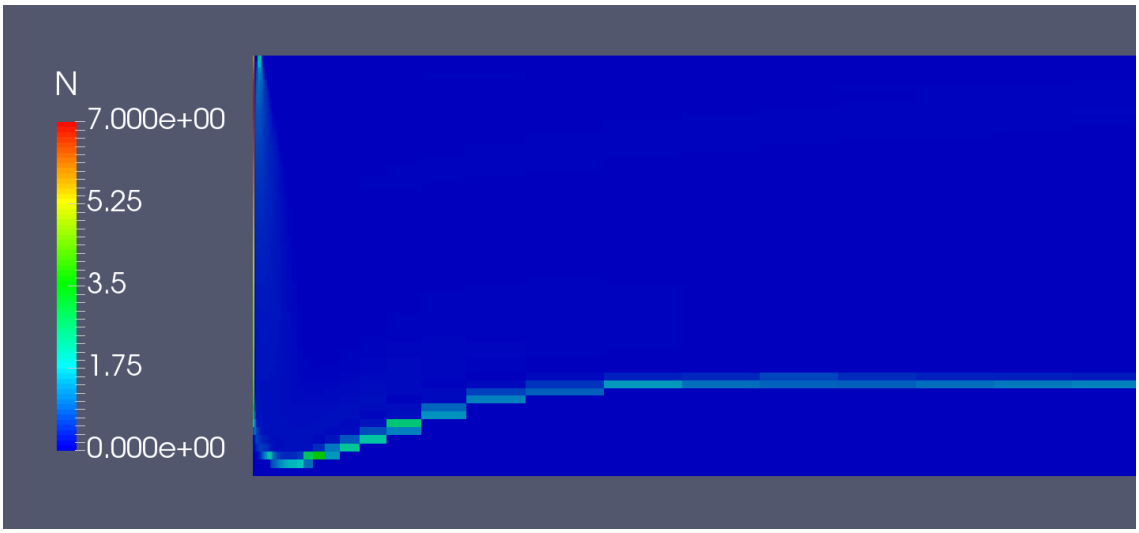

Figure 5.6: Bagnold number at the left side of the hopper at t=350s (Test 6)

As can be seen in Figure 5.6, the Bagnolds number is well below 40. The same is true for simulations at prototype scale. It is not needed to take into account the grain-grain interactions.

5.3. Moving mesh

First, it was tried to simulate sedimentation without a moving mesh (Figure 5.7). In case of sedimentation the sedimentation velocity was, however, too high. Once the sediment in a cell becomes fixated due to its high concentration, it affects the velocity in the cells around it as can be seen in Figure 5.7. This artificial roughness reduces the erosion flux in these cells. Hence, the sedimentation occurs faster than it should be.
Erosion was even impossible to reproduce. Once the concentration in a cell was low enough to make it liquid (change $H_{penalty}$ from 1 to 0) that cell would be shielded by its neighbours. In a few (or often even one) time steps, the cell would be filled again. A moving mesh was needed.

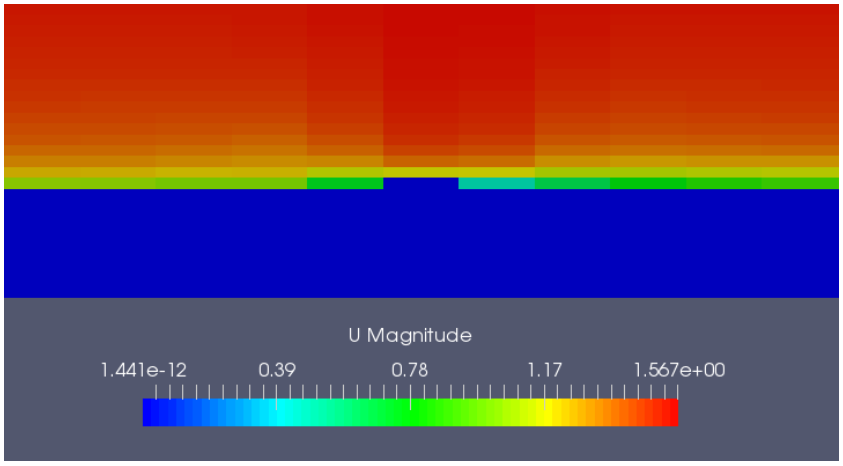

Figure 5.7: Influence of the bed on the flow

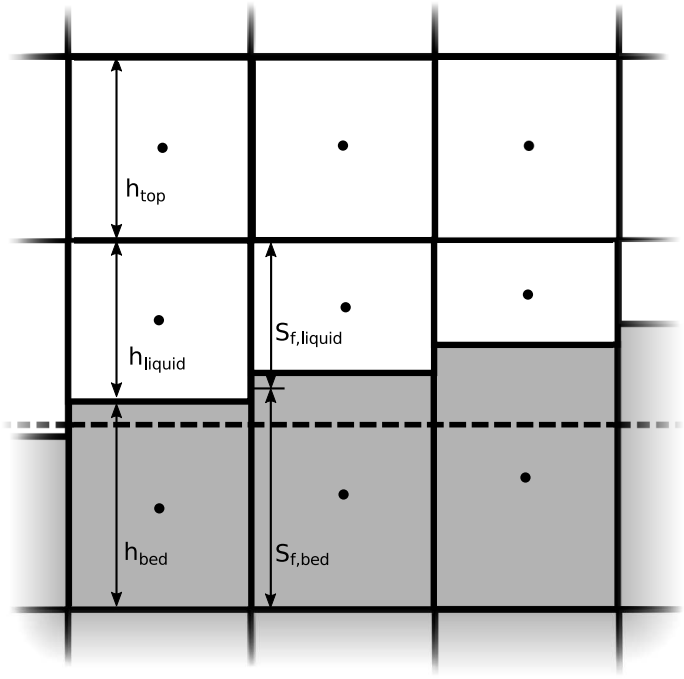

Figure 5.8: Moving mesh: the mesh follows the bed

`OpenFOAM` has already several moving meshes available. One example is the moving mesh in `InterDyMFoam`. It was decided, however, to develop a new moving mesh specially applicable for this situation. Inte-

grating a standard moving mesh in `driftFluxFoam`, takes a lot of effort. Furthermore, the standard moving meshes demand relatively large computation time. A more simple moving mesh can save a lot of computation time.
The design of the moving mesh is based on Van Rhee[49]. The mesh follows the bed. When the bed is rising, h_{liquid} is decreasing and h_{bed} is increasing (see Figure 5.8). The height of these cells are calculated every time step:

$$h_{bed}^{new} = h_{bed}^{old} + v_{sed}\Delta t \qquad \text{and} \qquad h_{liquid}^{new} = h_{liquid}^{old} - v_{sed}\Delta t \tag{5.30}$$

Since sediment becomes part of the bed, the concentration in the cell above the bed also has to be adjusted every time step. Conservation of mass gives:

$$\alpha_{liquid}^{old} h_{liquid}^{old} = \alpha_{liquid}^{new} h_{liquid}^{new} + \alpha_{bed}\Delta h \tag{5.31}$$

$$\alpha_{liquid}^{new} = \frac{\alpha_{liquid}^{old} h_{liquid}^{old} - \alpha_{bed}\Delta h}{h_{liquid}^{new}} \tag{5.32}$$

With Δh being positive in case of sedimentation. α_{bed} is used instead of α_{max}, because these are never exactly equal. MULES is not able to keep α_{bed} precisely at α_{max}. Using α_{bed} makes sure no mass is 'lost' or 'created'.

The face surfaces are calculated with the mean height of the adjacent cells as can be seen in Figure 5.8:

$$S_{f,liquid} = 0.5(h_{liquid,left} + h_{liquid,right}) \cdot \text{depth} \tag{5.33}$$

When h_{liquid} becomes too low, this creates instabilities. In that case, this cell is merged with the cell above it. This happens when h_{liquid} becomes smaller than 10% of its original height. After merging, the new cell has the following properties:

$$h_{merged} = h_{liquid} + h_{top} \tag{5.34}$$

$$\alpha_{merged} = \frac{\alpha_{liquid} h_{liquid} + \alpha_{top} h_{top}}{h_{liquid} + h_{top}} \tag{5.35}$$

Merging the cells above the bed means the bed cell has to be split. After splitting, both new cells simply have the concentration of the old bed cell. In case of erosion, h_{liquid} can become too big. When h_{liquid} becomes higher than 115% of its original height, it is split. This is done with similar formulas as Equations 5.34 and 5.35. Since this is simple bookkeeping, these formulas are omitted.
More information about the implementation of the moving mesh in `OpenFOAM` can be found in Appendix D.

Calculation sedimentation velocity
To calculate the movement of the bed with Equation 5.30, the sedimentation velocity needs to be determined. This done with Equation 2.21. The pickup is determined with Equation 2.23.

Influence of slope angle on the Erosion Flux
Now we have a moving mesh, the slope angle can also be calculated. The slope angle is needed for Equation 2.18. Figure 5.9 shows how the slope angle is calculated for the face in the middle:

$$\beta = tan^{-1}\frac{\Delta y}{\Delta x} \tag{5.36}$$

The slope angle is positive when the bed height is decreasing in the direction of the flow.
When the angle of a slope increases, the shear stresses in the slope also increase. These shear stresses can be calculated with the circle of Mohr. Incorporating these soil mechanics would be a lot of effort.

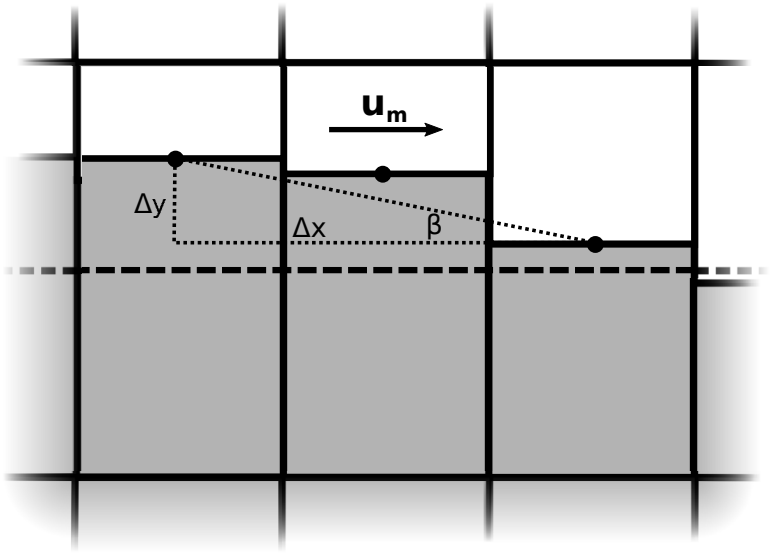

Figure 5.9: Slope of the bed

Instead, it is assumed that the maximum slope is the angle of internal friction. The slope angle is limited by increasing the erosion flux once the slope angle exceeds the angle of internal friction.

Mass conservation
The mass lost during a hopper simulation is calculated with:

$$M_{lost} = M_{cum,in} + M_{bed,start} - M_{cum,out} - M_{bed,end} - M_{suspended,end} \tag{5.37}$$

At the end of every hopper simulation, M_{lost} is less than 0.1% of $M_{cum,in}$.

5.4. 3D Simulations

The ability to do 3D simulations, opens up huge possibilities. Different inlet and overflow configurations could be simulated to design the optimal Trailing Suction Hopper Dredger.

To be able to simulate in 3D, the calculation of the slope angle (Equation 5.36) had to be applied to 3D.
In addition, parallel processing is necessary. Doing a 3D simulation with one processor simply requires too much time. Parallel processing is achieved by sending the bed height from each processor to the other processors. With these bed heights, the slope angle and mesh geometry at the processor patch can be calculated.
An example of a 3D simulation is shown in Figure 5.10. In the corners under the inlet, high velocities can be observed. In the corner, the entrainment is less, causing the jet to accelerate more. These high velocities can probably not be found in a real hopper. In this simulation, the inflow of mixture was still uniformly distributed over the width. In reality, the inflow velocities are higher in the middle.

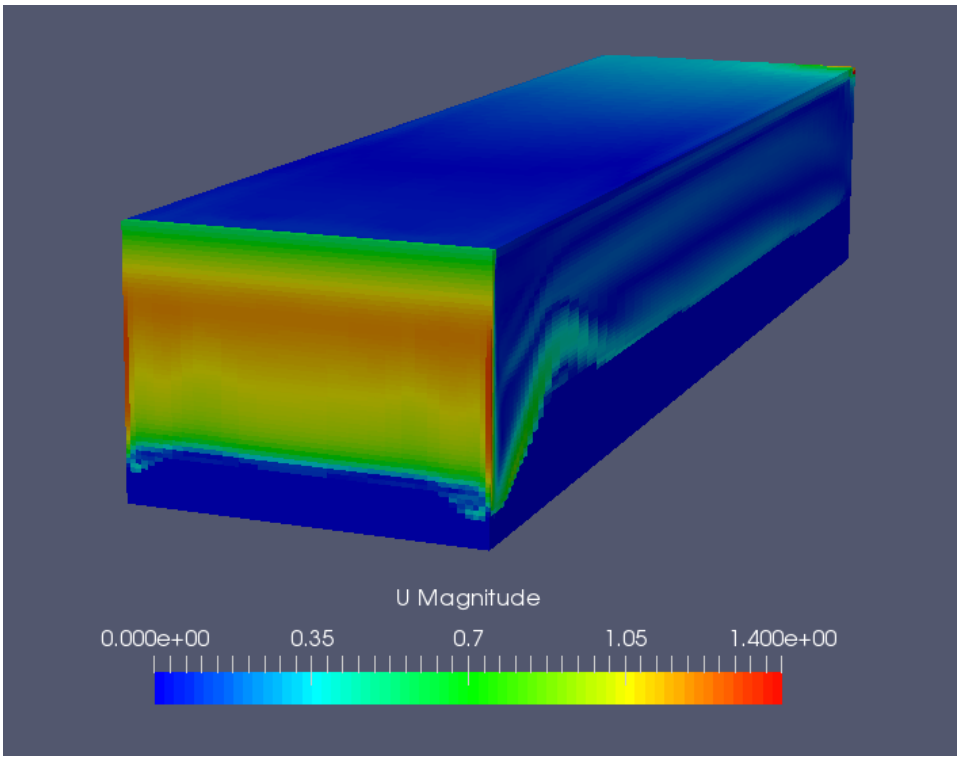

Figure 5.10: 3D simulation of Test 6 at t=650s.

6

Validation

This chapter is dedicated to the validation of the 2DV model with different benchmarks. In Paragraph 6.1, the settling of the model is validated with several settling experiments. Pickup of material is compared with the closed flume experiments of Van Rhee in Paragraph 6.2. Finally, the 2DV is model is compared with the hopper tests of Van Rhee.

6.1. Validation of settling

Using the settling in OpenFOAM
The current version of `driftFluxFoam` uses only one sand fraction. In `driftFluxFoam` this sand fraction is called the dispersed phase and has subscript *d*. The $\mathbf{u}_{k,m}$ of the dispersed phase is therefore called $\mathbf{u}_{d,m}$. For this reason the variable `Udm` can be found in `driftFluxFoam`. Since `driftFluxFoam` is using the mixture flux velocity, this `Udm` is not a real $\mathbf{u}_{d,m}$, but the $\mathbf{u}_{d,j}$ (for more explanation see Chapter 3.4). In other words, the $\mathbf{u}_{d,j}$ has to be used in `driftFluxFoam`, which, for cases with one fraction, is exactly the same as the hindered settling velocity: $w_0 \left(1-\alpha_d\right)^n$.

Settling experiments
Runge[54] and Van Rhee[49] have done settling experiments in a column with a height of 1.5 m and a diameter of 30 cm. The concentration was measured at several vertical positions with conductivity sensors. Although Van Rhee did measurements of the concentration over the whole height, only measurements from z = 0.90 m to z = 1.30 m are considered in this thesis. At the bottom of the column, not only settling takes place, but also sedimentation. For the time being, we only focus on settling. Sedimentation is validated in Paragraph 6.2. In the middle of the column, the influence of the PSD is too large. A full overview of all the experiments can be found in Appendix F.

Verification with an 1DV-advection model
The simulations have been compared with a simple 1DV-advection equation solved in MATLAB:

$$\frac{\partial c}{\partial t} + \frac{\partial \left(w_s c\right)}{\partial z} = 0 \tag{6.1}$$

For both `OpenFOAM` and the 1DV-model, a time step of 0.01s is used. In `OpenFOAM` a cell height of 0.01m was used and in the 1DV-model a cell height of 0.005m was used. In Appendix E, an numerical error analysis is shown in which the influence of the mesh, tolerance and time step was investigated. As expected, the 1DV-model and `OpenFOAM` give almost identical outcomes (Figure 6.1). It can be concluded that the settling is correctly implemented in `OpenFOAM`.
Runge used both a larger time step and cell height in his 1DV model, which resulted in a lot of numerical diffusion. This can clearly be seen in Figure 6.1.

Validation with the experiments

In Paragraph 2.1, several relations for the terminal settling velocity were given. All these relations were tried. It was concluded that the relation of Ferguson & Church in combination with Rowe gave the best fit. For the constants in Ferguson & Church[21], values of $C_1 = 18$ and $C_2 = 1.0$ are used. In Figures 6.1 and 6.2, `OpenFOAM` resembles the experiment well, but in the figures in Appendix F it can be seen that not all simulations fit the experiments that well. Causes are:

1. As explained earlier, the settling velocity is very sensitive to small variations in particle diameter and particle shape.
2. The PSDs of Runge were not totally uniform. This can be seen when experiment 42 is compared with `OpenFOAM`; the concentration in the experiment has a more gradual decrease.
   The PSDs of Van Rhee were much more graded than the PSDs of Runge. This caused the larger particles to move down and settle first, giving a larger settling velocity at the beginning. At the end of the experiment, only the smaller particles are left, causing smaller settling velocities at the end(Figure 6.2).
3. Experimental setups also have their inaccuracies.

Due to these phenomena, it was hard to choose the right equations for the settling. It is doubtful whether the choice of Ferguson & Church in combination with Rowe is the ideal one.

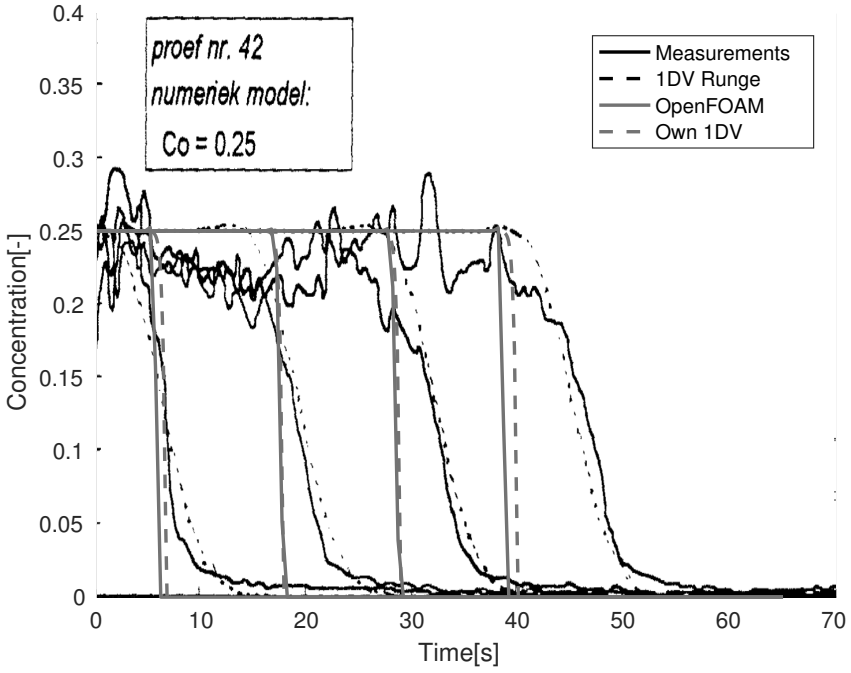

Figure 6.1: Experiment 42 of Runge compared with OpenFOAM and 1DV model, sensors at z = 0.9 m, z = 1.05 m, z = 1.20 m and z = 1.35 m are used, $D_{50} = 270\ \mu m$

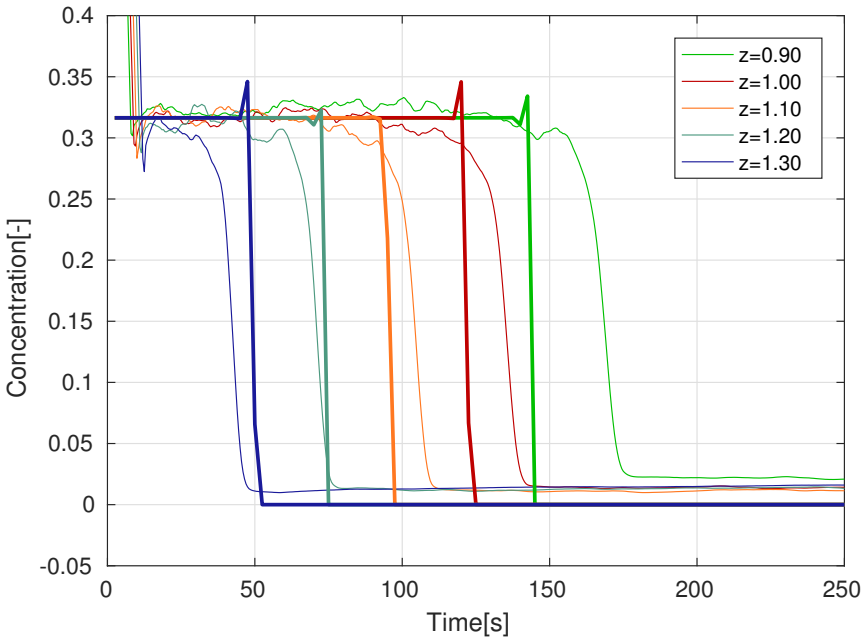

Figure 6.2: Experiment 4 of Van Rhee (thin lines) compared with OpenFOAM (thick lines), $D_{50} = 160\ \mu m$

6.2. Sedimentation validation

6.2.1. The experiments

Reduced sedimentation is validated by comparing the model with the experiments of Van Rhee[49]. In Paragraph 2.2 the experimental procedure is explained. An overview of the experiments is shown in Appendix H. In Figure 2.6 the PSDs of the different sands are shown. The model is compared with the experiments carried out with $D_{50} = 125\mu m$.

6.2.2. Simulations

Table 6.1: Boundary conditions

Patch	Variable	Type	Explanation
inlet	U	powerLawVelocityInlet	explained below
	alpha	fixedValue	
	p_rgh	fixedFluxExtrapolatedPressure	fixedGradient of p_{rgh} making sure ϕ_{HbyA} = 0
	nut	calculated	$\nu_t = C_\mu k^2/\epsilon$
	k	turbulentIntensityKineticEnergyInlet	explained below
	epsilon	turbulentMixingLengthDissipationRateInlet	explained below
outlet	U	inletOutlet	A zeroGradient outflow with fixedValue inflow (in this case U = 0) for the case of reverse flow
	alpha	zeroGradient	
	p_rgh	fixedFluxExtrapolatedPressure	
	nut	calculated	
	k	zeroGradient	
	epsilon	zeroGradient	
ref	U	inletOutlet	
	alpha	zeroGradient	
	p_rgh	fixedValue	p_{rgh} = 0
	nut	calculated	
	k	zeroGradient	
	epsilon	zeroGradient	
bottomWall	U	noSlip	
	alpha	zeroGradient	
	p_rgh	fixedFluxExtrapolatedPressure	
	nut	nutkRoughWallFunction	Equation 5.21
	k	kqRWallFunction	Wrapper around the zeroGradient
	epsilon	epsilonWallFunction	Equations 5.19 and 5.20
topWall	all	see bottomWall	
verticalWall	all	see bottomWall	
frontAndBack	all	empty	

It was decided to do these simulations in 2D. In 3D, there would be less turbulence, causing a diffusion coefficient which is lower. Nevertheless, the simulations are done in 2D. In 2D, the calculation time can already be more than an hour. In 3D, the calculation time would simply become too long.
The moving mesh is not able to cope with a non-orthogonal mesh. Therefore, it is not possible to make

a mesh with a diffuser. Instead, it was chosen to use a rectangular mesh over the whole length with dimensions 4.000 x 0.288 m. The number of cells was 160 x 80. In Appendix G, an error analysis is shown to check the influence of changes in the mesh, tolerance and time step.
Due to the turn and the butterfly valve, it can be assumed that the concentration at the inlet is uniform over the height.
In `OpenFOAM` it is necessary to select a point which determines the reference pressure. In `fvSolutions` a `pRefPoint` and `pRefValue` can be given. Unfortunately, this function doesn't work anymore in the newest version of `driftFluxFoam`. Another option is using the outlet as a reference. Several boundary conditions have specially been made for this purpose, but these also give problems. Therefore, an extra patch was added exactly in the middle of the outlet. This `ref` patch consists only of one face and is situated at z=0.144 m.

powerLawVelocityInlet
For the velocity at the inlet, the boundary condition `powerLawVelocityInlet` was used and adjusted for this purpose. The formula behind this BC is:

$$\frac{u_{local}}{u_{pipeaxis}} = \left(1 - \frac{r}{R}\right)^{\frac{1}{n}} \tag{6.2}$$

n depends on the Reynolds number. A frequently used value for n is 7 and is applicable for a wide range. This value is also used during the simulations.
Every simulation started with a high velocity at the inlet. After 4 seconds the velocity was lowered to its final velocity. The changing of the velocity was chosen to take 1 second, so at t = 5s the final velocity was reached.

turbulentIntensityKineticEnergyInlet
For the turbulent kinetic energy, k, the `turbulentIntensityKineticEnergyInlet` was used. The standard `turbulentIntensityKineticEnergyInlet` however uses the local velocity to calculate the local k. In the middle, the velocity is high which creates a high k and at the wall the velocity is low which creates a low k. In reality, it is the other way around: a high k at the wall and a low k in the middle. Therefore, the `turbulentIntensityKineticEnergyInlet` was adjusted. The new `turbulentIntensityKineticEnergyInlet` uses the average velocity instead of the local velocity. This gives a uniform profile of the k over the height. This is still not correct, but it is better than the standard `turbulentIntensityKineticEnergyInlet`. Now the following formula is used for k at the inlet:

$$k = 1.5 \cdot I \cdot U_{avg}^2 \tag{6.3}$$

I is the turbulence intensity. Russo & Basse [55] did simulations in ANSYS CFX to determine the turbulence intensity in a pipe. The simulations were done for water at 20 degrees Celsius. Boundary conditions for a smooth wall were used. The range of the simulations was $7 \cdot 10^5 < Re < 4 \cdot 10^7$. At the pipe axis the following relation was found for the turbulence intensity:

$$I_{pipeaxis} = 0.0853 Re^{-0.0727} \tag{6.4}$$

And for the average over the cross-sectional area:

$$I_{average} = 0.140 Re^{-0.0790} \tag{6.5}$$

Basse[5] also used experiments of the Princeton Superpipe to determine a relation for the turbulence intensity for both rough and smooth pipes. Experiments were carried out in the range of $8 \cdot 10^4 < Re < 6 \cdot 10^6$ for smooth wall:

$$I_{pipeaxis} = 0.0550 Re^{-0.0407} \tag{6.6}$$

And for the average over the cross-sectional area:

$$I_{average} = 0.317Re^{-0.110} \tag{6.7}$$

Also four experiments were carried out with a rough pipe. The turbulence intensity was about 10% higher than in a smooth pipe.

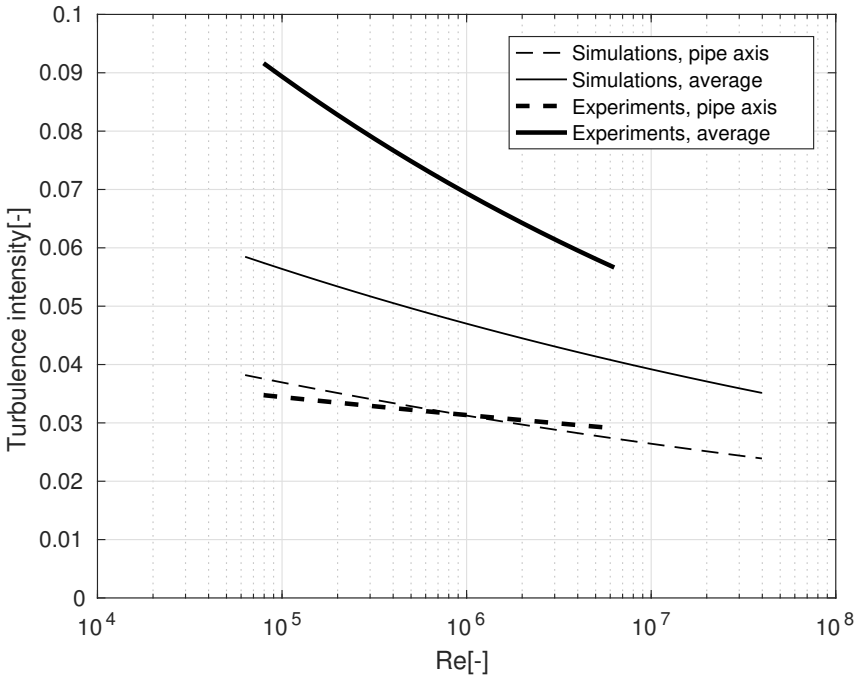

Figure 6.3: Turbulence intensity versus the Reynolds number in a smooth pipe

In the erosion experiments, a channel with dimensions 0.088 x 0.288m and velocities in the range of 0.5 - 1.5 m/s were used.

$$d_h = \frac{2hb}{h+b} = \frac{2 \cdot 0.288 \cdot 0.088}{0.288 + 0.088} = 0.135m \tag{6.8}$$

$$\begin{aligned} U = 0.5m/s \quad &\rightarrow \quad Re = \frac{Ud_h}{\nu} = 6.8 \cdot 10^4 \\ U = 1.5m/s \quad &\rightarrow \quad Re = \frac{Ud_h}{\nu} = 2.0 \cdot 10^5 \end{aligned} \tag{6.9}$$

Looking to Figure 6.3, an average turbulence intensity over the cross-sectional area of 0.07 can be assumed.

turbulentMixingLengthDissipationRateInlet
The dissipation of turbulent kinetic energy, ϵ, at the inlet is determined by the boundary condition `turbulentMixingLengthDissipationRateInlet`. This BC uses the formula:

$$\epsilon_{local} = \frac{C_\mu^{0.75} k_{local}^{1.5}}{d_h} \tag{6.10}$$

C_μ is 0.09 and d_h is 0.135 m.

Results
Exactly the same velocities and concentrations were used as during the measurements of Van Rhee. These values can be found in Appendix H. In `OpenFOAM`, the mass of the bed can easily be determined. The mass of the bed is used to calculate the mean bed height and sedimentation velocity. The results

are shown in Figure 6.4. For the validation with a concentration of 5%, 4 extra simulations were done. These extra simulations were done to see when the sedimentation velocity would become zero for a concentration of 5% in `OpenFOAM`.

The simulations very much follow the same trend as the experiments. It can be concluded that the simulation of reduced sedimentation satisfies the expected accuracy.

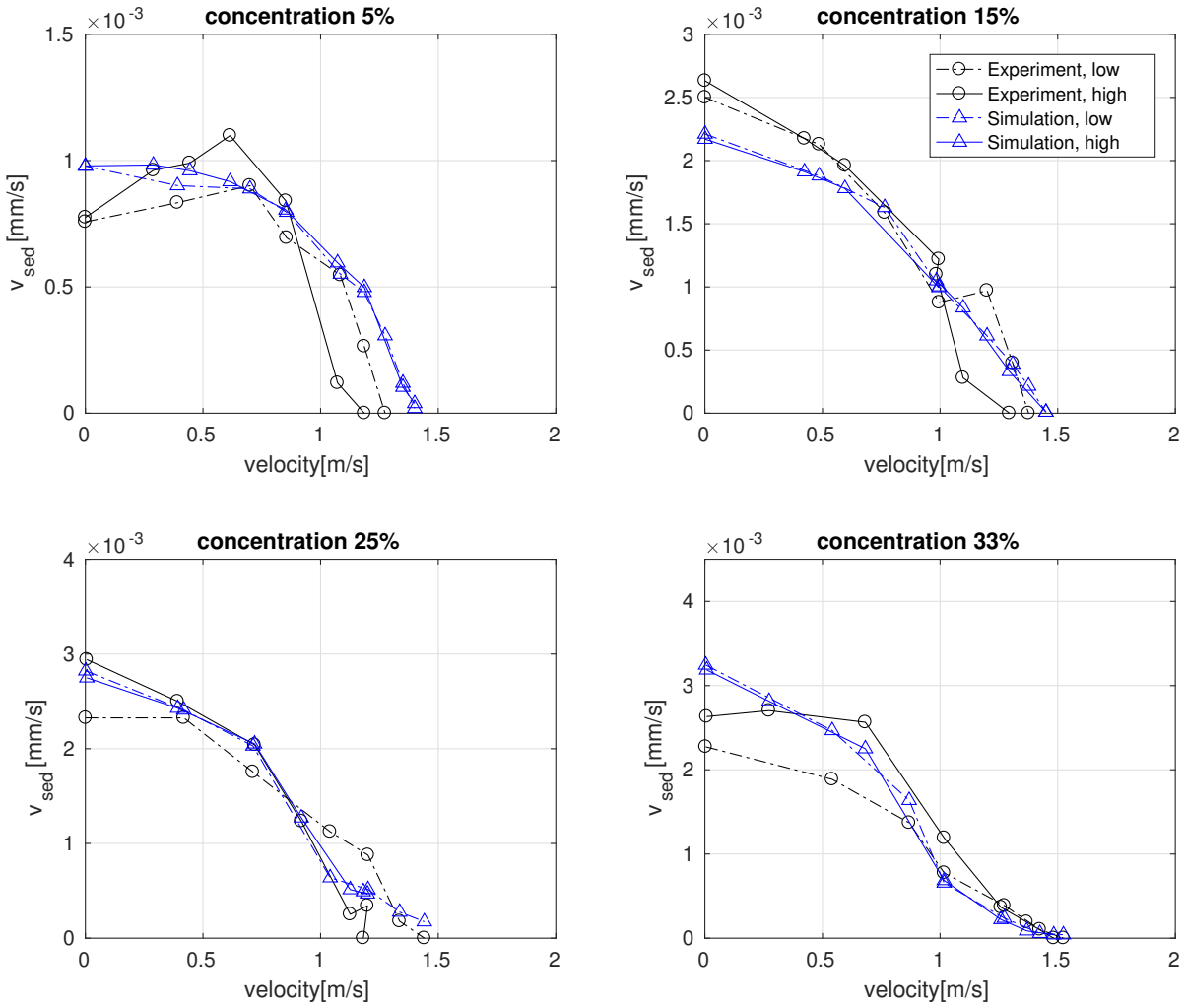

Figure 6.4: Flow velocity versus sedimentation velocity for different concentrations

6.3. Hopper validation

Figure 6.5 shows the mesh and Table 6.2 the corresponding boundary conditions. In Appendix I an analysis is shown to make sure no errors were caused by the settings of the time step, the tolerance of the pressure and the mesh.

As can be seen in Figure 6.5 the outlet consists of three faces. The face in the middle of the outlet is the pressure reference and is in Table 6.2 denoted as `ref`. The other two faces are called `outlet`.

The water surface is a rigid lid and cannot move. Obviously, it would be better if the water surface could move. Normally, the water level is below the overflow level before the loading starts. With this fixed rigid lid, this cannot be simulated. The moving of the water surface has to be added by Damen itself. For the time being, the height of the overflow is calculated with this formula (Hager[28]):

$$h_{water} - h_{overflow} = \left(\frac{q}{0.59\sqrt{g}} \right)^{\frac{2}{3}} \tag{6.11}$$

In which q is the flow rate per unit width.

Van Rhee[49] did measurements in a model hopper with dimensions 12 x 2.25 x 3.08 m(L x H x B). In addition, measurements were done in the TSHD called 'Cornelia'. The hopper of the Cornelia is 52 meters long, 11.5 meter wide and has a volume of 5000 m^3. The hopper, however, has a typical silo shape. The model can only handle rectangular domains, so a height of 5000/(52*11.5)=8.36 m is used.

The measurement at the Cornelia was done in the end of August 2001 near IJmuiden. At the end of August, the surface temperature of the seawater near IJmuiden is fluctuating between 18 and 20 degrees due to the tide and the weather. While dredging, sand is excavated at the seabed. Temperature of the water at the seabed is a bit lower and can be estimated to be between 16 and 18 degrees.
The settling velocities in Table 6.3 are determined by the iterative process with $\Psi = 0.7$. After a couple of simulations, it appeared that the settling velocities calculated by Ferguson & Church resulted in too large sedimentation velocities. Using the settling velocities calculated with the iterative method gave better agreement with the measurements. Also by using Garside instead of Rowe, the results improved.

Table 6.2: Boundary conditions of the hopper simulations

Patch	**Variable**	**Type**
inlet	U	fixedValue
	alpha	fixedValue
	p_rgh	fixedFluxExtrapolatedPressure
	nut	calculated
	k	turbulentIntensityKineticEnergyInlet
	epsilon	turbulentMixingLengthDissipationRateInlet
outlet	U	inletOutlet
	alpha	zeroGradient
	p_rgh	fixedFluxExtrapolatedPressure
	nut	calculated
	k	zeroGradient
	epsilon	zeroGradient
ref	U	inletOutlet
	alpha	zeroGradient
	p_rgh	fixedValue
	nut	calculated
	k	zeroGradient
	epsilon	zeroGradient
topWall	U	slip
	alpha	zeroGradient
	p_rgh	fixedFluxExtrapolatedPressure
	nut	calculated
	k	zeroGradient
	epsilon	zeroGradient
bottomWall	U	noSlip
	alpha	zeroGradient
	p_rgh	fixedFluxExtrapolatedPressure
	nut	nutkRoughWallFunction
	k	kqRWallFunction
	epsilon	epsilonWallFunction
verticalWall	all	see bottomWall
frontAndBack	all	empty

Table 6.3: Overview of the experiments of Van Rhee

Test	4	5	6	8	Cornelia
$Q_{mean}[m^3/s]$	0.100	0.099	0.137	0.075	6
α_{mean}[-]	0.26	0.21	0.27	0.30	0.175
α_{max}[-]	0.54	0.54	0.54	0.54	0.54
Water level at start$[m]$	1.25	1.25	1.25	1.25	
Bed level at start$[m]$	0.20	0.14	0.18		
$h_{overflow}[m]$	0.0676	0.0671	0.0834	0.0568	0.430
$D_{50}[\mu m]$	147	102	107	103	235
T$[^oC]$	16	16	16	16	16-18
$\nu_w[10^{-6}m^2/s]$	1.11	1.11	1.11	1.11	1.11-1.05
$rho_w[kg/m^3]$	998	998	998	998	1021
$w_0[mm/s]$	10.49	5.90	6.49	6.01	22.99-23.91

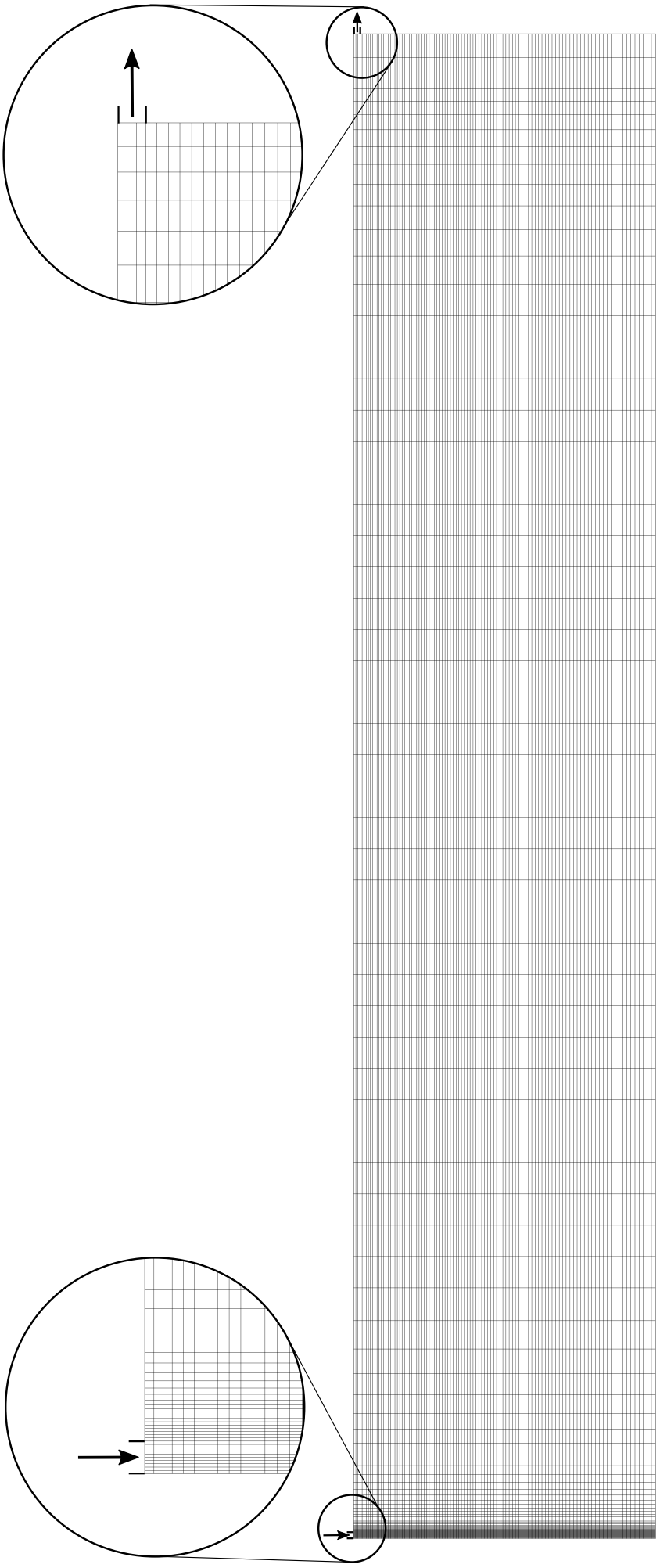

Figure 6.5: 100 x 60 mesh (12 x 2.33 m) with 20 cells in the refined section near the inlet

6.3.1. Velocity

The horizontal velocities during Test 8 are shown in Figures 6.6 and 6.7. Van Rhee used an electromagnetic velocity meter (EMS) to measure the horizontal velocity. At the beginning of the experiment the EMS was placed 30 cm from the bottom of the hopper (z = 0.30 m). Once the probe was buried, it would be relocated by 20 cm in vertical direction. This was done several times. Both in Figure 6.6 and Figure 6.7, the top graph shows the vertical position as a function of time. The bottom graph shows the horizontal velocity.
At the beginning and the end of the loading process, the highest velocities in the density current were measured. At the beginning of the experiment, the particle concentration in the hopper was low, causing the density difference between the incoming mixture and its surroundings to be high. The incoming mixture was therefore accelerated causing large velocities in the density current.
After some minutes, the concentration and density in the hopper had risen. This reduced the velocity of the negatively buoyant jet and the density current.
At the end of the experiment, the velocity in the density current rose again due to the decreasing cross-sectional area above the bed.

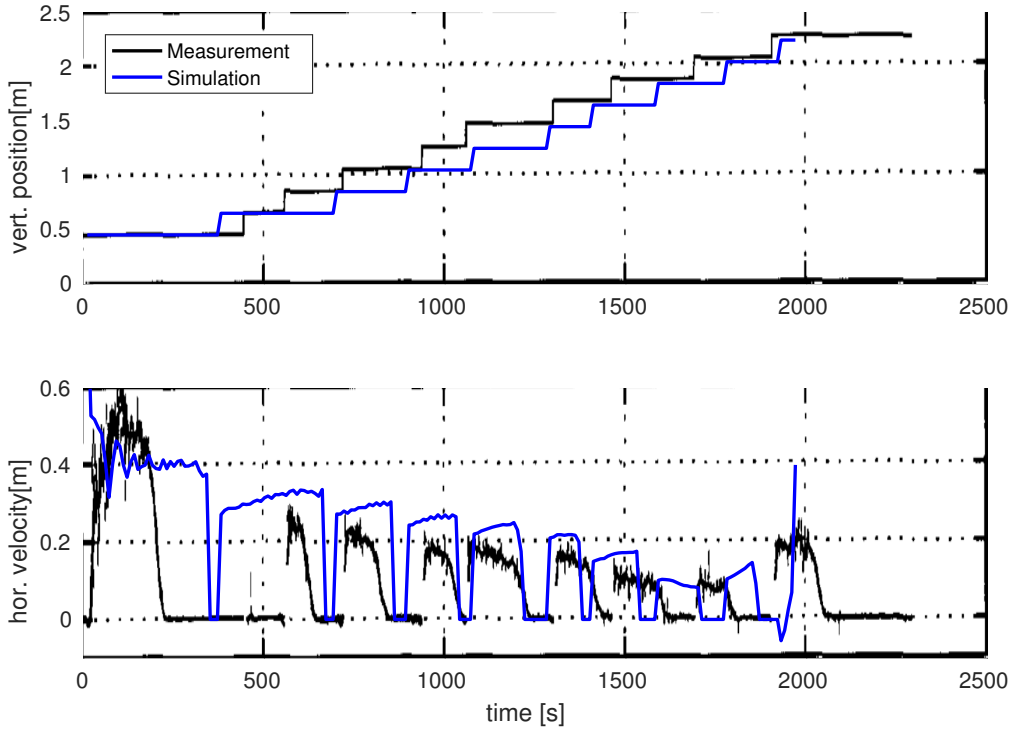

Figure 6.6: Horizontal velocity measured by EMS 1 during Test 8 (x = 3 m)

In the simulations, the velocities are a bit too high, but the trend is clearly similar. Causes for the higher velocities could be:

1. Water bubbles near the inlet due to the plunging of the mixture into the water. These water bubbles could reduce the density of the jet under the inlet causing the velocities to be lower.
2. During the validation of his model, Van Rhee encountered problems with jets. For the standard k-ϵ model, the spreading rate was too small resulting in larger velocities than the velocities in the experiments of Rodi[53]. This could also be the case in `OpenFOAM`. The 'realizable k-ϵ model' is developed to simulate flows with high shear rates, for example jets[57]. The jet was simulated with both the standard and realizable k-ϵ model. This is shown in Figure 6.8. The realizable k-ϵ model resulted, however, in higher velocities.

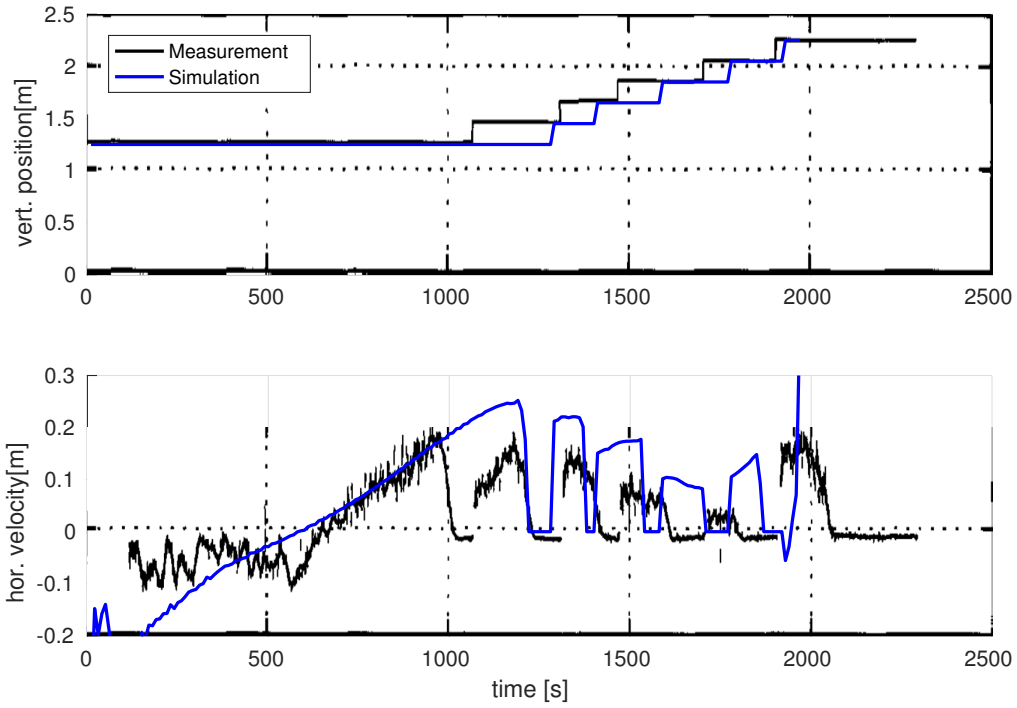

Figure 6.7: Horizontal velocity measured by EMS 2 during Test 8 (x = 3 m)

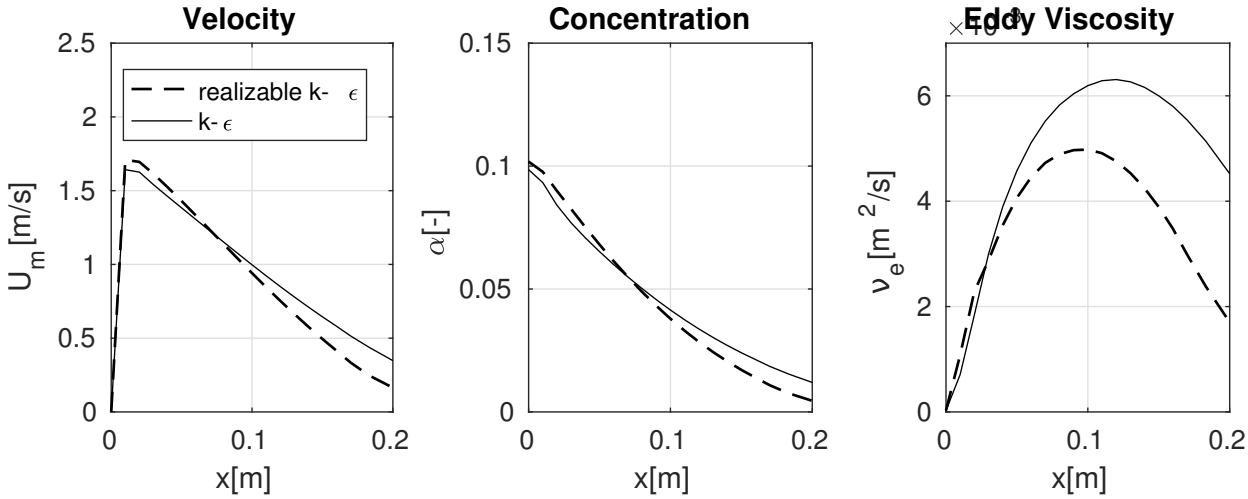

Figure 6.8: Different turbulence models at the inlet (z = 0.5 m, t = 50 s)

6.3.2. Concentration

During the tests, Van Rhee did measurements of the concentration over the height. In Figure 6.9, this is compared with the simulations.
At t = 640 s, t = 840 s and t = 1040 s, the concentration is a lot lower during the simulation. This is mainly caused by its high sedimentation velocity; the particles that are sedimented in the simulation, are still in solution in the measurement. The high sedimentation velocity during the simulation could be explained by a higher settling velocity, a lower erosion flux or a higher porosity.

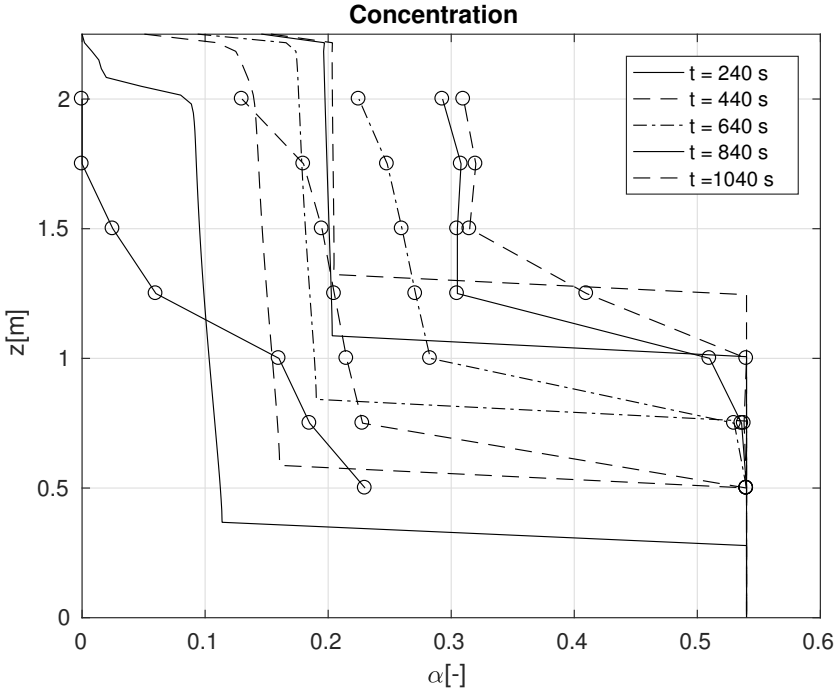

Figure 6.9: Measurements (circles) and simulation (lines) of the concentrations at x = 6 m (Test 6)

At t = 240 s, it can be seen that the sediment is more uniformly divided over the height of the hopper. This is partly caused by the fact that the model calculates with only one fraction. Calculating with multiple fractions would give more grading over the concentration profile. Van Rhee used multiple fractions in his computations. Nonetheless, he also encountered a profile which is too uniform. This shows that the modelling with a single fraction is not the only cause.
Probably, the ratio between the upward transport (by turbulent diffusion and the circulatory flow) and downward transport (by settling) is too large. Several causes could be thought of. Each possible cause was investigated. Unfortunately, without satisfactory results:

1. In Section 6.3.1, it was described that the velocities in the simulations are slightly higher than in during the tests of Van Rhee. These higher velocities could cause more transport of sediment over the height. To decrease the velocities, a second inlet was created just above the bed in the scour hole. Half of the sediment entered the hopper via the inlet at the top, and the other half entered via the inlet at the scour hole. The velocities in the density current decreased, but the mixing of sediment did not.

2. Figure 6.8 shows that the standard k-ϵ model results in a higher eddy viscosity than the realizable k-ϵ model. In Figure 6.10, a simulation with the realizable k-ϵ model is shown. Barely any difference can be observed when this figure is compared with Figure 6.9.

3. The turbulent diffusion coefficient Γ_t equals $\frac{\nu_t}{\sigma}$ in which ν_t is the eddy viscosity and σ the Schmidt number. In Figure 6.8, a Schmidt number of 1 was used. Schmidt numbers of different studies vary between 0.2 to 1.3 (Tominaga[61]). The influence of a higher Schmidt number was inves-

tigated by running the simulation with Schmidt numbers of up until 2; this didn't improve the results.

4. In Appendix A, the influence of the constant $c_{3\epsilon}$ of the k-ϵ model is described. In the simulation of Figure 6.9, a value of 1 was used for horizontal flow. A value of zero was tried, but this did not result in an improved concentration profile.

5. The hindered settling was calculated by the iterative method and Garside. This gives a rather low settling velocity. The iterative method in combination with Garside was chosen to make sure the sedimentation velocity would not become too high. This high sedimentation velocities could also be caused by an erosion flux which is too low. Increasing both the hindered settling and erosion flux could improve the concentration profile.
   To test this, a simulation was done with settling velocities calculated with Ferguson & Church. To compensate for the higher settling velocities, the pickup flux was doubled. The sediment was still distributed too uniformly.

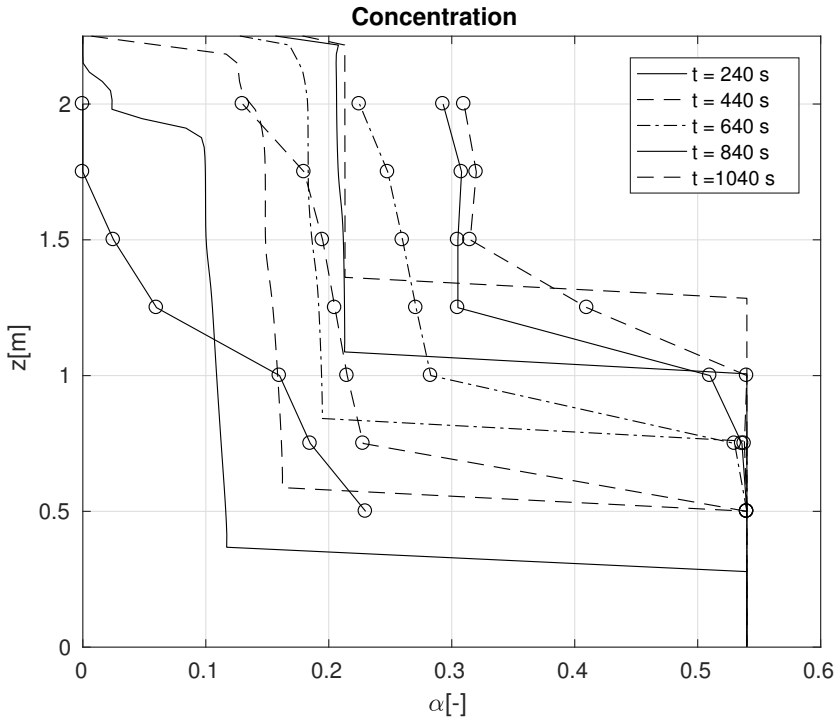

Figure 6.10: Measurements (circles) and simulation (lines) of the concentration at x = 6 m with realizable k-ϵ (Test 6)

6.3.3. Overflow loss

The overflow losses of Test 4, 5, 6, 8 and the Cornelia are shown in Figures 6.11 to 6.16. The cumulative overflow losses are defined as:

$$OV_{cum} = \frac{\int_0^t \alpha_{out}(t) Q_{out}(t)}{\int_0^t \alpha_{in}(t) Q_{in}(t)} \tag{6.12}$$

And the overflow flux is defined as:

$$OV_{flux} = \frac{\alpha_{out}(t) Q_{out}(t)}{\alpha_{in}(t) Q_{in}(t)} \tag{6.13}$$

In Figure 6.12 the hopper load is used. The hopper load in this case is defined as the total volume of grains (without pore volume) inside the hopper per unit width, which is equal to the sum of the settled sand and the amount of sand still in suspension.

For Test 4, the simulation resembles the measurement very well. This is against every expectation. Since only the D_{50} is simulated, it could be expected that the overflow losses would be lower. With multiple fractions, the smaller fractions are pushed upwards. These smaller fractions then cause the overflow losses to be higher than a simulation with a single fraction.
The overflow losses during the simulations of Test 5, 6, 8 and the Cornelia are as expected. The overflow losses of these simulations are lower than the measurements.
At the end of simulations 6 and 8, an interesting phenomenon can be observed: a sudden drop in the outflow concentration. This is due to the clean layer of water which is pushed out at these moments.

Multifraction Drift Flux solver
At this moment, `driftFluxFoam` can only calculate with one particle fraction. In summer 2018, `OpenFOAM` will release a version of the `driftFluxFoam` solver which will be able to calculate with multiple fractions. This solver is being developed in collaboration with Frans Van Grunsven of the TU Delft. When this solver is available, the code developed during this thesis can be implemented in that solver.

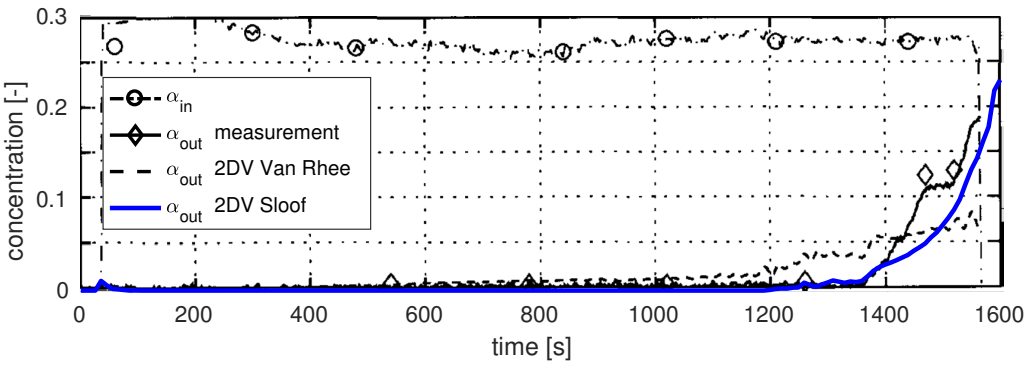

Figure 6.11: Measured and computed concentrations (Test 4)

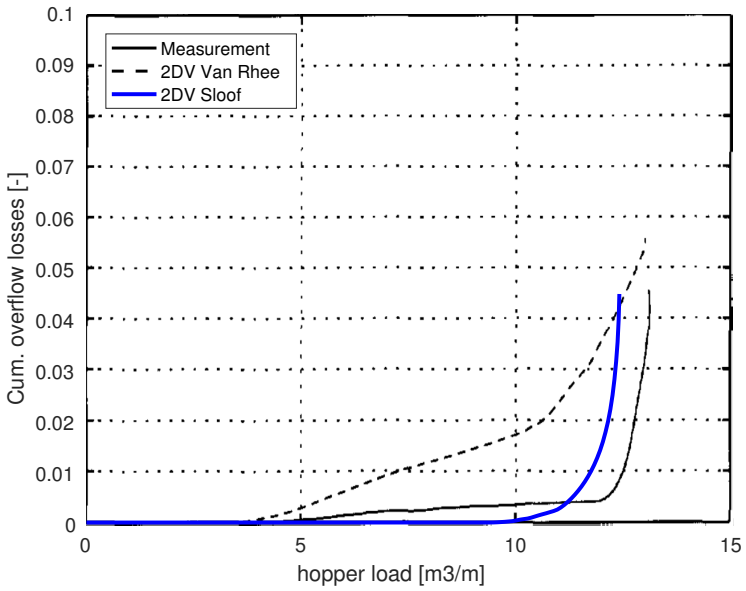

Figure 6.12: Cumulative overflow losses vs. hopper load (Test 4)

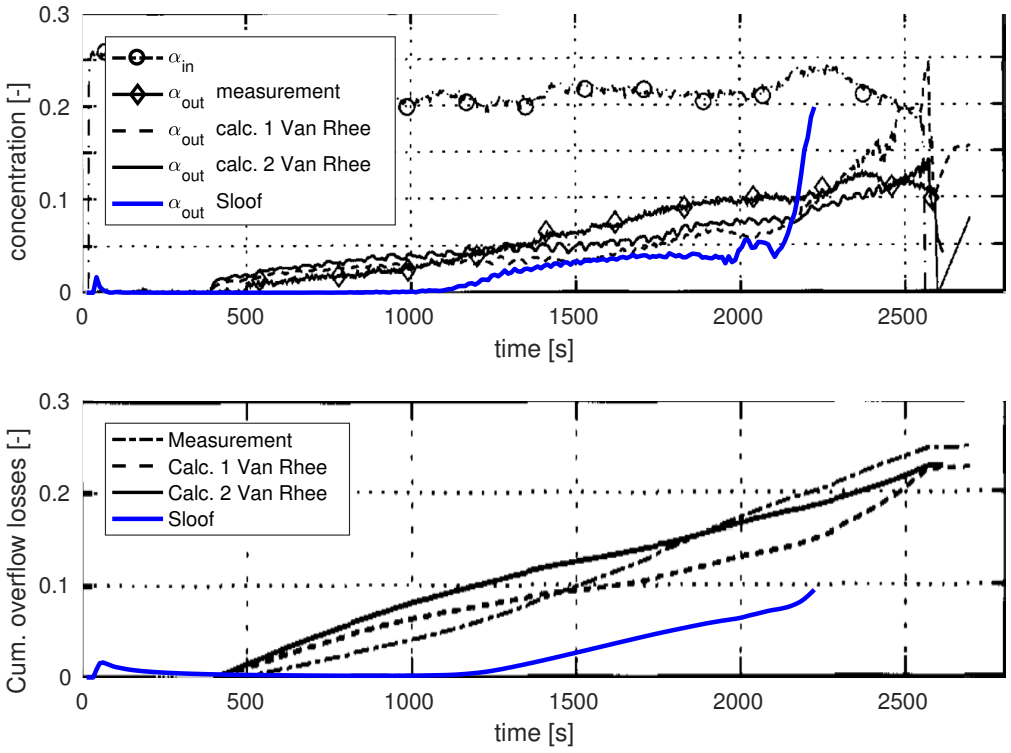

Figure 6.13: Concentrations and cumulative overflow losses (Test 5)

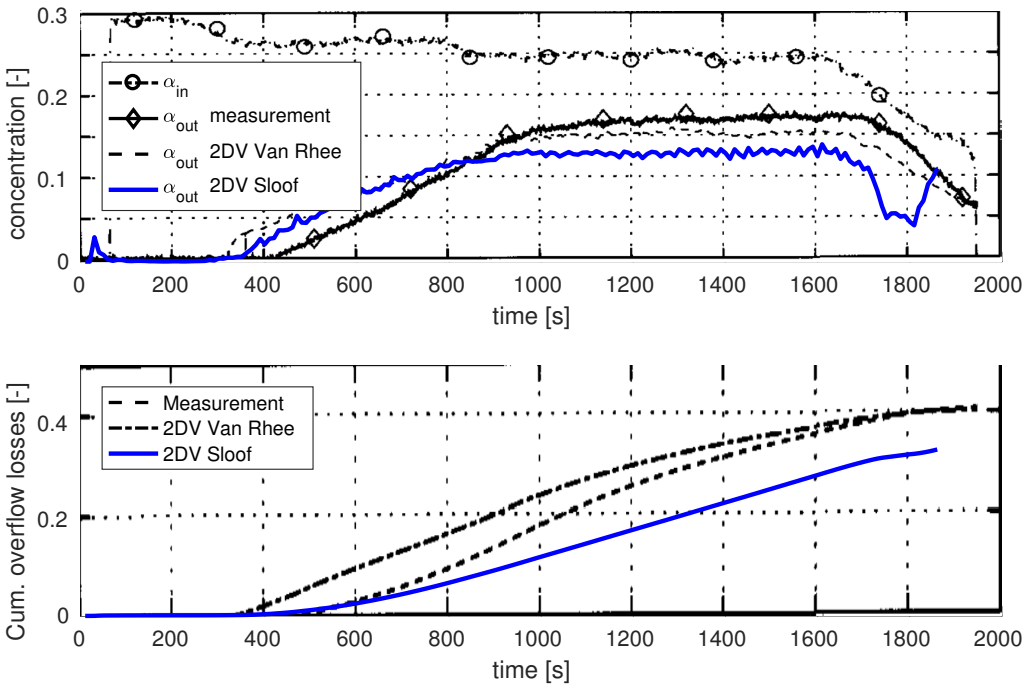

Figure 6.14: Concentrations and cumulative overflow losses (Test 6)

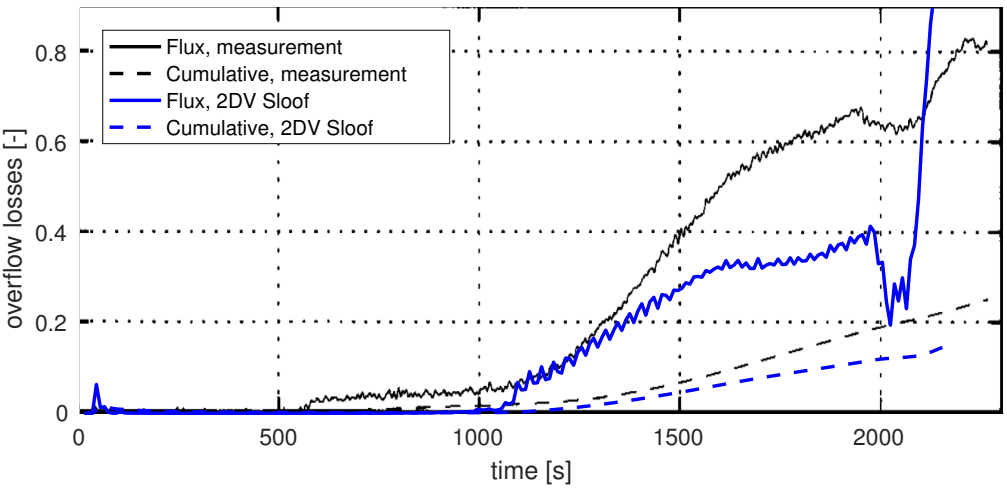

Figure 6.15: Overflow fluxes and cumulative overflow losses (Test 8)

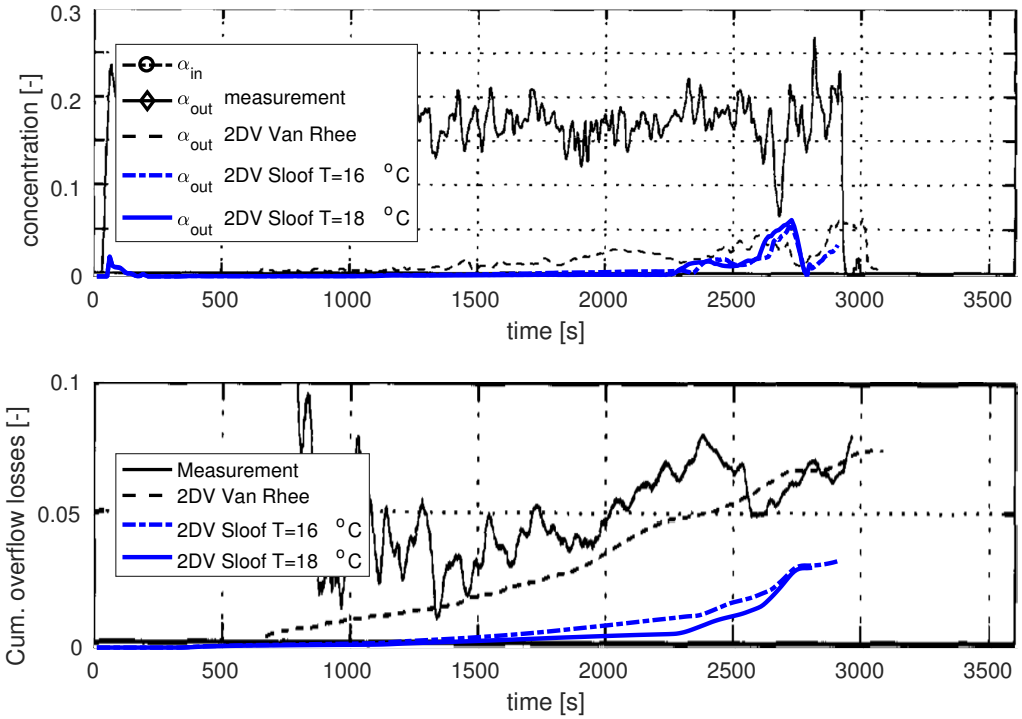

Figure 6.16: Concentrations and cumulative overflow losses for the Cornelia

7

Observations

In the previous chapter, it was described how the 2DV model was developed. This 2DV model gives a deeper insight in the phenomena in the hopper. In this chapter, these observations are described.

7.1. Flow Pattern

Figure 7.1 shows the flow pattern at the beginning of Test 8, which was simulated with the 2DV model of this thesis. Van Rhee described the flow in the hopper by means of Figure 1.4. This is very similar compared to the flow pattern in Figure 7.1.
At the end of the loading cycle, the flow pattern changed. This is shown in Figure 7.2.

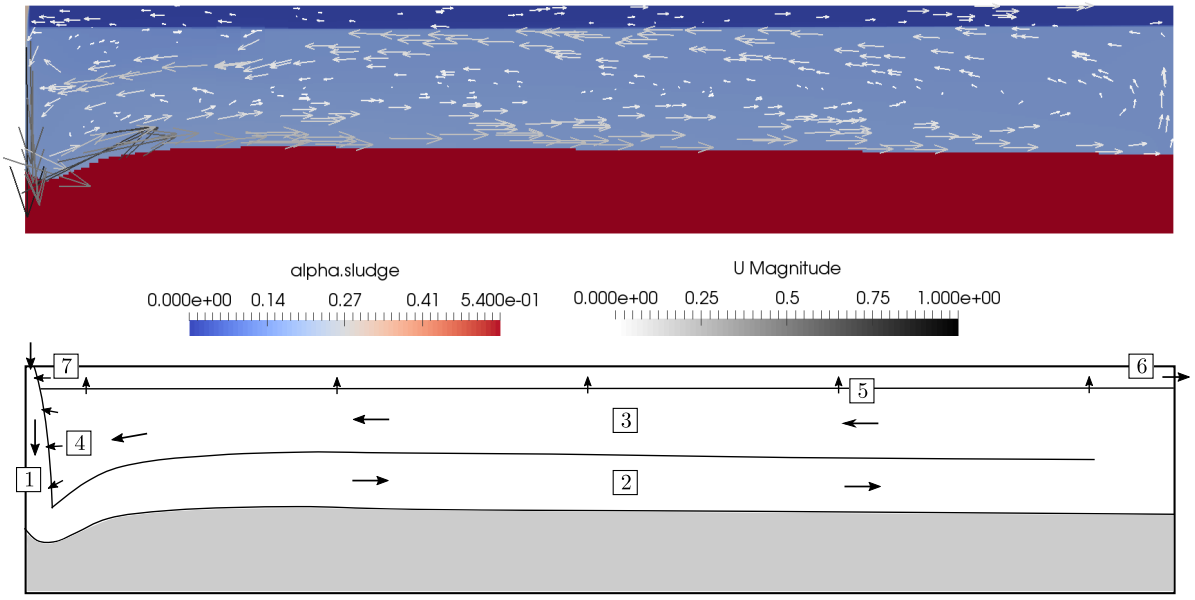

Figure 7.1: Simulation Test 8 (t = 800 s) and schematized overview.

In zone 1, a buoyant jet can be found. Subsequently, the mixture flows as a density current over the bed (zone 2). Above the density current, a return current can be observed (zone 3). The mixture of the return current is entrained into the buoyant jet in zone 4. At the top of the hopper, a relatively clean layer of water is present. Particles settling down are causing the water to flow upwards. This

water and the smaller particles of the Particle Size Distribution are pushed into the top layer over the whole length of the hopper, depicted by number 5. Since the PSD was not taken into account during the simulation, the concentration in the top layer was 0%. In reality, this will be a concentration of a few percent.
Part of this relatively clean water in the top layer is entrained in the jet (number 7). The remaining water flows through the overflow (number 6).

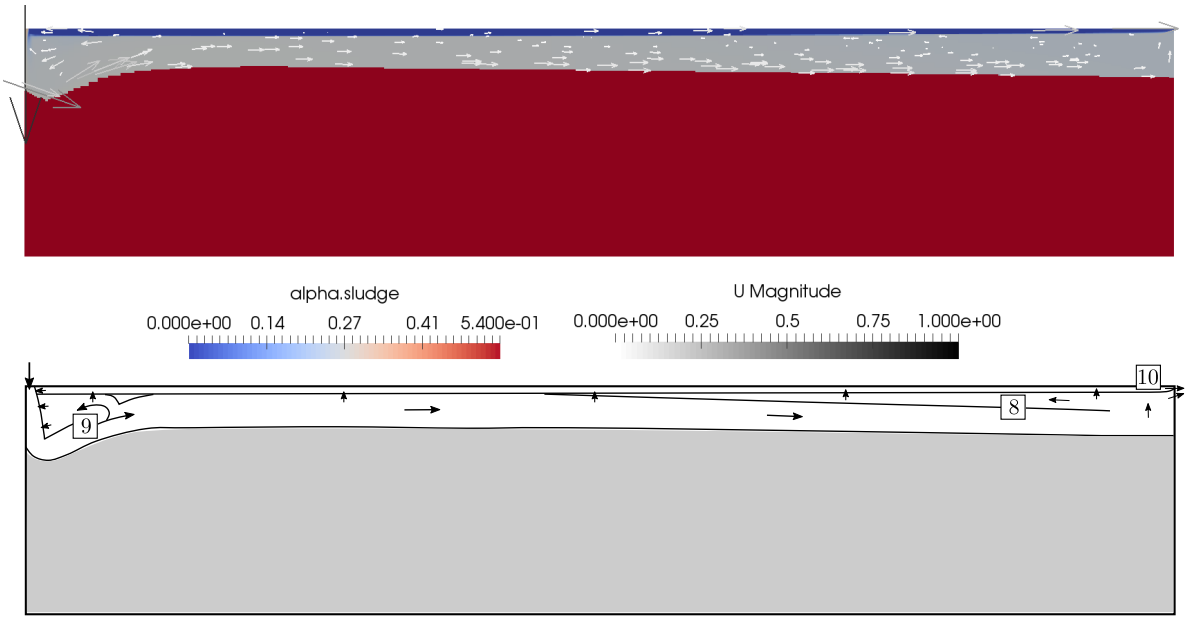

Figure 7.2: Simulation Test 8 (t = 1700 s) and schematized overview.

Approaching the end of the cycle, the flow pattern changes due to the decrease in cross-sectional area. It is hard to give a general description of the flow at the end of the cycle, since it strongly depends on the bed morphology, the settling velocity and flow rate. In many cases, though, the flow is similar to Figure 7.2.
Contrary to Figure 7.1 where a large return current was present, in Figure 7.2 this large return current is not possible due to the small cross-sectional area above the bed. Instead, a small return current is observed in zone 8. The particles in this area settle into the density current. The water is pushed into the top layer.
Part of the mixture coming out of the erosion pit is directly entrained into the jet (number 9). The remaining mixture flows as a density current towards the overflow. At the overflow (number 10), both water from the bottom and top layer are flowing out of the hopper resulting in large overflow losses.

7.2. Eddy viscosity and turbulent diffusion

The eddy viscosity is an important parameter in most hopper models (see Section 4), since the eddy viscosity is a measure for the amount of turbulent diffusion. A better understanding of the eddy viscosity in hoppers is important for future research.
The eddy viscosity during the simulations is shown in Figure 7.3. It was decided to show the eddy viscosity at t = 800 s and t = 1700 s, since the flow pattern at these moments are different. At t = 800 s, a large return current can be observed. At t = 1700 s, the return current is negligible.

In the simulations, both in the bottom and top layer, a parabolic profile for the eddy viscosity can be seen. It is not possible for eddies to travel from the bottom layer to the top layer. Due to the large density gradient, all turbulent energy is destructed at the interface of these layers. Hence, the eddy viscosity and turbulent diffusion is nearly zero at this interface. This in turn, reinforces the concentration

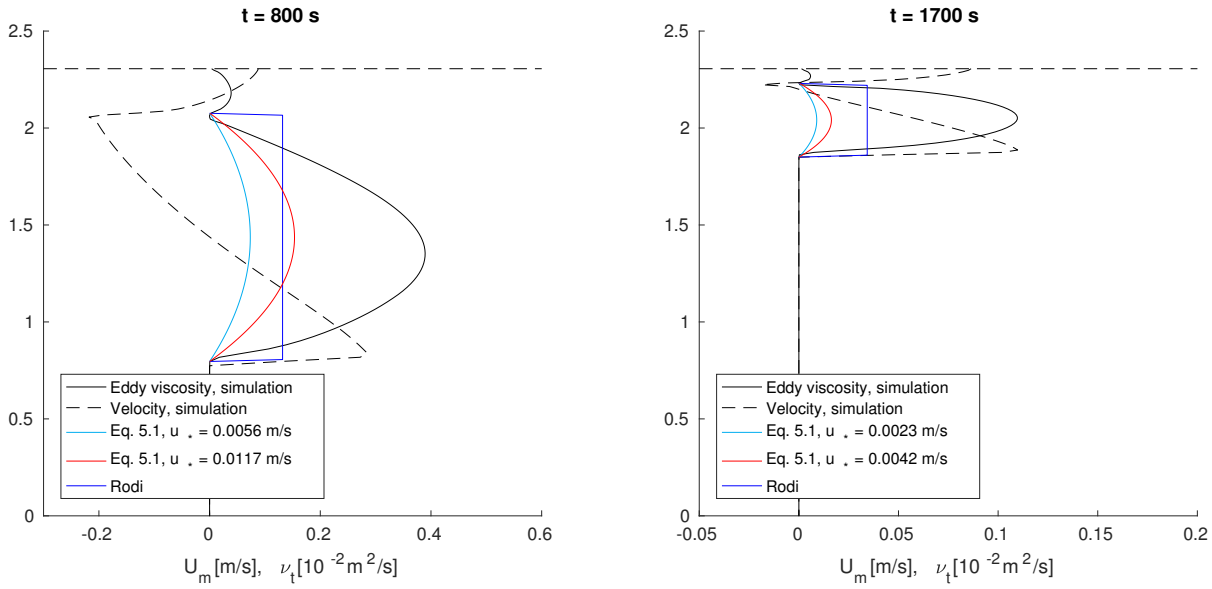

Figure 7.3: Simulation Test 8 (t = 1700 s) and schematized overview.)

gradient.

In open channel flow, the eddy viscosity can be described by the following parabolic profile. It is interesting to check whether the same formula applies to hopper flow.

$$\nu_t = \kappa u_* y \left(1 - \frac{y}{h}\right) \tag{7.1}$$

The shear velocity, u_*, can be calculated with the boundary condition for k (Equation C.12): $u_* = k^{0.5}/C_\mu^{0.25}$. The k at the bottom is available in the simulation. This results in an u_* of 0.0056 m/s and 0.0023 m/s for t=800s and t=1700s, respectively.
The shear velocity can also be calculated with the boundary layer theory for flat plates described by White[64] (Chapter 7.4 of his book) based on Blasius[6]:

$$c_f \approx \frac{0.027}{Re_x^{1/7}} \tag{7.2}$$

This gives shear velocities of 0.0117 m/s and 0.0042 m/s for t=800s and t=1700s, respectively.
Alternatively, the eddy viscosity can be determined by Prandtl's Mixing Length Model:

$$\nu_t = \ell_m^2 \left|\frac{\partial u}{\partial z}\right| \tag{7.3}$$

In which ℓ_m is the mixing length. Rodi[53] proposes $\ell_m = 0.09 h_0$ for density currents, in which h_0 is the height of the density current. At t=800s, h_0 is 0.65 m and at t=1700s h_0 is 0.36 m. It could also be argued to take height of the whole bottom layer for h_0 (1.28 m and 0.38 m, respectively), since eddies can freely travel throughout the whole bottom layer due to the small density gradient in this layer. In Figure 7.3, for h_0 the height of the density current is taken.
In Figure 7.3, it can clearly be seen that the turbulence in a hopper is higher than determined by Equation 7.1 and Rodi[53].

Transport by the circular flow
At t = 800 s the mixture circulates through the hopper. The mixture flows towards the end of the hopper and is transported back by the return current. This mixes the material in the hopper.
A measure for the turbulent diffusive transport in open channel flow is:

$$k_t = O(u_* h) \tag{7.4}$$

In addition, a measure for the advective mixing by circulatory flow can be determined:

$$k_{circ} = O(\frac{h^2}{t}) \tag{7.5}$$

In which t is the time needed for the flow to reach the end of the hopper: $t = L/U$. Dividing Equation 7.5 by Equation 7.4 gives an idea about the amount of mixing contributed by the circulatory flow:

$$\frac{k_{circ}}{k_t} \approx \frac{\frac{h^2 U}{L}}{u_* h} = \frac{Uh}{u_* L} = \frac{0.29 \cdot 1.28}{0.0117 \cdot 12} = 2.6 \tag{7.6}$$

The mixing due to the circulatory flow at t = 800 s is approximately 2.6 times as big as the turbulent mixing in case of open channel flow. Note that in the hopper the eddy viscosity is higher than for open channel flow. It can be concluded that the circulatory flow and the turbulent diffusion have approximately the same contribution to the mixing in a hopper.
This also explains why there is still perfect mixing at t = 1700 s. At t = 1700 s there is no circulatory flow anymore, but the turbulence is strong enough to maintain perfect mixing.

7.3. Top layer

For the change of the overflow losses over time, the behaviour of the top layer is determining. In Figure 7.4, both for the simulation and the measurement, clearly, three phases can be distinguished. The transition between these 3 phases is completely determined by the physics of the top layer:

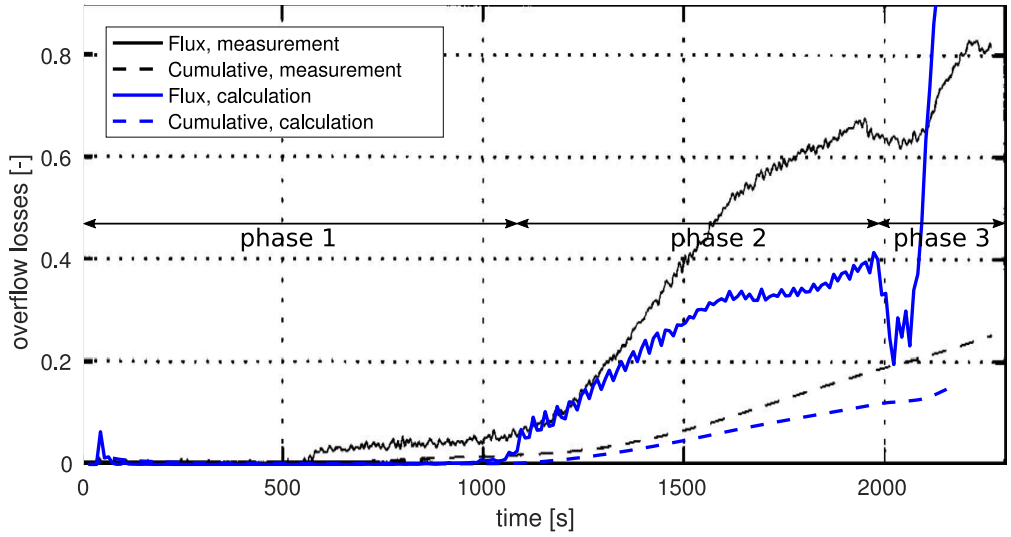

Figure 7.4: Overflow fluxes and cumulative overflow losses (Test 8)

- Phase 1: During Phase 1, the concentration gradient between the top and bottom layer is below the overflow height. This can also bee seen in Figure 7.5 when looking to the concentration profile of t = 800s. Since the top layer has a larger thickness than the overflow, only water from the top layer flows through the overflow. The overflow concentration equals the concentration of the top layer.
- Phase 2: The concentration gradient is at the overflow height (Figure 7.5). Both water from the bottom and top layer flows through the overflow.
- Phase 3: Due to the decrease in cross-sectional area, the layered structure becomes unstable and dissolves.

The rest of this paragraph will take a closer look at these phases.

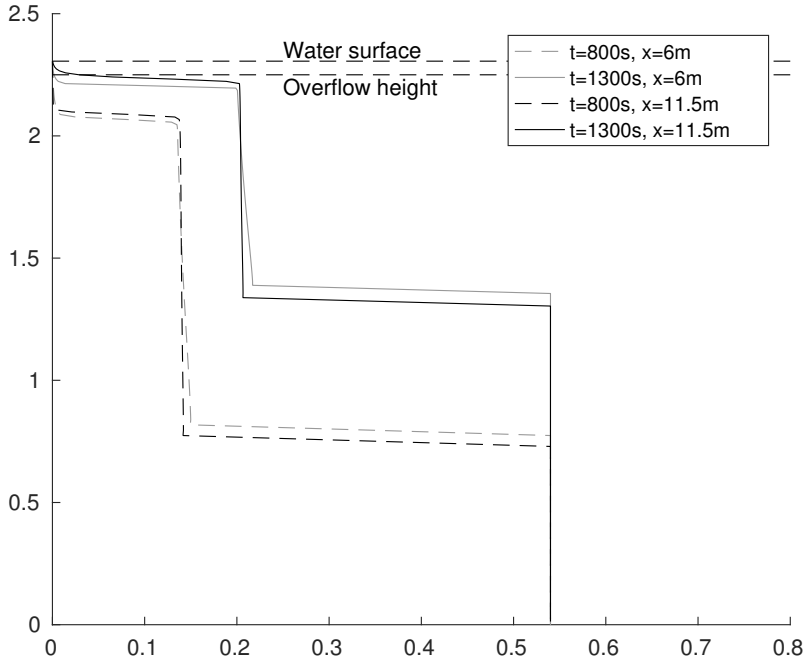

Figure 7.5: Concentration over the height (Test 8)

7.3.1. Phase 1

During Phase 1, the interface between the top and bottom layer is below the overflow height. The vertical velocity of the interface w_i equals the vertical velocity of the particles at (or just under) the interface: w_d. An equation for w_d can be derived.

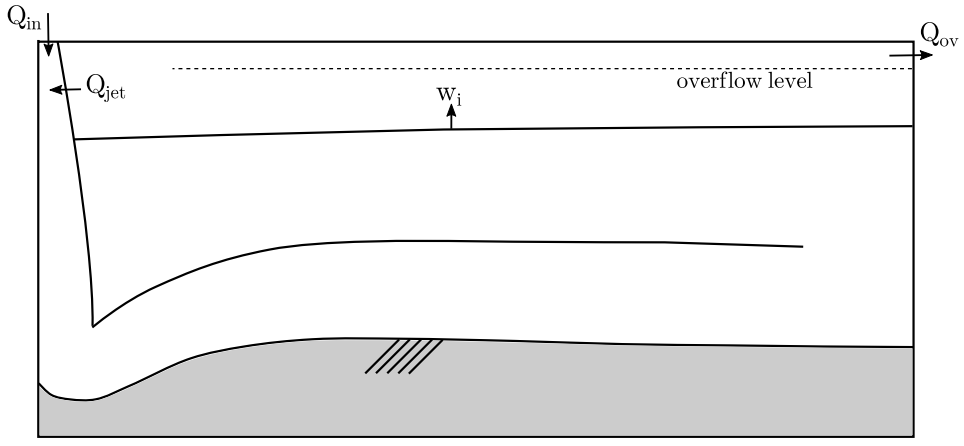

Figure 7.6: Schematic overview Phase 1.

The mixture flux velocity in z-direction (Equation 3.20) is:

$$j_z = (1 - \alpha_d)w_f + \alpha_d w_d \tag{7.7}$$

In which w_f is the velocity of the water fraction and w_d the velocity of the dispersed phase, i.e. the sand particles. At the interface, the upward volume flux is $Q_{in} + Q_{jet}$. Therefore:

$$j_z = \frac{Q_{in} + Q_{jet}}{WL} \tag{7.8}$$

Where W and L are the width and length of the hopper. The slip velocity can be calculated with:

$$w_f - w_d = -w_0 \left(1 - \alpha_d\right)^{n-1} \tag{7.9}$$

In which w_0 is negative, since the terminal settling of a particle in a quiescent fluid is downward. The water velocity w_f (Equation 7.9) and the mixture flux velocity (Equation 7.8) can be substituted in Equation 7.7. From this follows:

$$w_i = w_d = \frac{Q_{in} + Q_{jet}}{WL} + (1 - \alpha_d) w_0 \left(1 - \alpha_d\right)^{n-1} \tag{7.10}$$

The relations of Yannopoulos[67] could have been used to estimate Q_{jet}, but these calculated flow rates did not appear to be realistic when being compared with the simulations. A rough estimate was made by looking to the velocities in the simulations:

$$Q_{jet} = 0.1 U_{in} W h_t \tag{7.11}$$

In which U_{in} is the velocity of the mixture entering the hopper and h_t is the thickness of the top layer. Equation 7.11 has an accuracy of approximately $\pm$ 50%. More research is needed to find a better estimate of Q_{jet}.

Equation 7.10 gives a lot of insight into the course of the overflow losses over time. In test 4 (Figure 6.11) for instance, w_i is very small due to a relatively large particle size. Hence, Phase 1 is present throughout almost the whole loading cycle. At t = 1400 s, the interface has not yet reached the overflow height, but the interface is already becoming unstable and Phase 3 has started. This explains why Phase 2 is not present in Test 4.

7.3.2. Phase 2

In Phase 2, the interface is at the overflow height. In Figure 7.7, it can be seen that part of the water going through the overflow comes from the top layer: $Q_{ov,t}$. The remaining water comes from the bottom layer: $Q_{ov,b}$. Equations for these flow rates can be derived.

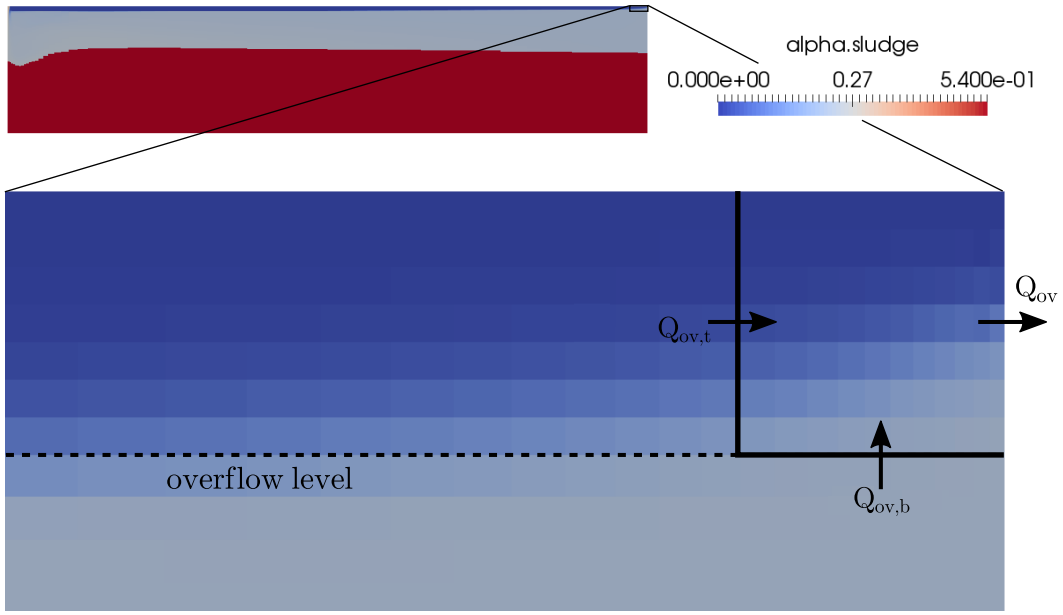

Figure 7.7: Concentration near the overflow (Test 8).

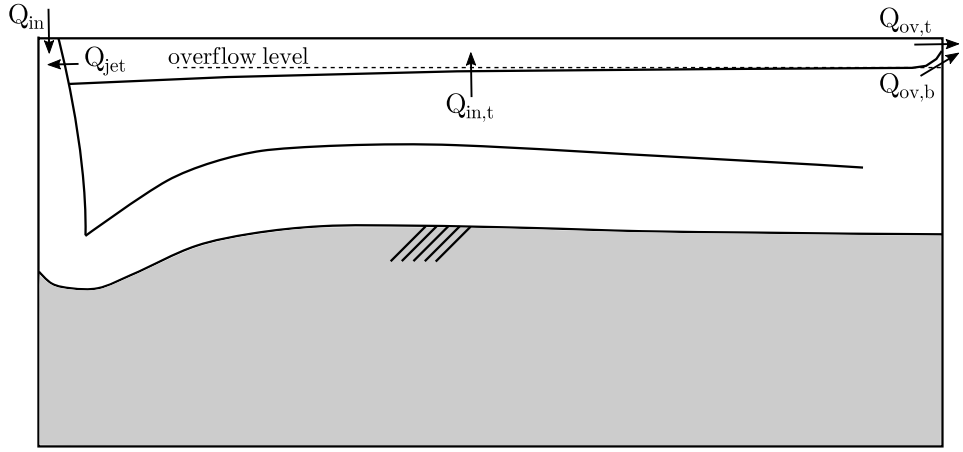

Figure 7.8: Schematized overview Phase 2.

Again, the flow can be described by the mixture flux velocity in z-direction:

$$j_z = (1 - \alpha_d) w_f + \alpha_d w_d \tag{7.12}$$

This time, the concentration gradient stays in place, meaning $w_d = 0$. By definition, the water velocity then equals the slip velocity:

$$w_f = -w_0 \, (1 - \alpha_d)^{n-1} \tag{7.13}$$

Note that w_0 is negative. This can be substituted in Equation 7.12, obtaining:

$$j_z = -(1 - \alpha_d) w_0 \, (1 - \alpha_d)^{n-1} \tag{7.14}$$

The volume flux of water pushed into the top layer is then:

$$Q_{in,t} = -(1 - \alpha_d) w_0 \, (1 - \alpha_d)^{n-1} \, WL \tag{7.15}$$

Part of this water is entrained by the jet. The rest flows through the overflow:

$$Q_{ov,t} = -(1 - \alpha_d) w_0 \, (1 - \alpha_d)^{n-1} \, WL - Q_{jet} \tag{7.16}$$

Exactly the same formula can be derived using a different philosophy. The vertical velocity of the interface can be calculated with Equation 7.10. When this layer exceeds the overflow level, the concentrated water above the overflow, flows through the overflow:

$$Q_{ov,b} = w_i WL = Q_{in} + Q_{jet} + (1 - \alpha_d) w_0 \, (1 - \alpha_d)^{n-1} \, WL \tag{7.17}$$

The water flowing through the overflow via the clean layer is then:

$$Q_{ov,t} = Q_{in} - Q_{ov,b} = -(1 - \alpha_d) w_0 \, (1 - \alpha_d)^{n-1} \, WL - Q_{jet} \tag{7.18}$$

Note, that Equation 7.16 and Equation 7.18 are exactly the same.

$Q_{ov,t}$ and $Q_{ov,b}$ can also be obtained from the simulations. The same square/frame as in Figure 7.7 is created at the overflow. The flow rate going through the faces on the vertical line is $Q_{ov,t}$ and the flow rate going through the faces on the horizontal line is $Q_{ov,b}$. Since it is hard to determine the right position of the interface, two frames are made for every simulation. The results are shown in Figure 7.9.

It can be seen that Equation 7.16 approaches the flow rates in the simulations very well. It can also be observed that quite some water of the top layer is entrained in the jet (the difference between $Q_{in,t}$ and $Q_{ov,t}$). This 'loss' of clean water can easily be avoided by placing a vertical plate next to the inlet. This would reduce the overflow losses significantly.

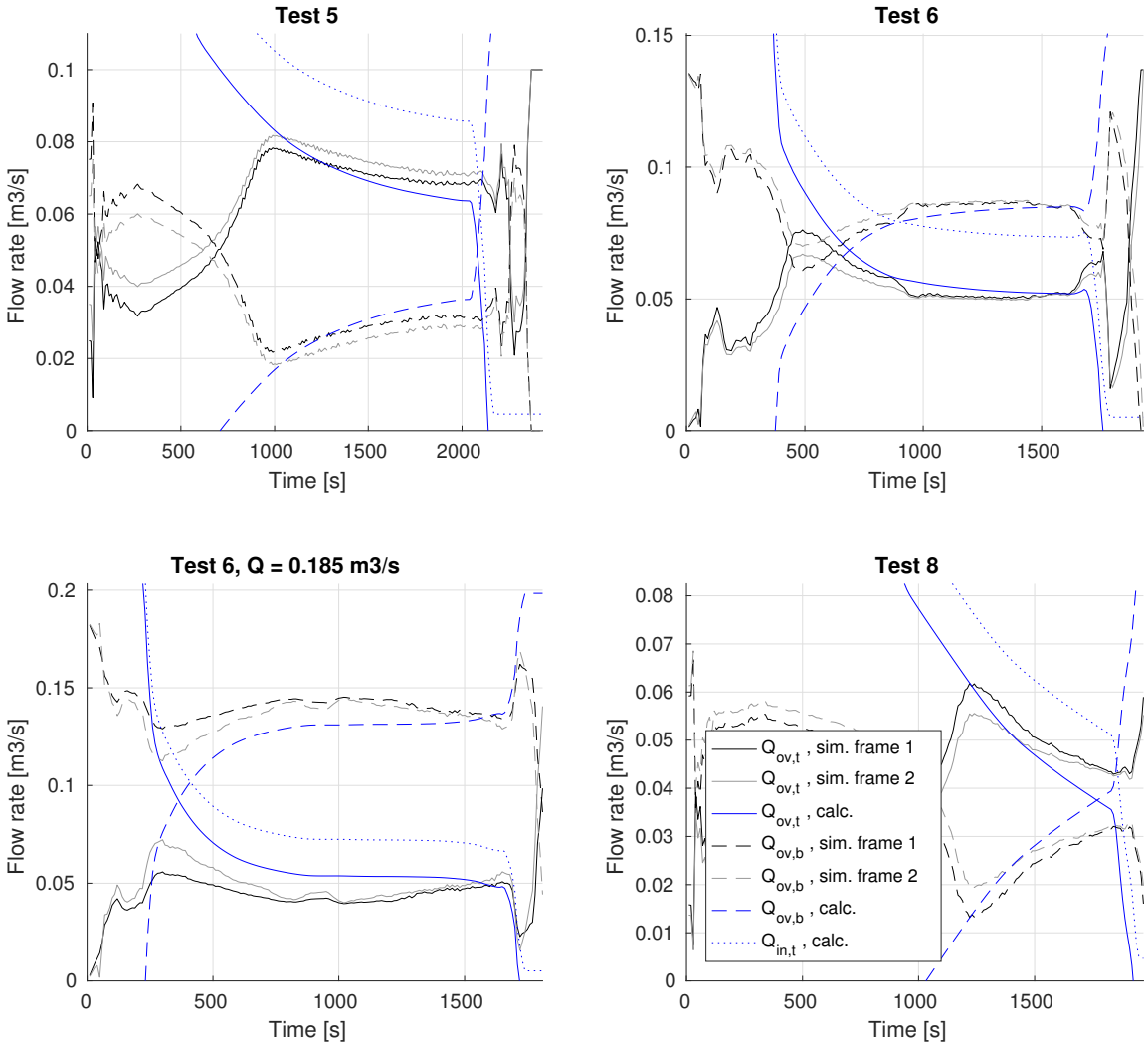

Figure 7.9: Ratio of flow rates through the overflow.

7.3.3. Phase 3

The last phase starts when the interface becomes unstable. This can be seen in Figure 7.4 at t = 2000 s. The top layer is pushed through the overflow. Therefore, a temporary decrease of the overflow concentration can be observed. The top layer is not always pushed through the overflow. The top layer can also be mixed with the bottom layer.

The moment of instability can be estimated with the Richardson number. The Flux Richardson Number is a measure of the turbulence destruction divided by the shear production and is defined as:

$$Ri_f = -\frac{g\overline{\rho' w'}}{\rho \overline{u' w'} \frac{\partial u}{\partial z}} \tag{7.19}$$

From the eddy viscosity concept of Boussinesq follows:

$$\overline{\rho' w'} = \nu_t \frac{\partial \rho}{\partial z} \quad \text{and} \quad \overline{u' w'} = \nu_t \frac{\partial u}{\partial z} \tag{7.20}$$

By substituting this in Equation 7.19, the following is obtained:

$$Ri_f = -\frac{g\frac{\partial \rho}{\partial z}}{\rho\left(\frac{\partial u}{\partial z}\right)^2} \tag{7.21}$$

Preferably, a formulation of the Bulk Richardson Number is obtained to determine the starting point of phase 3:

$$Ri_b = -\frac{g\frac{\Delta \rho}{\Delta z}}{\rho\left(\frac{\Delta U}{\Delta z}\right)^2} \tag{7.22}$$

The velocity and density differences ($\Delta\rho$ and ΔU) can easily be estimated, but Δz is unknown. In the simulations, it can be seen that Δz is very small. It is assumed that $\Delta z = 0.1h_b$ in which h_b is the height of the bottom layer. It was also observed that the critical Richardson Number is generally reached at the beginning of the hopper where $U_t \approx 0$. The velocity in the bottom layer is then: $U_b = Q/W/h_b$. The Bulk Richardson Number can be obtained:

$$Ri_b = \frac{g\frac{\Delta \rho}{0.1h_b}}{\rho_{mean}\left(\frac{Q/W/h_b}{0.1h_b}\right)^2} = \frac{0.1g}{\rho_{mean}}\frac{\Delta\rho W^2 h_b^3}{Q^2} \tag{7.23}$$

In table 7.1, it can be seen that the average moment of instability is at a Bulk Richardson number of 0.25. All simulation were done with only one fraction. In reality, the particle diameters of the grains differ, resulting in a smoother concentration gradient. With polydisperse sand, the flow is expected to become unstable for higher Bulk Richardson Numbers.

Table 7.1: Moment of instability and the corresponding Richardson Number

	Moment of instability[s]	$Q\left[\frac{m^3}{s}\right]$	$h_t[m]$	$h_b[m]$	$\rho_t\left[\frac{kg}{m^3}\right]$	$\rho_b\left[\frac{kg}{m^3}\right]$	$W[m]$	$Ri_b[-]$
Test 4	1080	0,100	0,380	0,189	999	1220	3,08	0,63
Test 5	2140	0,100	0,092	0,121	999	1280	3,08	0,20
Test 6	1660	0,137	0,060	0,196	999	1329	3,08	0,53
Test 6, high flow rate	1600	0,185	0,073	0,189	999	1367	3,08	0,29
Test 8	1890	0,075	0,065	0,093	999	1430	3,08	0,24
Cornelia	2120	6,0	1,328	0,719	1021	1222	11,5	0,12
Cornelia $D_{50} = 180\mu m$	3060	6,0	0,964	0,468	1021	1236	11,5	0,04
Cornelia, high flow rate	2020	7,0	0,964	0,779	1021	1244	11,5	0,12
Cornelia, high flow rate	1950	8,0	0,903	0,717	1021	1252	11,5	0,08
Mean								0,25
Standard deviation								0,20

8

Layer Model

With the knowledge described in Chapter 7, a rather simple model can be made. First, the model was developed for only one fraction. This is described in Paragraph 8.1. In addition, an attempt was done to expand the model to multiple fractions. This is described in Paragraph 8.2.

8.1. Monodisperse Layer Model

Due to the large eddy viscosity and circulatory flow in the bottom layer, it can be assumed that the bottom layer is perfectly mixed. With conservation of mass, the following equation can be obtained for the concentration of the bottom layer:

$$h_b A \frac{\partial \alpha_b}{\partial t} = Q_{in}\left(\alpha_{in} - \alpha_{out}\right) - v_{sed} A \left(\alpha_{max} - \alpha_b\right) - w_i A \alpha_b \tag{8.1}$$

In which A is the horizontal area of the hopper. The second term at the right-hand side represents the mass going into the bed. The third therm represents the decrease in concentration, because the height of the bottom layer increases. Equation 8.1 can be discretized into:

$$\alpha_b^{n+1} = \alpha_b^n + \frac{Q_{in}\left(\alpha_{in} - \alpha_{out}\right)}{h_b^n A}\Delta t - \frac{\left(z_{bed}^{n+1} - z_{bed}^n\right)\left(\alpha_{max} - \alpha_b^n\right)}{h_b^n} - \frac{\left(z_i^{n+1} - z_i^n\right)\alpha_b^n}{h_b^n} \tag{8.2}$$

In which z_{bed} is the vertical position of the bed calculated by:

$$z_{bed}^{n+1} = z_{bed}^n + v_{sed}\Delta t = z_{bed}^n + \frac{-w_0\left(1 - \alpha_b^n\right)^n}{\alpha_{max} - \alpha_b^n}\Delta t \tag{8.3}$$

In equation 8.2, z_i is the vertical position of the interface between the bottom and top layer. The determination depends on the phase. The settling velocity was calculated with Ferguson & Church. Hindered settling was accounted for with Rowe.

Phase 1
If z_i is smaller than the overflow height (z_{ov}), z_i is calculated by:

$$z_i^{n+1} = z_i^n + w_i \Delta t \tag{8.4}$$

The starting position of the interface, z_i^1, is two-thirds of the total height of the hopper. When the density current enters the hopper, it normally takes up about one-third of the height. The returning density current takes up approximately another one-third of the height.
w_i is calculated by Equation 7.10. It is assumed that the concentration of the top layer is zero, so α_{out} is also zero in this phase.

Phase 2
When z_i is larger than $z_{overflow}$, the position of the interface stays constant, i.e. equal to the overflow height. $Q_{ov,b}$ is then calculated by:

$$Q_{ov,b} = w_i A \tag{8.5}$$

For the overflow concentration, it follows:

$$\alpha_{out} = \alpha_b \frac{Q_{ov,b}}{Q_{in}} \tag{8.6}$$

Phase 3
Every time step, the Bulk Richardson Number is calculated with equation 7.23. When it becomes smaller than 0.25, the third phase starts. It is assumed that at this moment the bottom and top layer are mixed, i.e. the hopper becomes perfectly mixed over its total height. This means z_i equals the water surface and α_{out} equals α_b.

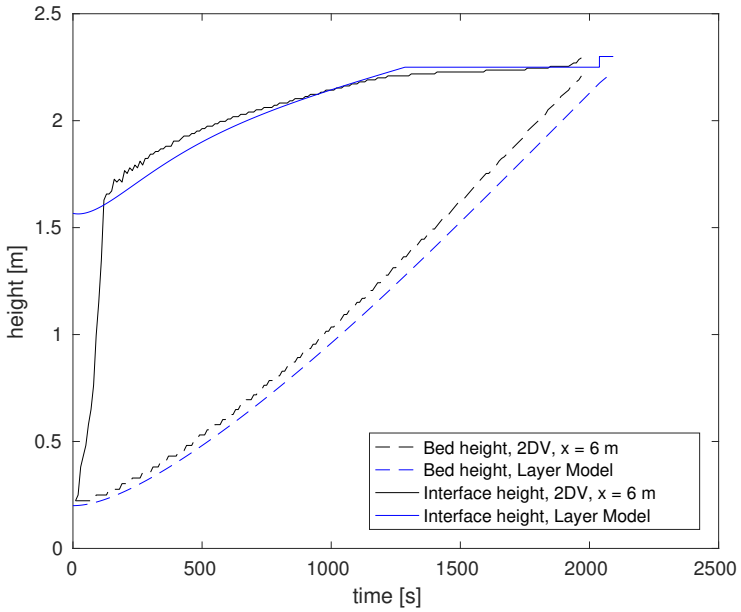

Figure 8.1: Height of bed and concentration inteface over time (Test 8)

In Figure 8.1, the position of the bed and interface calculated with the new Layer Model are shown. It can be seen that the model shows very good resemblance with the 2DV model.

The overflow losses of the Layer Model are also compared with the measurement of Van Rhee and the 2DV of this thesis. In Figure 8.2 the hopper load is used. The hopper load in this case is defined as the total volume of grains (without pore volume) inside the hopper per unit width, which is equal to the sum of the settled sand and the amount of sand still in suspension. The overflow flux in Figure 8.5 is defined as in Equation 6.13.

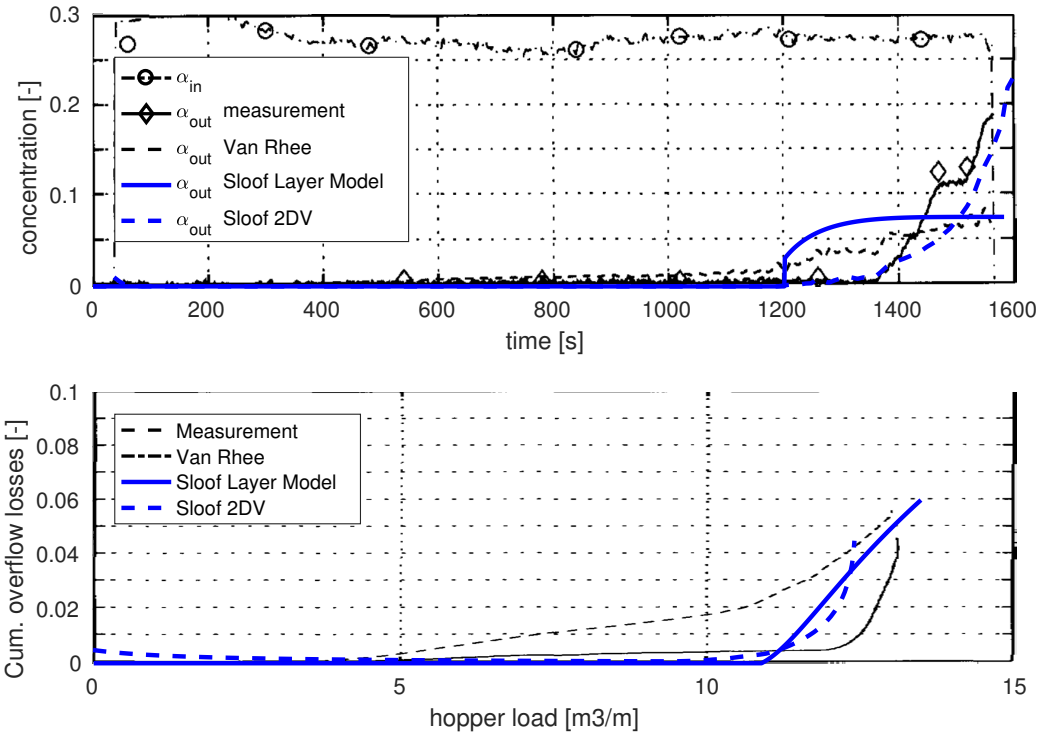

Figure 8.2: Concentrations and cumulative overflow losses (Test 5)

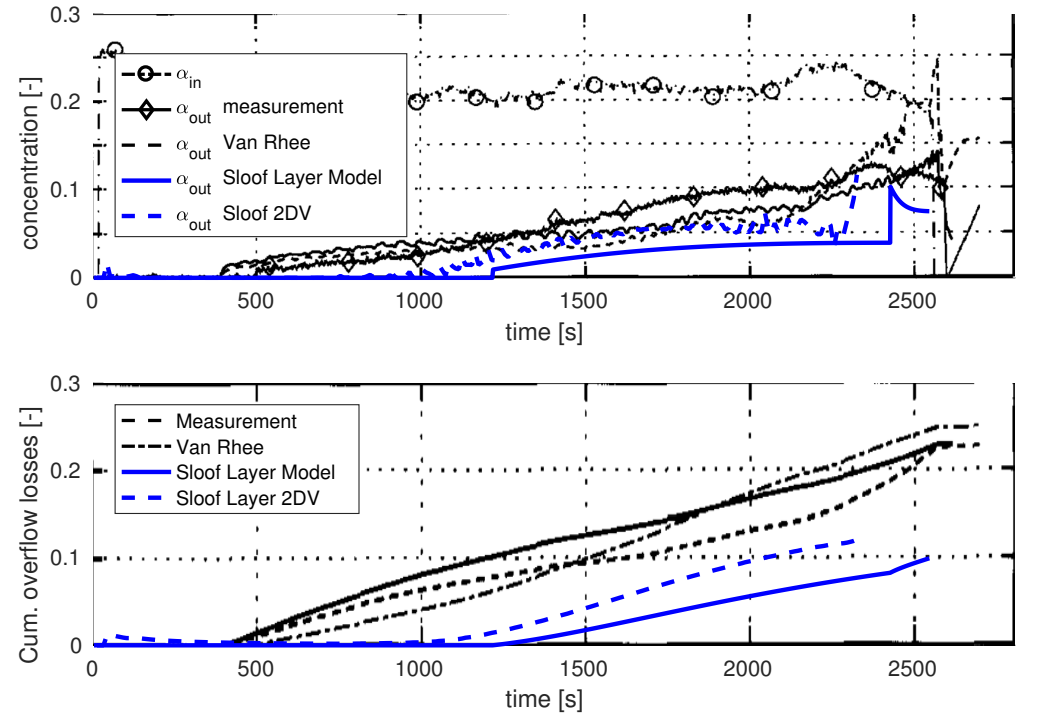

Figure 8.3: Concentrations and cumulative overflow losses (Test 5)

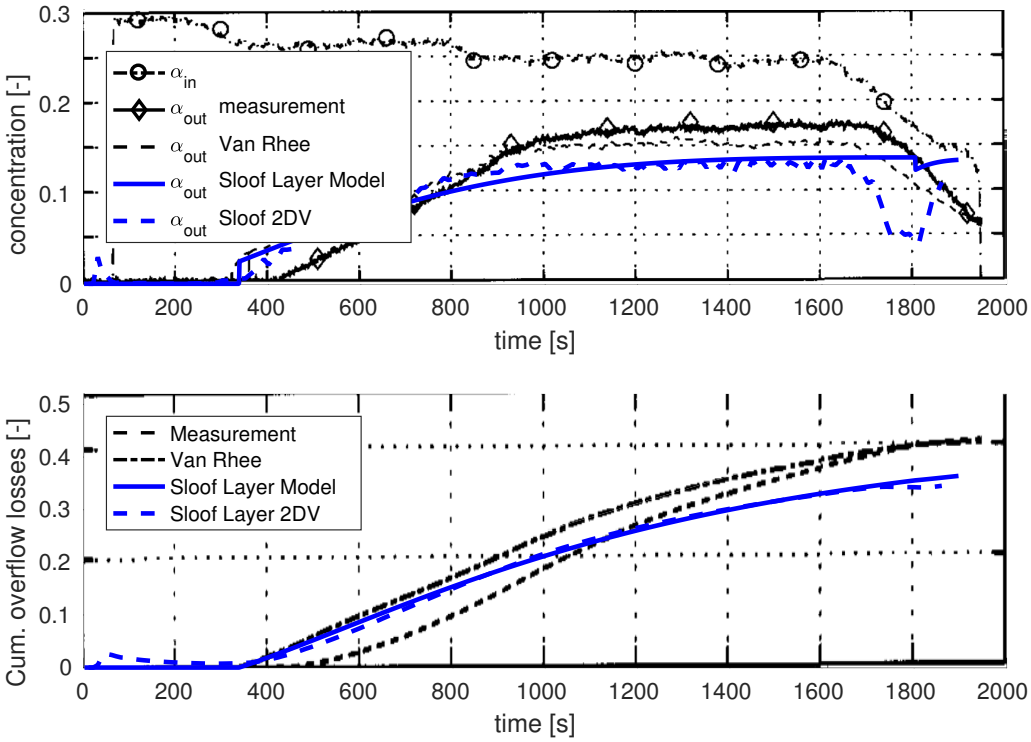

Figure 8.4: Concentrations and cumulative overflow losses (Test 6)

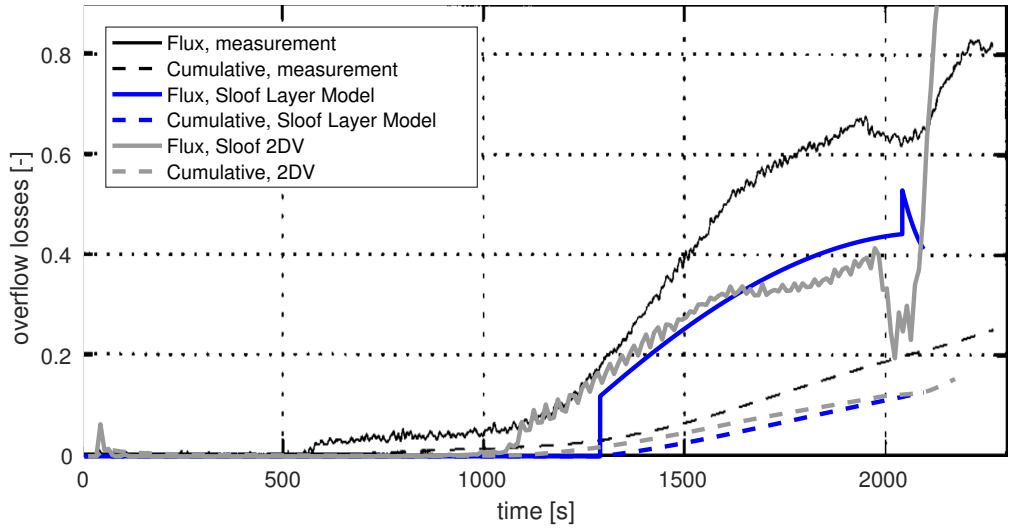

Figure 8.5: Overflow fluxes and cumulative overflow losses (Test 8)

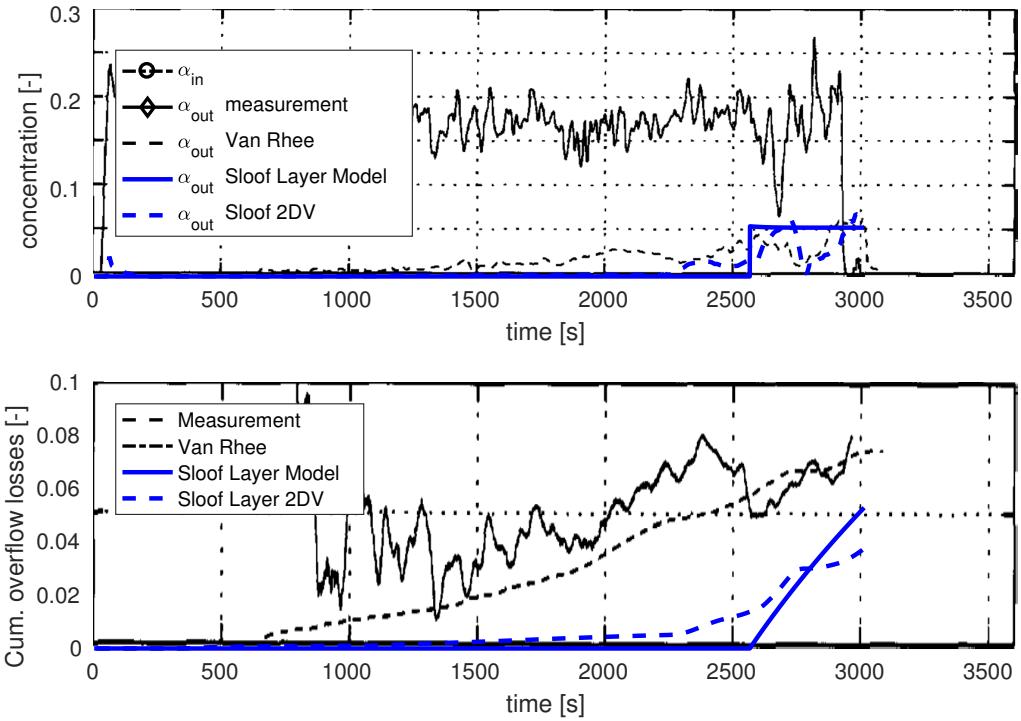

Figure 8.6: Concentrations and cumulative overflow losses for the Cornelia, T = 18°C.

Due to its simplicity, the model has extremely short calculation times. The calculation time is between one and two seconds. In Figures 8.1 to 8.6, it can be seen that the results of the monodisperse 2DV model of this thesis can very well be reproduced with the Layer Model. The starting point of the different phases can be modelled correctly and the overflow losses of the 2DV model can be reproduced. Compared to the measurements, the overflow losses are too low. This difference is probably caused by the absence of a Particle Size Distribution. Hence, the influence of the PSD was incorporated in the Layer Model. This is described in the following paragraph.

8.2. Polydisperse Layer Model

Equation 8.2 was adjusted for polydisperse sediment:

$$\alpha_{k,b}^{n+1} = \alpha_{k,b}^{n} + \frac{Q_{in}\alpha_{k,in} - Q_{ov,b}\alpha_{k,b} - Q_{k,i} + Q_{k,jet}}{h_b^n A}\Delta t - \frac{\left(z_{bed}^{n+1} - z_{bed}^{n}\right)\left(\alpha_{k,bed} - \alpha_{k,b}^{n}\right)}{h_b^n} - \frac{\left(z_i^{n+1} - z_i^{n}\right)\alpha_{k,b}^{n}}{h_b^n} \tag{8.7}$$

In which $Q_{k,i}$ is the volume flux of fraction k over the interface and $Q_{k,jet}$ the particle transport from the top layer to the bottom layer by the jet. The sedimentation velocity is calculated with:

$$v_{sed} = \frac{-\sum_{k=1}^{N} w_k \alpha_{k,b}^{n}}{\alpha_{max} - \sum_{k=1}^{N} \alpha_{k,b}^{n}} \tag{8.8}$$

The vertical fraction velocity w_k is the vertical component of Equation 3.22:

$$w_k = j_z + w_{k,r} - \sum_{k=1}^{N} w_{k,r}\alpha_{k,b} \tag{8.9}$$

Near the bed, j_z is zero. At the interface between the top and bottom layer, j_z is $(Q_{in} + Q_{jet})/A$. The fraction concentration in the bed is calculated with:

$$\alpha_{k,bed} = \frac{(-w_k + v_{sed})\,\alpha_{k,b}}{v_{sed}} \tag{8.10}$$

The vertical velocity of the interface between the bottom and top layer is assumed to be the average particle velocity:

$$w_i = \frac{\sum_{k=1}^{N} w_k \alpha_{k,b}}{\sum_{k=1}^{N} \alpha_{k,b}} \tag{8.11}$$

The determination of the fraction flux over the interface $Q_{k,i}$ depends on the concentration in the top layer. For the concentration profile in the top layer, various assumptions can be done. In this thesis two assumptions have been tried: a perfectly mixed top layer and a Hunt profile.

Perfectly mixed top layer
A mass balance for the sediment in the top layer is derived:

$$\alpha_{k,t}^{n+1} = \alpha_{k,t}^{n}\frac{h_t^n}{h_t^{n+1}} + \frac{Q_{k,i} - Q_{k,jet} - Q_{ov,t}\alpha_{k,t}^{n}}{h_t^n A}\Delta t \tag{8.12}$$

The particles entrained by the jet are calculated with:

$$Q_{k,jet} = Q_{jet}\alpha_{k,t} \tag{8.13}$$

The transport of particles over the interface is calculated with:

$$Q_{k,i} = \left(w_{k,b}\alpha_{k,b} - w_{k,t}\alpha_{k,t}\right) WL \tag{8.14}$$

In which $w_{k,b}$ is fraction velocity in the bottom layer and $w_{k,t}$ the fraction velocity in the top layer.

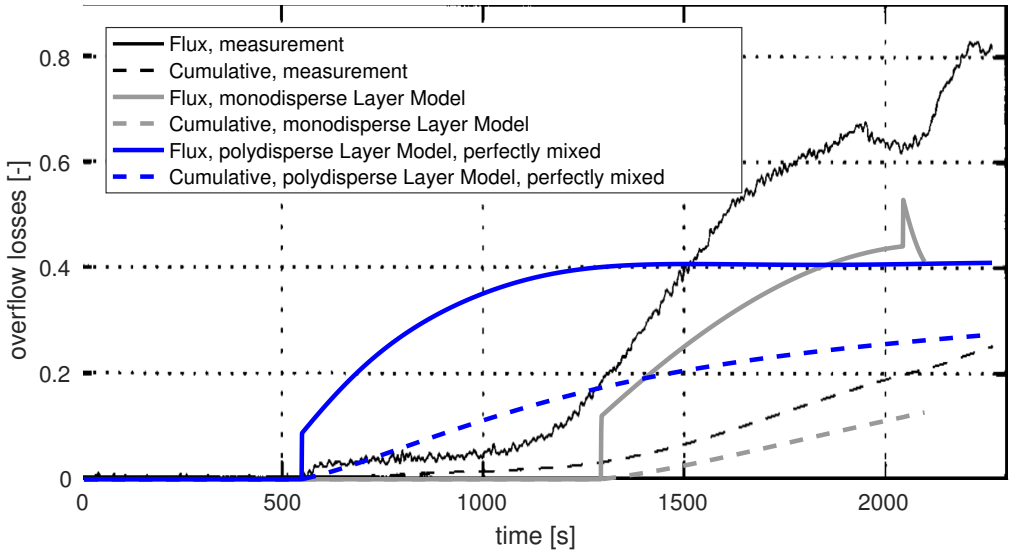

Figure 8.7: Overflow fluxes and cumulative overflow losses (Test 8)

Hunt profile

In open channel flow with monodisperse sediment a Rouse profile can be observed. Hunt[30] adjusted the Rouse profile for polydisperse sediment. For the derivation of the Hunt profile, a parabolic profile of the turbulent diffusivity is assumed, which is the case in the top layer of a hopper as can be seen in Figure 7.3. The concentration profile over the height is:

$$\alpha_{k,t}(z) = \frac{\alpha_{k,ref}\left(Z(z)/Z_{ref}\right)^{-\gamma_k}}{1 - \sum_{k=1}^{N} \alpha_{k,ref}\left(1 - \left(Z(z)/Z_{ref}\right)^{-\gamma_k}\right)} \tag{8.15}$$

In which:

$$Z(z) = \frac{(z - z_i)/h_t}{1 - (z - z_i)/h_t} \quad \text{and} \quad Z_{ref} = \frac{(z_{ref} - z_i)/h_t}{1 - (z_{ref} - z_i)/h_t} \tag{8.16}$$

z_i is the position of the interface. z_{ref} is the reference height where the fraction concentrations $\alpha_{k,ref}$ are known. In this case the known fraction concentrations are the fraction concentrations at the interface: $\alpha_{k,b}$. The reference height would then be z_i. Z_{ref} is then zero, which results in dividing by zero in Equation 8.18. Instead, an arbitrary value of $z_i + 0.01h_t$ was chosen for z_{ref}. This value can be changed to calibrate the model.
γ_k is defined as $w_{k,0}/(\kappa u_*)$. This means hindered settling is not taken into account. Since the concentrations in the top layer are low, this only causes minor errors. The shear velocity at the top layer in the simulation of Test 8 is 0.0159 m/s and 0.0072 m/s at t = 800 s and t = 1700 s, respectively. An average shear velocity of 0.01 m/s is used.

The concentration of each fraction going through the overflow via the top layer can be calculated with:

$$\alpha_{k,t,out} = \frac{\int_{z_{ov}}^{z_w} \alpha_{k,t}(z)dz}{z_w - z_{ov}} \tag{8.17}$$

In which z_w is the height of the water surface and z_{ov} the overflow height. The volume flux of particles leaving the top layer can be obtained with:

$$Q_{k,t,out} = Q_{ov,t}\alpha_{k,t,out} = Q_{ov,t}\frac{\int_{z_{ov}}^{z_w}\alpha_{k,t}(z)dz}{z_w - z_{ov}} \tag{8.18}$$

In which $Q_{ov,t}$ is the mixture flow rate leaving the hopper via the top layer: $Q_{in} - Q_{ov,b}$. It was assumed that the particles entering the top layer instantaneously leave the hopper, meaning $Q_{k,i} = Q_{k,t,out}$ and $Q_{k,jet} = 0$. The particle fluxes $Q_{k,i}$ and $Q_{k,jet}$ are needed for the mass balance of the bottom layer: Equation 8.7.

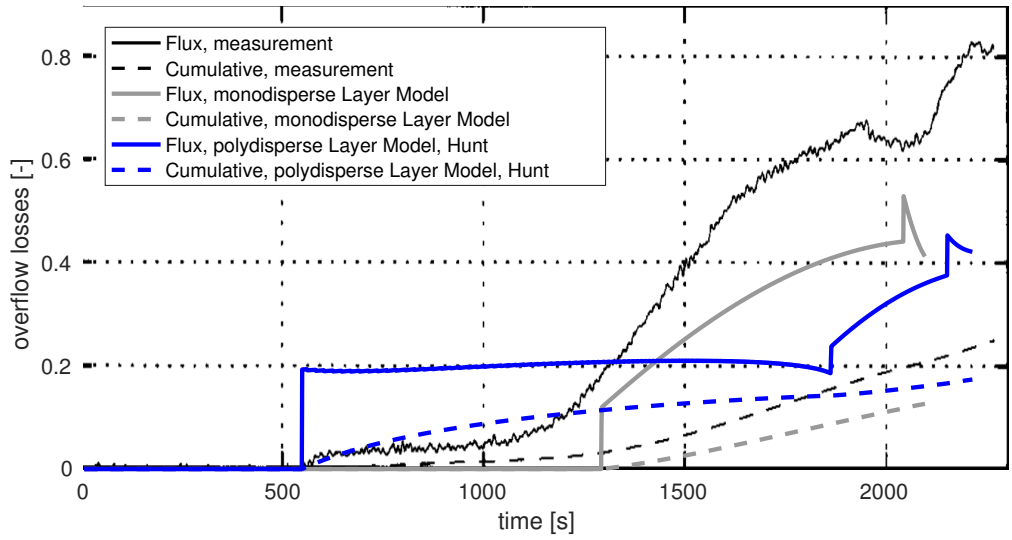

Figure 8.8: Overflow fluxes and cumulative overflow losses (Test 8)

For both the model where the top layer is assumed to be perfectly mixed (Figure 8.7) and the model where the Hunt profile is applied (Figure 8.8), the overflow concentration of the top layer is too high in the beginning of the loading cycle. At the end of the loading cycle, the overflow concentration is too low. The concentration in the top layer needs to be modelled in a different way. More research is needed to determine the concentration in the top layer.

In addition, it is advisable to do research about the phenomena in a hopper with polydisperse sediment. Once the 2DV model of this thesis is extended and is capable of computing with a PSD, the physics of the top layer can be investigated more thoroughly. The presence of multiple particle sized could, for instance, make the concentration gradient between the top and bottom layer less sharp, causing less turbulence destruction and a different eddy viscosity profile as found in Figure 7.3.

9

Conclusions and Recommendations

9.1. Conclusions 2DV model

Settling
The model was compared with several settling experiments. It became clear that the hindered settling velocity is very sensitive to the shape and size of the particles. This is a main contributor to the inaccuracy of the model.

Reduced sedimentation
A moving mesh was needed to simulate reduced sedimentation. The model was validated with the closed flume experiments of Van Rhee. The results of the model corresponded well with the experiments. By using a pickup function erosion could also be modelled.

Velocities in the hopper
The velocities in the hopper are slightly too high. This could be caused by the turbulence modelling in the jet. Another explanation could be the presence of air bubbles which normally slow down the jet.

Concentrations in the hopper
The sediment is mixed too uniformly over the height of the hopper. This is partly caused by simulating with only one fraction. However, this cannot be the only cause. It was tried to decrease the mixing in several ways without satisfactory result.

Overflow losses
The overflow losses are generally too low. This is exactly the expected outcome, since only one fraction is simulated instead of a Particle Size Distribution.

Calculation Time
When calculating with multiple processors a 2D hopper simulation is done in one and a half hours. This is a very good achievement for a calculation like this. Making a database and doing interpolations once a loading time is needed, gives calculation times which are well within the demands of Damen.

3D simulations
The ability to do 3D simulations opens up huge possibilities. Different inlet and overflow configurations could be simulated to design the optimal Trailing Suction Hopper Dredger.

9.2. Conclusions Layer Model

Modelling with one fraction
A relatively simple model has been developed which has extremely short calculation times. The start

of the different phases were predicted well. Just like the 2DV model, the calculated overflow losses are too low. The results of the Layer Model are in strong agreement with the 2DV model.

Modelling with multiple fractions
It was not possible to determine the concentrations in the top layer yet. Therefore, calculations with multiple fractions were not in agreement with the measurements.

9.3. Recommendations 2DV model

Particle Size Distribution
At this moment, the model can only calculate with the D_{50}. Doing calculations with the PSD would improve both the concentration profile and estimation of the overflow losses. When the multifraction version of `driftFluxFoam` is available, the code developed during this thesis should be implemented in that solver.

Concentrations in the hopper
Calculating with multiple fractions would improve the concentration profiles in the hopper. To make further improvements, more research is needed into the cause of the large diffusion over the height.

Moving rigid lid
With a moving rigid lid it is possible to simulate a lower water level at the beginning of the simulation. In addition, it would be possible to simulate the varying height of the water above overflow level. It would be even better to simulate a free surface with a VOF-solver like `interFoam` of `interDyMFoam`.

Silo shape of hoppers
Modelling the silo shape in 2D calculations would improve the results.

More measurements with TSHDs
At prototype scale, the model is only validated for the Cornelia. Comparing the model with more measurements would improve the trust in its results and can give more insights. The slip velocity can be calculated with:

9.4. Recommendations Layer Model

Flow rate entrained into the jet
A rough estimate for Q_{jet} was used in the Layer Model; a better estimate is advisable.

Vertical plate next to the inlet
A vertical plate next to the inlet prevents the entrainment of water out of the top layer into the jet. This could reduce the overflow losses.

Modelling of the top layer concentration
It was not possible to model the concentration in the top layer yet. It is recommended to try different approaches to model the concentration in the top layer. The slip velocity can be calculated with: **More research with 2DV model with PSD**
The governing phenomena of hopper sedimentation with monodisperse sediment are well described in this thesis. The presence of multiple fractions can have influence on these processes. Once the 2DV model can calculate with a PSD, it is recommended to investigate the physics of the top layer more thoroughly with multiple fractions.

Bibliography

[1] Aliseda, A., Cartellier, A., Hainaux, F., Lasheras, F.C. (2002) "Effect of preferential concentration on the settling velocity of heavy particles in homogeneous isotropic turbulence." J. Fluid Mech. 468, pp. 77-105.

[2] Angot, P., Bruneau, C.H., Frabrie, P. (1999). "A penalization method to take into account obstacles in viscous flows". Numerische Mathematik, 81, pp. 497–520.

[3] Baldock, T.E. (2003). "Settling velocity of sediments at high concentrations". Coast. Eng., 51, pp. 91-100

[4] Bagnold, R.A. (1954). "Experiments on a gravity-free disperion of large solid spheres in a Newtonian fluid under shear". Proc. R. Soc. Lond. A., 225, pp. 49-63

[5] Basse, N.T. (2017), "Turbulence intensity and the friction factor for smooth- and rough-wall pipe flow", Fluids, vol. 2.

[6] Blasius, H.(1908) "Boundary Layers in Liquids with Low Viscosity"(in German), J. Math. Phys. , 56 , pp. 1-37.

[7] Blocken, B. (2007) "Cfd simulation of the atmospheric boundary layer: wall function problems." Atmospheric Environment, 41, pp. 238-252.

[8] Braaksma, J., Klaassens, J. B., Babuska R., de Keizer, C.(2007). "A computationally efficient model for predicting overflow mixture density in a hopper dredger". Terra et Aqua, 106, pp. 16-25.

[9] Brennan, D. (2001). "The numerical simulation of two-phase flows in Settling Tanks". PhD thesis, Imperial College of Science, Technology and Medicine, Department of Mechanical Engineering, London.

[10] Brouwers, J.J.H. (2007) "Dissipation equals production in the log layer of wall-induced turbulence." Physics of fluids, 19

[11] Brownlie, W. R., Brooks, N. H. (1981). "Compilation of alluvial channel data: laboratory and field". WM Keck Laboratory of Hydraulics and Water Resources, California Institute of Technology Pasadena, CA.

[12] Camp T. R. (1936). "A study of the rational design of settling tanks." Sewage Works Journal 8(5), pp, 742-758.

[13] Camp, T.R. (1943). "The effect of turbulence on retarded settling." Proceedings of the 2nd Hydraulics Conference, University of Iowa, Studies in Engineering, Bulletin 27, pp. 307-317.

[14] Cebeci, T., Smith, A. M. 0. (1974). Analysis of Turbulent Boundary Layers. New York: Academic Press

[15] Celik, I.B. (1999). "Introductory turbulence modeling". Lecture Notes, West Virginia University.

[16] Cheng , N. S. (1997). "Simplified settling velocity formula for sediment particle". Journal of Hydraulic Engineering, American Society of Civil Engineers, v. 123, pp. 149-152.

[17] Chieng, C. C., Launder, B. E. (1980). "On the Calculation of Turbulent Heat Transport Downstream From an Abrupt Pipe Expansion." Numerical Heat Transfer, 3, pp. 189-207

[18] Choi, S., García, M. H. (2002). "k–ϵ turbulence modeling of density currents developing two dimensionally on a slope." J. Hydraul. Eng., 128(1), pp. 55–63.

[19] Costa, P. (2016) "Universal Scaling Laws for Dense Particle Suspensions in Turbulent Wall-Bounded Flows" Phys. Rev. Lett. 117, 134501

[20] Dobbins, W. E. (1943). "The effect of Turbulence on Sedimentation." Proc. Am. Soc. Civil Engineers, Vol. 69, No. 2, pp. 235-262.

[21] Ferguson, R., Church, M. (2004). "A Simple Universal Equation for Grain Settling Velocity". Journal of Sedimentary Research, vol. 74, n. 6, pp. 933–937

[22] Jensen, J.H., Saremi, S. (2014). "Overflow concentration and sedimentation in hoppers" J. Waterw., Port, Coast. Ocean Eng., ASCE, 40.

[23] Garside, J., Al-Dibouni, M.R. (1977). "Velocity-Voidage Relationships for Fluidization and Sedimentation in Solid-Liquid Systems" Ind. Eng. Chem., Process Des. Dev., Vol. 16, No. 2, pp. 206-214.

[24] Goeree, J.C., Van Rhee, C., Bugdayci, H.H. (2013). "Numerical sediment simulation using a continuous flow-model." Multiphase, 16, pp. 323-335, BHR Group, Bedford, UK.

[25] Goeree, J.C. (2016). "Concentration and Velocity Profiles of Sediment-Water Mixtures using the Drift Flux Model" The Canadian Journal of Chemical Engineering, 94, pp. 1048-1058.

[26] Groot, J. (1981). "Rapport Beunbezinking". Papendrecht: Royal Boskalis Westminster.

[27] Han, Z., Reitz, Z.D. (1995). "Turbulence modeling of internal combustion engines using RNG $k-\epsilon$ models" Comb. Sci. Tech. 106, 267 (1995).

[28] Hager, W.H. (1987). "Lateral outflow over side weirs." J. Hydr. Eng., ASCE, 113(4), pp. 491–504.

[29] Henkes, R.A.W.M., Van Der Vlugt, F.F., Hoogendoorn, C.J. (1991). "Natural Convection Flow in a Square Cavity Calculated with Low-Reynolds-Number Turbulence Models." Int. J. Heat Mass Transfer, 34, pp. 1543-1557.

[30] Hunt, J. N. (1969). "On the turbulent transport of a heterogeneous sediment." Q. J. Mech. Appl. Math., 22, pp. 235-246.

[31] Konijn, B.J. (2016). "Numerical simulation methods for dense-phase dredging flows". PhD thesis, Universiteit Twente, the Netherlands

[32] Kotsovinos, N.E. (1977). "Plane turbulent buoyant jets. Part 1. Integral properties". J. Fluid Mech., 81, pp. 25-44.

[33] Márquez Damián, S. (2013) "An extended mixture model for the simultaneous treatment of short and long scale interfaces". Ph.D. thesis Facultad de Ingeniería y Ciencias Hídricas (FICH), Instituto de Desarrollo Tecnológico para la Industria Química (INTEC), Universidad Nacional del Litoral.

[34] Menter, F.R. (1992). "Influence of freestream values on k-ω turbulence model predictions." AIAA Journal, Vol. 30, No. 6.

[35] Miedema, S.A., Vlasblom, W. (1996). "Theory of Hopper Sedimentation". 29th Annual Texas A&M Dredging Seminar, New Orleans.

[36] Miedema, S.A., Rhee, C. van (2007) "A sensitivity analysis on the effects of dimensions and geometry of Trailing Suction Hopper Dredges". WODCON, Orlando, USA.

[37] Miedema, S.A. (2008), "An Analytical Approach To The Sedimentation Process In Trailing Suction Hopper Dredgers". Terra et Aqua, 112, pp. 15-25. A&M Dredging Seminar, New Orleans: WEDA.

[38] Miedema, S.A. (2009). "The effect of the bed rise velocity on the sedimentation process in hopper dredges". Journal of Dredging Engineering, Vol. 10, No. 1 , pp. 10-31.

[39] Miedema, S.A. (2012). "Dredging Processes, The Loading Process of a Trailing Suction Hopper Dredge." Lecture Notes, Delft University of Technology.

[40] Ooijens, S. (1999). ”Adding Dynamics to the Camp Model for the Calculation of Overflow Losses”. Terra et Aqua, 76, pp. 12-21.

[41] Pal, D., Ghoshal, K. (2013) ”Hindered settling with an apparent particle diameter concept”. Advances in Water Resources, 60, pp. 178–187.

[42] Parker, G., Fukushima, Y., and Pantin, H. M. (1986). ”Self-accelerating turbidity currents”. J. Fluid Mech., 171, pp. 145-181.

[43] Patel, V. P., Rodi, W., Scheuerer, G. (1985). ”Turbulence Models for Near-Wall and Low Reynolds Number Flows: A Review.” AIAA Journal, 23, pp. 1308-1319

[44] Pattijn, S. (1999). ”Non-linear, low-Reynolds, two-equation turbulence models”. PhD disseration, Dep. Flow Mechanics, Heat and Incineration, Ghent University.

[45] Picano, F. (2015) ”Turbulent channel flow of dense suspensions of neutrally buoyant spheres.” J. Fluid Mech., 764, pp. 463–487

[46] Poletto, M., Joseph, D.D. (1995). ”Effective density and viscosity of a suspension”. J. Rheol., 39, pp.323-343.

[47] Richardson, J. and Zaki, W. (1954). ”Sedimentation and Fluidisation: Part I”. Transactions of the Institution of Chemical Engineers, 32, pp. 35-53

[48] Van Rijn, L. C. (1984). ”Sediment pick-up functions”. Journal of Hydraulic Engineering, 110(10), pp.1494–1502.

[49] Van Rhee, C. (2002). ”On the sedimentation process in a Trailing Suction Hopper Dredger”. PhD thesis, TU Delft, the Netherlands

[50] Van Rhee, C., Talmon, A. (2010). ”Sedimentation and erosion of sediment at high solids concentration”. Proceedings of Hydrotransport 18, pp. 211-222, BHR Group, Bedford, UK.

[51] Van Rhee, C. (2015). ”Slope failure by unstable breaching”. Maritime Engineering, 184, pp. 84-92

[52] Rodi, W. (1993) ”Turbulent Buoyant Jets and Plumes”. Oxford, Pargamon.

[53] Rodi, W. (1993) ”Turbulence Models and their Application in Hydraulics”. 3rd ed., Balkema, Rotterdam.

[54] Runge, A.C. (1999). ”Eendimensionale beschouwing van de bezinking van hoog geconcentreerde zandwatermengsels onder turbulente omstandigheden”. TU Delft, Faculteit Civiele Techniek en Geowetenschappen, sectie Waterbouwkunde

[55] Russo, F., Basse, N.T. (2016). ”Scaling of turbulence intensity for low-speed flow in smooth pipes”, Flow Meas. Instrum., 52, pp. 101–114.

[56] Sequeiros, O.E. (2010). ”Characteristics of velocity and excess density profiles of saline underflows and turbidity currents flowing over a mobile bed”. Journal of Hydraulic Engineering, 136, pp. 412–434.

[57] Shih, T.H., Liou, W. W. Shabbir, A., Yang, Z. and Zhu, J. (1994). ”A New k–e Eddy Viscosity Model for High Reynolds Number Turbulent Flows—Model Development and Validation”. NASA TM-106721.

[58] Sobera, M., Kleijn, C. (2008) “T-RANS Simulations of Subcritical Flow with Heat Transfer Past a Circular Cylinder Surrounded by a Thin Porous Layer,” Journal of Flow, Turbulence and Combustion 80 (4), pp. 531-546.

[59] Spearman, J. (2013) ”TASS Software - User Guide for TASS version 4.0”. HR Wallingford

[60] Thomas, D.G. (1965). ”Transport Characteristics of Suspensions: VIII” J. Colloid Sci., 20, pp. 267-277

[61] Tominaga, Y., Stathopoulos, T. (2007) ”Turbulent Schmidt numbers for CFD analysis with various types of flowfields” Atmospheric Environment, 41, pp. 8091–8099.

[62] Wang, L.P., Maxey, M. R. (1993) ”Settling velocity and concentration distribution of heavy particles in homogeneous isotropic turbulence.” J. Fluid Mech. 256, pp. 27–68.

[63] Weij, D. (2017) Private Communication. Technical University Delft.

[64] White, F.M. (2003) ”Fluid Mechanics”. WCB/McGraw-Hill, Boston, MA, USA.

[65] Yakhot, V., Orszag, S.A. (1986). ”Renormalization group analysis of turbulence. 1. Basic theory.” J. Sci. Comput., 1(1), pp. 3–51.

[66] Yang, Z., and Shih, T.H. (1993). ”New time scale based $k - \epsilon$ model for near-wall turbulence”. AIAA Journal, Vol. 31, No.7, pp. 1191–1198.

[67] Yannopoulos, P. C. (2006). ”An improved integral model for plane and round turbulent buoyant jets”. J. Fluid Mech., 547, pp. 267–296

Nomenclature

Greek Symbols

α	Concentration	$[-]$
α_b	Concentration in the bottom layer of the 'Layer Model'	$[-]$
α_b	Near bed concentration	$[-]$
α_k	Concentration of fraction k	$[-]$
α_{bed}	Concentration in the bed cell	$[-]$
α_d	Concentration of the dispersed phase	$[-]$
$\alpha_{k,b}$	Concentration of fraction k in the bottom layer of the 'Layer Model'	$[-]$
$\alpha_{k,t}$	Concentration of fraction k in the top layer of the 'Layer Model'	$[-]$
α_{liquid}	Concentration in the cell above the bed	$[-]$
α_{max}	Maximum concentration used by MULES	$[-]$
α_{merged}	Concentration in the cell after merging	$[-]$
α_n	Coefficients belonging to the neighbour cells in the FvMatrix of the momentum equation	$[-]$
α_p	Coefficients on the diagonal in the FvMatrix of the momentum equation	$[-]$
α_t	Total concentration, sum of all the particle fractions	$[-]$
β	Slope angle	$[^\circ]$
Δ	Specific sediment density	$[-]$
$\dot{\gamma}$	Shear rate	$[1/s]$
ϵ	Dissipation of turbulent kinetic energy	$[J/(kg \cdot s)]$
Γ	Diffusion coefficient	$[m^2/s]$
Γ_t	Turbulent diffusion coefficient	$[m^2/s]$
κ	Von Karman constant	$[-]$
μ	Dynamic viscosity	$[Pa \cdot s]$
μ_m	Mixture viscosity (dynamic)	$[Pa \cdot s]$
μ_t	Turbulent eddy viscosity (dynamic)	$[Pa \cdot s]$
μ_{eff}	Effective viscosity: summation of eddy and molecular viscosity (dynamic)	$[Pa \cdot s]$
ν	Kinematic viscosity	$[m^2/s]$
ν_m	Mixture viscosity (kinematic)	$[m^2/s]$
ν_t	Turbulent eddy viscosity (kinematic)	$[m^2/s]$
ν_{eff}	Effective viscosity: summation of eddy and molecular viscosity (kinematic)	$[m^2/s]$
ω	The specific turbulence dissipation rate	$[1/s]$
Φ	Pickup flux	$[-]$
ϕ	Angle of internal friction	$[^\circ]$

ϕ_g	Contribution of the hydrostatic pressure to the volume flux through a face	$[m^3/s]$
ϕ_{HbyA}	Volume flux through a face without the contribution of the pressure	$[m^3/s]$
$\phi_{p_{rgh}}$	Contribution of the dynamic pressure to the volume flux through a face	$[m^3/s]$
Ψ	Shape factor	$[-]$
ρ	Density	$[kg/m^3]$
ρ_k	Density of fraction k	$[kg/m^3]$
ρ_m	Mixture density	$[kg/m^3]$
ρ_s	Solids density	$[kg/m^3]$
ρ_w	Water density	$[kg/m^3]$
σ	Schmidt number	$[-]$
τ	Shear stress	$[Pa]$
τ_k	Kolmogorov time scale	$[s]$
τ_p	Particle relaxation time	$[s]$
τ_y	Yield stress	$[Pa]$
θ	Shields number	$[-]$
θ_{cr}	Critical shields number	$[-]$
θ'_{cr}	Critical shields number adjusted for high speed and slope	$[-]$

Roman Symbols

ℓ_m	Mixing length (in Prandtl's Mixing Length Model)	$[m]$
$\mathbf{I}$	Identity matrix	$[-]$
$\mathbf{j}_m$	Mixture flux velocity vector	$[m/s]$
$\mathbf{m}_k$	Coupling force between the faces	$[kg/(m^2 \cdot s^2]$
$\mathbf{S}$	Deformation tensor	$[1/s]$
$\mathbf{S}_f$	Surface vector of a face	$[m^2]$
$\mathbf{T}_m$	Viscous stress tensor	$[Pa]$
$\mathbf{T}_m^t$	Turbulent stress tensor	$[Pa]$
$\mathbf{u}$	Velocity vector	$[m/s]$
$\mathbf{u}_f$	Velocity at the face	$[m/s]$
$\mathbf{u}_k$	Velocity vector of fraction k	$[m/s]$
$\mathbf{u}_m$	Mixture centre of mass velocity vector	$[m/s]$
$\mathbf{u}_n$	Velocity in the cell centre of a neighbouring cell	$[m/s]$
$\mathbf{u}_p$	Velocity in the cell centre	$[m/s]$
$\mathbf{u}_{k,j}$	Velocity of k with respect to the 'flux velocity'	$[m/s]$
$\mathbf{u}_{k,m}$	Diffusion velocity, the velocity of k with respect to the 'mixture centre of mass velocity'	$[m/s]$
$\mathbf{u}_{k,r}$	Slip velocity vector of fraction k	$[m/s]$
C	Constant for rough wall function	$[-]$
C_1	Emperical constant Ferguson & Church	$[-]$

C_2	Emperical constant Ferguson & Church	$[-]$
C_D	Drag coefficient	$[-]$
c_k	Mass fraction of k	$[m]$
c_μ	Constant of the k-ϵ model, $C_\mu = 0.09$	$[-]$
D	Particle diameter	$[m]$
d	Pipe diameter	$[m]$
D_*	Bonneville parameter	$[-]$
D_{50}	Mass median particle diameter: diameter for which 50% is finer	$[m]$
d_H	Hydraulic diameter	$[m]$
E	Erosion flux	$[kg/(m^s \cdot kg)]$
g	Gravitational acceleration	$[m/s^2]$
H	Height of the hopper	$[m]$
h_{bed}	Height of the bed cell (in the moving mesh)	$[m]$
h_b	Height of the bottom layer in the 'Layer Model'	$[m]$
h_{liquid}	Height of the cell above the bed (in the moving mesh)	$[m]$
h_{merged}	Height of the cell after merging (in the moving mesh)	$[m]$
$h_{overflow}$	Height of the water above the overflow	$[m]$
h_t	Height of the top layer in the 'Layer Model'	$[m]$
h_{water}	Height of the water above the bed	$[m]$
I	Turbulence intensity	$[-]$
k	Turbulent kinetic energy	$[J/kg]$
L	Length of the hopper	$[m]$
N	Bagnold number	$[-]$
n	Hindered settling exponent	$[-]$
n_0	Porosity	$[m]$
n_k	Hindered settling exponent for fraction k	$[-]$
OV_{cum}	Cumulative overflow losses	$[-]$
OV_{flux}	Overflow flux	$[-]$
P	Production of turbulent kinetic energy	$[J/(kg \cdot s)]$
p	Pressure	$[Pa]$
P_b	Buoyant dissipation of turbulent kinetic energy	$[J/(kg \cdot s)]$
p_{rgh}	Dynamic pressure	$[Pa]$
Q	Flow rate	$[m^3/s]$
q	Flow rate per unit width	$[m^3/(m \cdot s)]$
Q_{in}	Flow rate coming into the hopper	$[m^3/s]$
Q_{jet}	Flow rate entrained into the jet from the top layer	$[m^3/s]$
Q_{out}	Flow rate going out the hopper	$[m^3/s]$
$Q_{ov,b}$	Part of the flow rate going through the overflow coming from the bottom layer	$[m^3/s]$

$Q_{ov,t}$	Part of the flow rate going through the overflow coming from the top layer	$[m^3/s]$
Q_s	Flow rate of solids	$[m^3/s]$
Re	Bulk Reynolds Number	$[-]$
Re_p	Reynolds Particle Number	$[-]$
Ri_b	Bulk Richardson Number	$[-]$
Ri_f	Flux Richardson Number	$[-]$
S	Sedimentation flux	$[kg/(m^s \cdot kg)]$
St	Stokes number	$[-]$
t	Time	$[s]$
U	Depth averaged horizontal velocity	$[m/s]$
u	Horizontal velocity	$[m/s]$
u	Shear velocity	$[m/s]$
u_*	Shear velocity	$[m/s]$
u_+	Non-dimensional velocity near the wall	$[-]$
v_0	Hopper load parameter	$[m/s]$
v_{sed}	Sedimentation velocity	$[m/s]$
W	Width of the hopper	$[m]$
w	Vertical velocity	$[m/s]$
w_0	Terminal settling velocity single grain	$[m/s]$
w_d	Vertical velocity of the dispersed phase	$[m/s]$
w_f	Vertical velocity of the water phase	$[m/s]$
w_i	Vertical velocity of the interface in the 'Layer Model'	$[m/s]$
w_k	Vertical velocity of fraction k	$[m/s]$
w_s	Hindered settling velocity	$[m/s]$
$w_{k,0}$	Terminal settling velocity single grain of fraction k	$[m/s]$
$w_{k,r}$	Vertical slip velocity of fraction k	$[m/s]$
y_+	Non-dimensional wall distance	$[-]$
z_{bed}	Vertical position of the bed	$[m]$
z_i	Vertical position of interface in the 'Layer Model'	$[m]$

A

(U)RANS models

In Paragraph 3.5 the idea behind turbulence modelling was explained. In `OpenFOAM`, several RANS models are available. A discussion about the different models is given in this appendix.

Standard k-ϵ model
In a k-ϵ model the turbulent eddy viscosity is calculated with:

$$\nu_e = c_\mu \frac{k^2}{\epsilon} \tag{A.1}$$

The k is the turbulent energy and ϵ is the dissipation of turbulent energy. Both are calculated with their own transport equation.

$$\frac{\partial k}{\partial t} + \frac{\partial (uk)}{\partial x} + \frac{\partial (wk)}{\partial z} = \frac{\partial}{\partial x}\left(\frac{\nu_e}{\sigma_k}\frac{\partial k}{\partial x}\right) + \frac{\partial}{\partial z}\left(\frac{\nu_e}{\sigma_k}\frac{\partial k}{\partial z}\right) + P + P_b - \epsilon \tag{A.2}$$

$$\frac{\partial \epsilon}{\partial t} + \frac{\partial (u\epsilon)}{\partial x} + \frac{\partial (\epsilon k)}{\partial z} = \frac{\partial}{\partial x}\left(\frac{\nu_e}{\sigma_\epsilon}\frac{\partial \epsilon}{\partial x}\right) + \frac{\partial}{\partial z}\left(\frac{\nu_e}{\sigma_\epsilon}\frac{\partial \epsilon}{\partial z}\right) + c_{1\epsilon}\frac{\epsilon}{k}P + c_{1\epsilon}c_{3\epsilon}\frac{\epsilon}{k}P_b - c_{2\epsilon}\frac{\epsilon^2}{k} \tag{A.3}$$

The coefficients can for example be found in Celik[15]. The k-ϵ model has certain advantages and disadvantages. It has a good convergence rate and relatively low memory requirements. The biggest disadvantages are inaccuracy with adverse pressure gradients, strong curvature to the flow.

During the validation of his model, Van Rhee[49] also encountered problems with jets. For neutrally buoyant jets the spreading is too small. This resulted in velocities which were too high. For buoyant jets, the spreading is even less than for the neutrally buoyant jets. It is unclear if this was caused by the k-ϵ model or the settings during the simulations.

`OpenFOAM` has two versions of the standard k- model: `kEpsilon` and `buoyantKEpsilon`. In `kEpsilon` the buoyancy term P_b is omitted. In this thesis, `buoyantKEpsilon` is used.

By default, in $c_{3\epsilon}$ is one in `buoyantKEpsilon`. Inspired by the work of Henkes[29], $c_{3\epsilon}$ is also multiplied by a factor $\tanh(v/u)$ in `buoyantKEpsilon`. This means that in horizontal flow $c_{3\epsilon}$ is zero and in vertical flow $c_{3\epsilon}$ is one.
Choi & Garcia[18] gave an overview of different researches about the $c_{3\epsilon}$. For vertical flow, $c_{3\epsilon}$ should indeed be one. For horizontal flow, experiments show mixed results. For stably stratified flows, $c_{3\epsilon}$ varies between zero and 0.5. For unstable horizontal flows, $c_{3\epsilon}$ can be expected to be one.
In figure A.1, it can be seen that $c_{3\epsilon}$ has some influence. A low $c_{3\epsilon}$ causes more stratification. In this thesis, the $\tanh(v/u)$-term is omitted. If that is a good choice can be questioned. Keeping the overview of Choi in mind, a term of $0.3 + 0.7\tanh(v/u)$ would probably be better. Some more research is advisable.

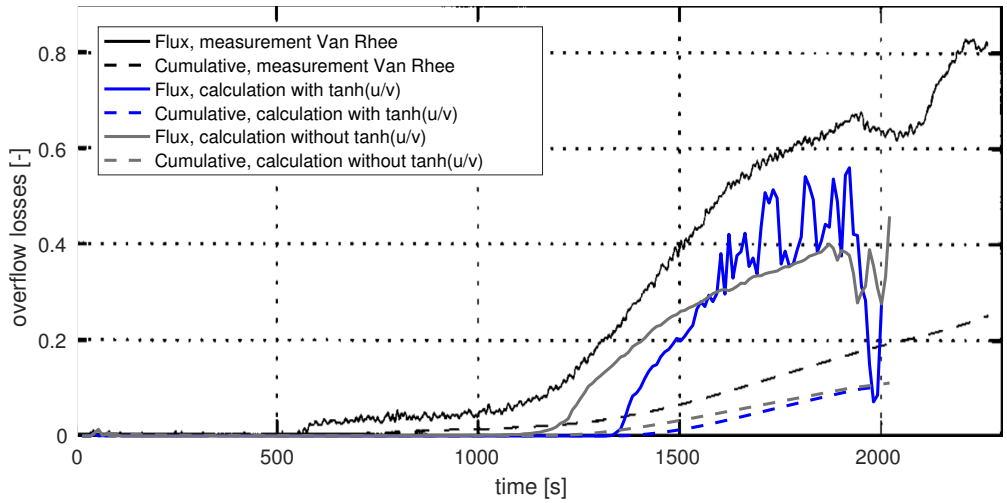

Figure A.1: Influence of $c_{3\epsilon}$ on the overflow losses of Test 8. An inlet of 8 cm, which is rather big, and a very fine mesh was used. The flux is defined as $\frac{\alpha_{out}(t)Q_{out}(t)}{\alpha_{in}(t)Q_{in}(t)}$.

RNG-k-ϵ model

The RNG-k-ϵ model is derived from the instantaneous Navier–Stokes equations by using a mathematical technique called renormalization group theory[58][65]. It has a correction that reduces the modeled turbulence in presence of large vortical structures. Therefore, it has improved accuracy in rotating flows.

One of the differences with the standard k-ϵ model is a varying $c_{2\epsilon}$:

$$c_{2\epsilon}^{*} = c_{2\epsilon} - \frac{\eta\left(1-\frac{\eta}{\eta_0}\right)}{1+\gamma\eta^3} \tag{A.4}$$

Where γ=0.012 and η_0=4.38.

$$\eta = \sqrt{\frac{P}{c_\mu \epsilon}} \tag{A.5}$$

The rest of the coefficients differ only slightly from the standard $k-\epsilon$ model and can for example be found in Han[27] or Van Rhee[49]. Van Rhee[49] did several tests with the RNG-k-ϵ model. In some situations it resulted in improvements, but sometimes the results became worse.

Realizable-k-ϵ model

The realizable-k-ϵ model is another variation on the standard k-ϵ model. The main difference is the calculation of c_μ:

$$c_\mu = \frac{1}{A_0 + A_s\frac{kU^*}{\epsilon}} \tag{A.6}$$

For the determination of A_s, A_0, U^* and the other variables the reader is referred to Shih[57]. Also the transport equations of k and ϵ are different than in the standard k-ϵ model. Shih validated the realizable model for jets. The spreading rate with the realizable model is closer to measurement results the standard k-ϵ model.

k-ω model

In the k-ω model the eddy viscosity is calculated by:

$$\nu_e = \frac{k}{\omega} \tag{A.7}$$

Both the kinetic energy k and The specific dissipation rate ω are calculated with their respective transport equation. The k-ω model is more accurate than k-ϵ near the wall. Therefore, it performs significantly better for adverse pressure gradients and separation. In the freestream outside the boundary

layer, k-ϵ gives better performance since the ω-equation shows a strong sensitivity in this region[34]. In addition, the need of high mesh resolution near the wall causes extra calculation time.

SST-k-ω model
The SST-k-ω model is a combination of k-ω and k-ϵ. k-ω is used near the wall and k-ϵ is used in the rest of the domain. This also leads to more calculation time. Just like the standard k-ω model, it is too much effort to implement this model in `driftFluxFoam`.

B

Relative Viscosity

In the past, much research has been done to determine the relative viscosity. In Figure B.1 a small collection of research is shown. It can be seen that a large scatter is present in different measured results. This is due to the large variation in particle diameters, liquid viscosities and shear rates.

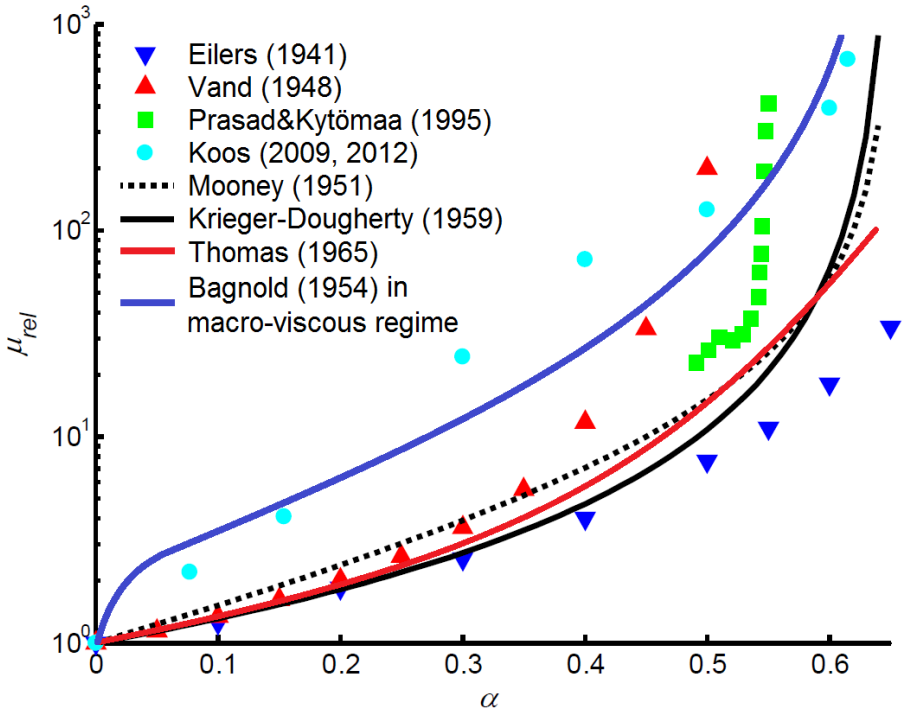

Figure B.1: Relative viscosity in the macro viscous regime. This figure is made by Konijn[31]. Relations of Thomas and Bagnold are added.

In this thesis the relation of Thomas[60] is used:

$$\mu_{rel} = 1 + 2.5\alpha + 10.05\alpha^2 + A\exp(B\alpha) \tag{B.1}$$

In which A and B are 0.00273 and 16.6 respectively. Thomas fitted his relation on measurements of 5 researches. These researches used particle diameters in the range of 0.099 to 124 μm. The accuracy in this range is $\pm$ 13% at a solids concentration of 50% and particle sizes between 0.099 and 240 μm.

Previous research on viscosities mainly has been done with rheometers. Poletto[46] used an alternative method to find the mixture viscosity. By letting a larger particle settle in a mixture of smaller particles

Table B.1: Particle diameter and fluid viscosity of the different experiments

Experiment	$D_{50}[\mu m]$	Liquid viscosity $[mPa \cdot s]$	Apparatus
Eilers (1941)	2.7	>1000	Concentric cylinders
2*Vand (1948)	2*50-80	2*80	Concentric cylinders
			Capillary rheometer
2*Prasad&Kytömaa (1995)	2*3175	55	2*Concentric cylinders
		70	
Koos(2009)	3340	1.7	Concentric cylinders
4*Koos et al. (2012)	6320	10.8	4*Concentric cylinders
	3220	2.5	
	2930	35.5	
	3040	35.5	
Thomas (1965)	0.099-240		
Bagnold (1954)	1320	10-70	

the viscosity of the mixture with the smaller particles could be determined. Poletto compared his measurements with several relations. The emperical relation of Thomas had good agreement with these experiments.

C

Derivation Boundary Conditions

In the log-layer, the dissipation of turbulent kinematic energy equals the production (Brouwers[10]):

$$\rho\epsilon = P \tag{C.1}$$

$$\rho\epsilon = \tau\frac{\partial u}{\partial y} \tag{C.2}$$

$$\rho\epsilon = \rho u_*^2\frac{\partial u}{\partial y} \tag{C.3}$$

$\frac{\partial u}{\partial y}$ can be calculated by taking the derivative of equation 3.33 or 3.40. This both leads to:

$$\frac{\partial u}{\partial y} = \frac{u_*}{\kappa y} \tag{C.4}$$

Equation C.4 can be substituted in equation C.3:

$$\epsilon = \frac{u_*^3}{\kappa y} \tag{C.5}$$

Equation C.1 can also be used to derive an equation for k:

$$\rho\epsilon = P \tag{C.6}$$

$$\rho\epsilon = \tau\frac{\partial u}{\partial y} \tag{C.7}$$

The shear stress can be calculated with:

$$\tau_e = \mu_e\frac{\partial u}{\partial y} = C_\mu\frac{k^2}{\epsilon}\frac{\partial u}{\partial y} \tag{C.8}$$

Substitution in equation C.7 leads to:

$$\rho\epsilon = \rho C_\mu\frac{k^2}{\epsilon}\frac{\partial u}{\partial y}\frac{\partial u}{\partial y} \tag{C.9}$$

Substitution of equation C.4 leads to:

$$\epsilon^2 = C_\mu k^2 \frac{u_*^2}{\kappa^2 y^2} \tag{C.10}$$

By using C.5 we get:

$$\frac{u_*^6}{\kappa^2 y^2} = C_\mu k^2 \frac{u_*^2}{\kappa^2 y^2} \tag{C.11}$$

$$k = \frac{u_*^2}{C_\mu^{0.5}} \tag{C.12}$$

The equations C.5 and C.12 can often be found in literature and are the basis of a lot of CFD-calculations. Van Rhee[49], for instance, uses these equations.

In `OpenFOAM`, the usage of wall functions is slightly different. Since equations C.5 and C.12 can give instabilities, `OpenFOAM` uses a method which is more stable.
During a high-Reynolds calculation, the boundary condition for the k is the `kqRWallFunction`, which is a simple wrapper around the zero-gradient condition. For a high-Reynolds calculation of ϵ the `epsilonWallFunction` is frequently used. To get the `epsilonWallFunction`, equation C.12 needs to be substituted into equation C.5:

$$\epsilon = \frac{C_\mu^{0.75} k^{1.5}}{\kappa y} \tag{C.13}$$

To calculate the k correctly at the first grid-cell, the production of turbulent kinetic energy, P, needs to be calculated correctly. `epsilonWallFunction` therefore does a correction for the production. This seems very easy, because in the log-layer the production equals the dissipation (calculated with equation C.13). `OpenFOAM` does something different, though:

$$P = \tau \frac{\partial u}{\partial y} = \mu_{eff} \frac{\partial u}{\partial y} \frac{\partial u}{\partial y} \tag{C.14}$$

$$P = \mu_{eff} \frac{\partial u}{\partial y} \frac{u_*}{\kappa y} \tag{C.15}$$

In which $\mu_{eff} = \mu_e + \mu_{mixture}$ and μ_e is the turbulent eddy viscosity and $\mu_{mixture}$ is the viscosity of the fluid. Interestingly, only the eddy viscosity is sometimes taken into account to calculate the production of turbulent energy (for example in C.8). In other instances, both the fluid viscosity and eddy viscosity are taken into account (equation C.3 and C.14). Equation C.12 can be substituted for u_*:

$$P = \mu_{eff} \frac{\partial u}{\partial y} \frac{k^{0.5} C_\mu^{0.25}}{\kappa y} \tag{C.16}$$

To calculate the velocity in the first grid-cell, the viscosity at the wall needs to be calculated correctly. These corrections are done in the boundary conditions for the viscosity. All these boundary conditions rely on the following principle:

$$\tau = \mu_{wall} \frac{\partial u}{\partial y} \tag{C.17}$$

$$\rho_w u_*^2 = \mu_{wall} \frac{u}{y} \tag{C.18}$$

$$\rho_w u_*^2 = \mu_{wall} \frac{u}{y} \tag{C.19}$$

$$\mu_{wall} = \frac{\rho_c y u_*^2}{u} \tag{C.20}$$

Now, a smooth or rough wall function can be used to get a formulation of μ_{wall}. For a smooth wall, equation 3.33 is for example used:

$$\mu_{wall} = \frac{\rho_w \kappa y u_*}{\ln(E y_+)} = \frac{\mu_w \kappa y_+}{\ln(E y_+)} \tag{C.21}$$

$$\nu_{eff} = \frac{\nu_w \kappa y_+}{\ln(E y_+)} \tag{C.22}$$

In this thesis the `nutkRoughWallFunction` is used. The `nutkRoughWallFunction` uses equation C.22, but then divides E by a factor $1 + Ck_s^+$ just like in formula 3.39. This factor $1 + Ck_s^+$ accounts for the roughness.

D

Implementation Moving Mesh

To implement a moving mesh in `OpenFOAM`, the height of the cells need to be adjusted. Figure D.1 shows how the cell properties are calculated in `OpenFOAM`. First, the face centres and face areas are calculated in the function `calcFaceCentresAndAreas()`. The coordinates of the corner points are used for this. After that the cell centres and cell volumes are calculated in the function `calcCellCentresAndVols()`. The other functions use these values.

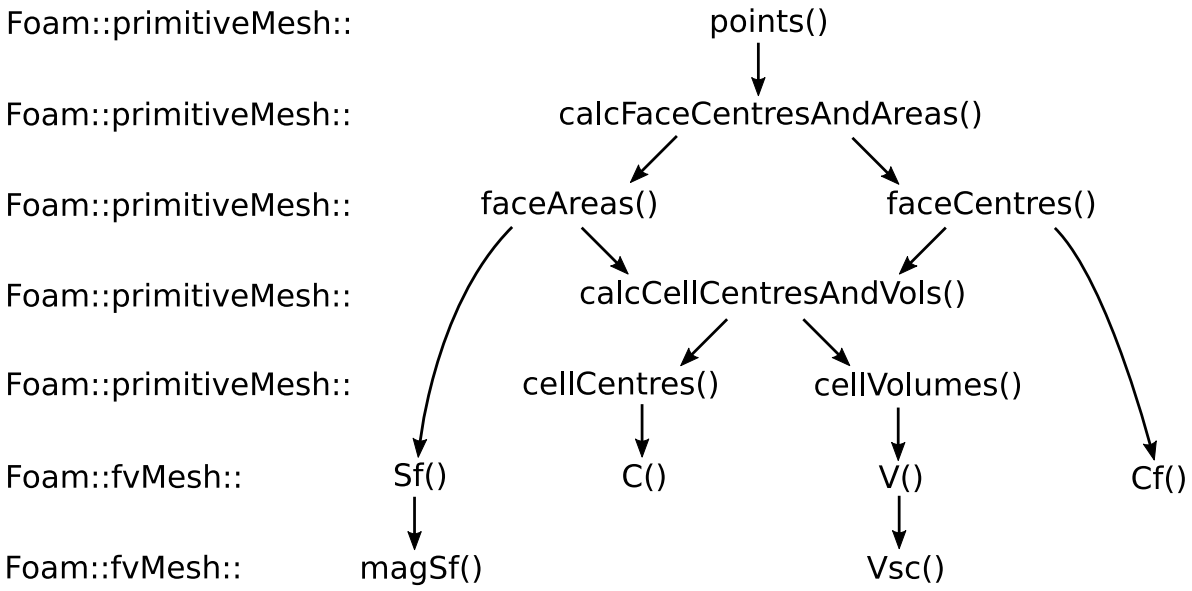

Figure D.1: Overview of how the cell properties are calculated in `OpenFOAM`

It seems easiest to adjust the values in the functions `points` or `calcFaceCentresAnd- Areas()`. However, in `primitiveMesh` the order of the cell and face numbers is different than in `fvMesh`. Therefore, it was decided to change the functions in `fvMesh`. Fortunately, `OpenFOAM` uses a lot of pointers. The fields made in `Sf()`, `magSf()`, `C()`, `V()`, `Vsc()` and `C()` also use pointers. By making these pointers public, the fields in these functions can be adjusted every time step.

E

Numerical Error Analysis Settling Simulations

In Chapter 6.1, experiments with settling columns were used to validate the settling in the 2DV model. To do this validation, it was first needed to investigate the numerical error. That analysis is shown in this appendix.

The numerical uncertainty of a CFD prediction is composed of three contributions: the round-off error, the iterative error and the discretization error.
The round-off error is caused by the precision of the machine. For example, *a double* calculated by a 32 bit machine has 15 digits. This is enough to assume that the round-off error in this case is negligible.
One has an iterative error when an equation is solved implicitly. The equation is written in matrix form: $A\Psi = B$. This matrix system is solved iteratively until the error is smaller than the given tolerance. So depending on a given tolerance the iterative error will be big or small. A small tolerance gives a small iterative error, but it will cause the calculation time to be longer.
The discretization error is caused by the approximation of the derivatives in the equations. The error depends on Δx, Δt and the type of the schemes used.

First, the influence of the mesh, or in other words Δx, was investigated (Figure E.1). A Δx of 0.01 m is sufficient, which results in 150 cells over the height.

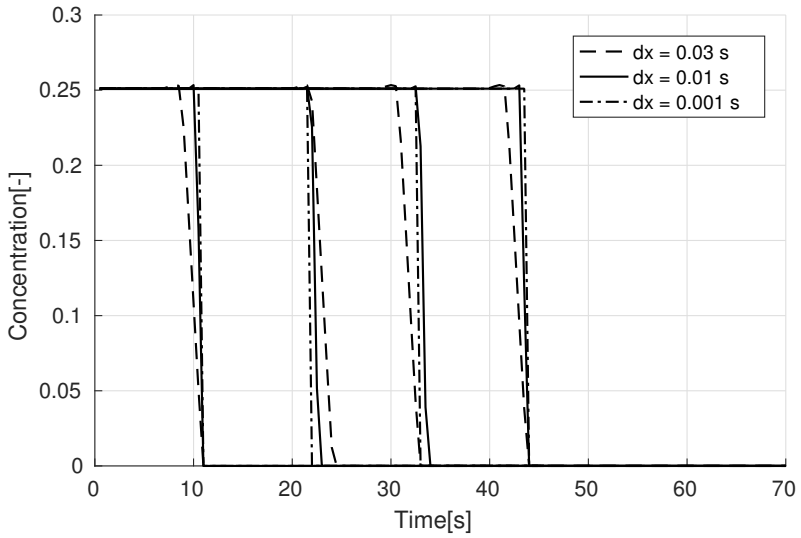

Figure E.1: Experiment 42 of Runge: influence of Δx, concentration at z = 0.9 m, z = 1.05 m, z = 1.20 m and z = 1.35 m, $D_{50} = 270\ \mu m$

Secondly, the time step is investigated. The results are shown in Figure E.2. The time step should be made $0.1\ s$ or lower.

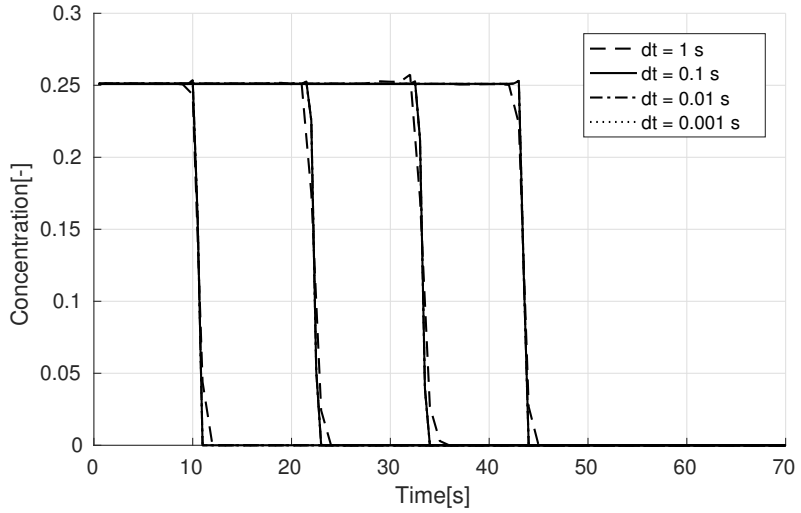

Figure E.2: Experiment 42 of Runge: influence of Δt, concentration at z = 0.9 m, z = 1.05 m, z = 1.20 m and z = 1.35 m, $D_{50} = 270\ \mu m$

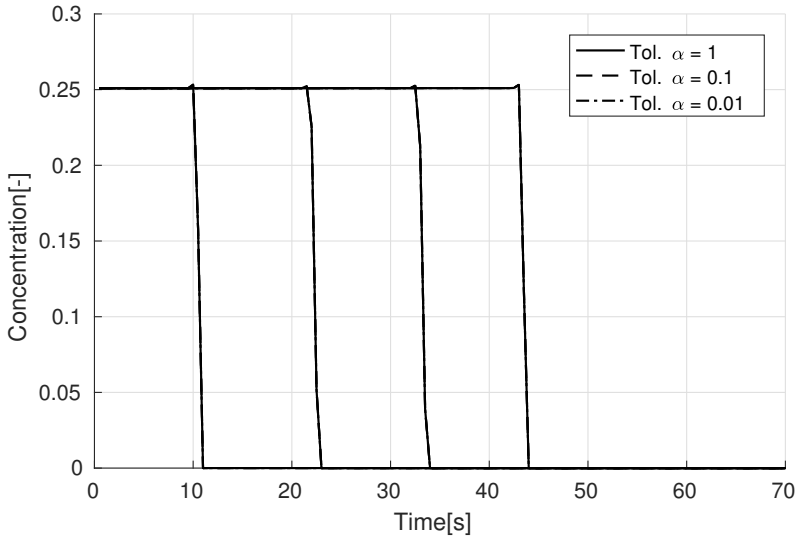

Figure E.3: Experiment 42 of Runge: influence of tolerance for the concentration, concentration at z = 0.9 m, z = 1.05 m, z = 1.20 m and z = 1.35 m, $D_{50} = 270\ \mu m$

At last, the iteration errors are investigated by varying the tolerances. The concentration tolerance is varied in Figure E.3. It can be seen that the tolerance has no influence, which is surprising. The reason can be found when a look is taken at the log file of the simulations. In the log files, many lines like the one below can be found:

```
smoothSolver: Solving for alpha.sludge, Initial residual = 0.00954204, Final
residual = 7.1623e-17, No Iterations 1
```

At least, one iteration is done. In that iteration, a very low error (or residual) is reached as can be seen in the line above. It is not needed to get a lower error, so the given tolerance for the concentration is irrelevant in case of the settling simulations.

The same holds for the tolerance of the pressure. A typical line in one of the log files is:

```
DICPCG: Solving for p_rgh, Initial residual = 0.0974585, Final residual =
8.06646e-18, No Iterations 1
```

One iteration is sufficient. It does not matter which tolerance is chosen to solve the pressure equation.

Table E.1: Overview of the settings

Setting	**Value**
Δt	10^{-1} s
Δx	0.01 m
tolerance p_{rgh}	Irrelevant
tolerance α	Irrelevant

F

Settling experiments

In this appendix, different settling experiments are compared with the model in OpenFOAM and a simple 1DV-model (equation 6.1). The terminal settling velocities in Table F.1 are calculated with the relation of Ferguson & Church[21] with $C_1 = 18$ and $C_2 = 1.0$.

Table F.1: Experiments of Runge[54] and Van Rhee[49]

Experiment	$D_{50}[\mu m]$	α_0[%]	T[^oC]	α_{max}	w_0[mm/s]
42 of Runge	270	25.1	24.7	-	37.4
46 of Runge	270	16.0	21.7	-	36.1
50 of Runge	270	5.5	17.9	-	34.2
108 of Runge	80	24.3	24.2	-	5.52
112 of Runge	80	15.2	21.2	-	5.19
116 of Runge	80	4.6	18.8	-	4.92
1 of Van Rhee	80	26.16	26.44	55.86	5.76
2 of Van Rhee	80	32.57	29.51	55.86	6.08
3 of Van Rhee	160	14.65	17.47	55.86	15.8
4 of Van Rhee	160	31.64	27.63	55.86	18.7

According to Runge, the c_0 in Experiment 50 was 5.5%. Figure F.4 shows a different α_0. It is unclear what the real α_0 was. The same can be observed for Experiment 116.

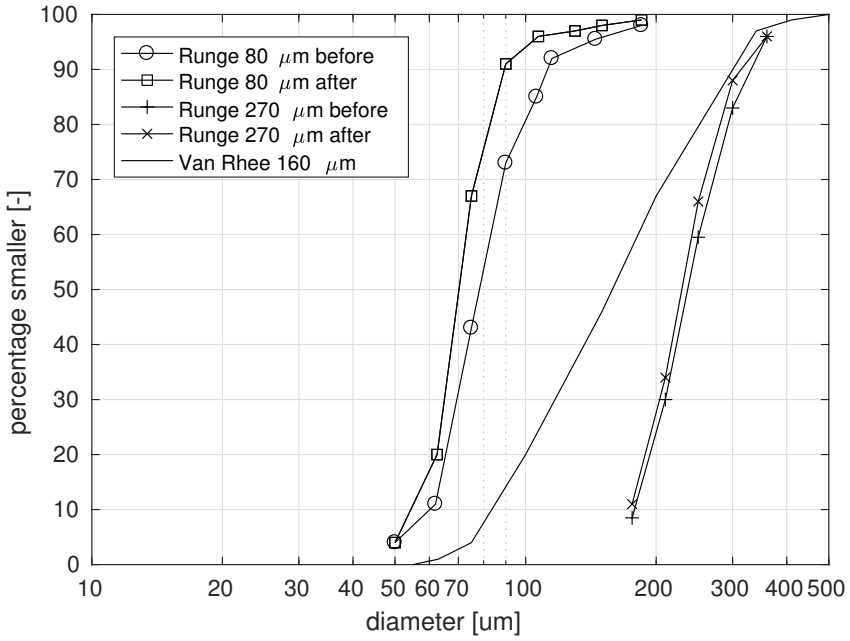

Figure F.1: Particle Size Distributions of Runge and Van Rhee

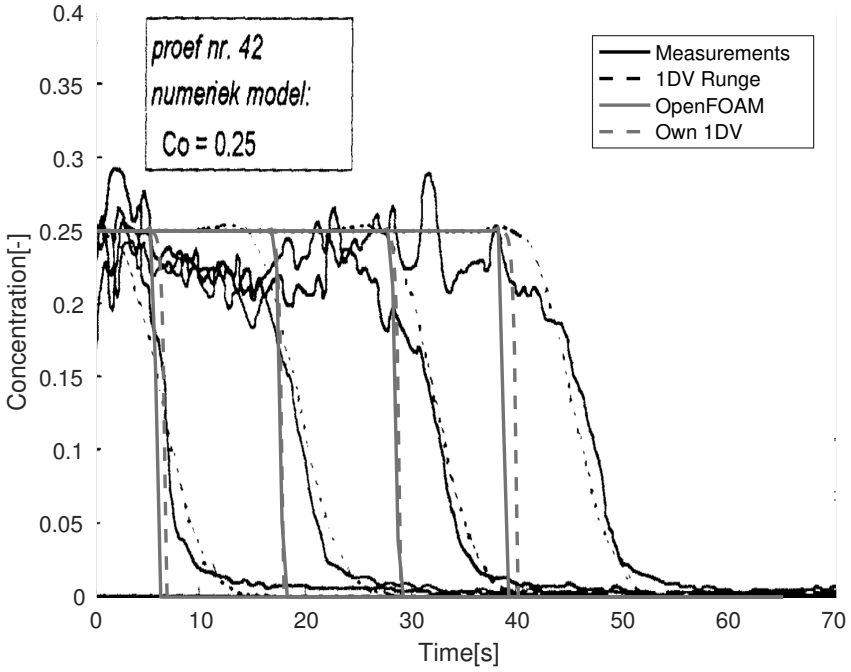

Figure F.2: Experiment 42 of Runge, sensors at z = 0.9 m, z = 1.05 m, z = 1.20 m and z = 1.35 m are used, $D_{50} = 270\ \mu m$

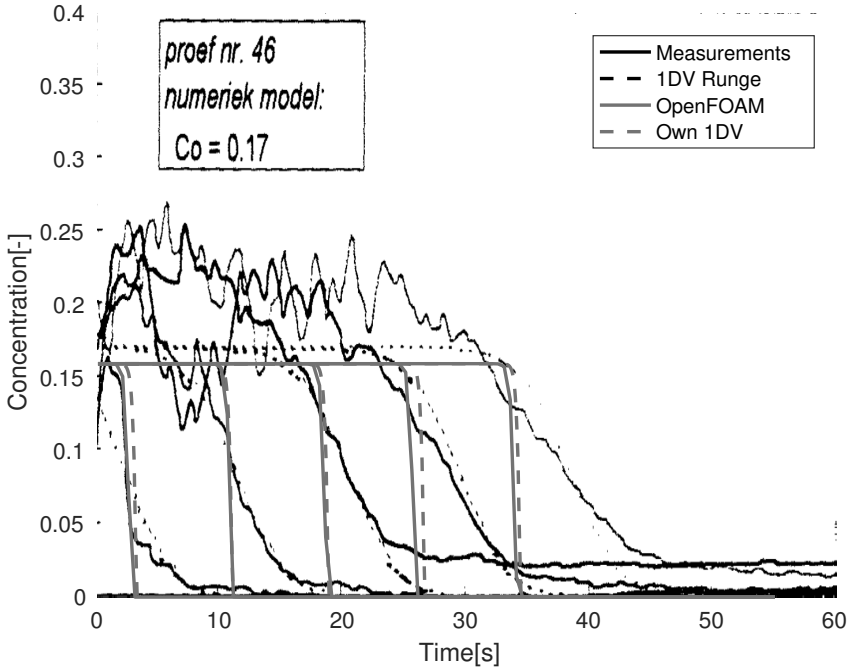

Figure F.3: Experiment 46 of Runge, sensors at z = 0.75 m, z = 0.9 m, z = 1.05 m, z = 1.20 m and z = 1.35 m are used, $D_{50} = 270\ \mu m$

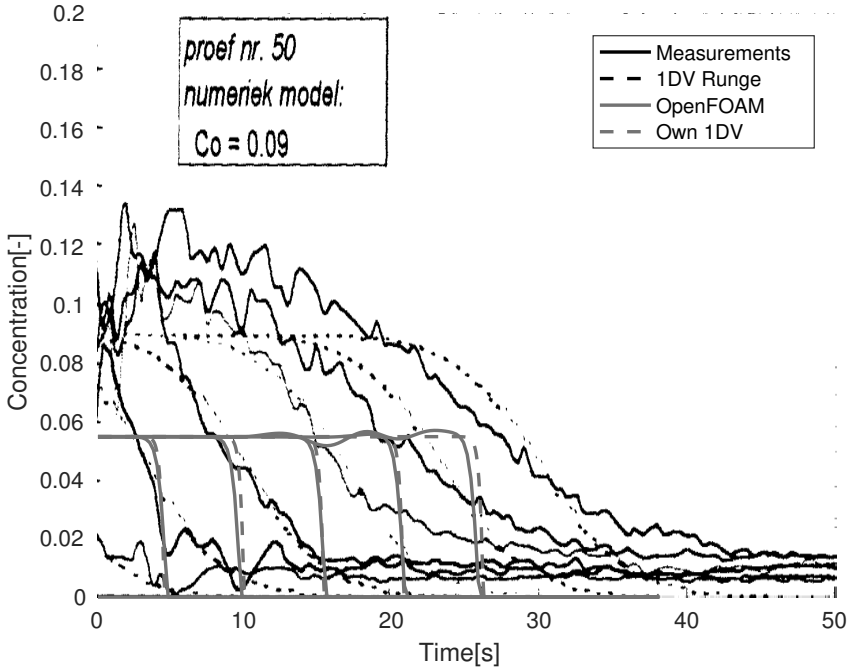

Figure F.4: Experiment 50 of Runge, sensors at z = 0.45 m, z = 0.60 m, z = 0.75 m, z = 0.90 m, z = 1.05 m and z = 1.20 m are used, $D_{50} = 270\ \mu m$

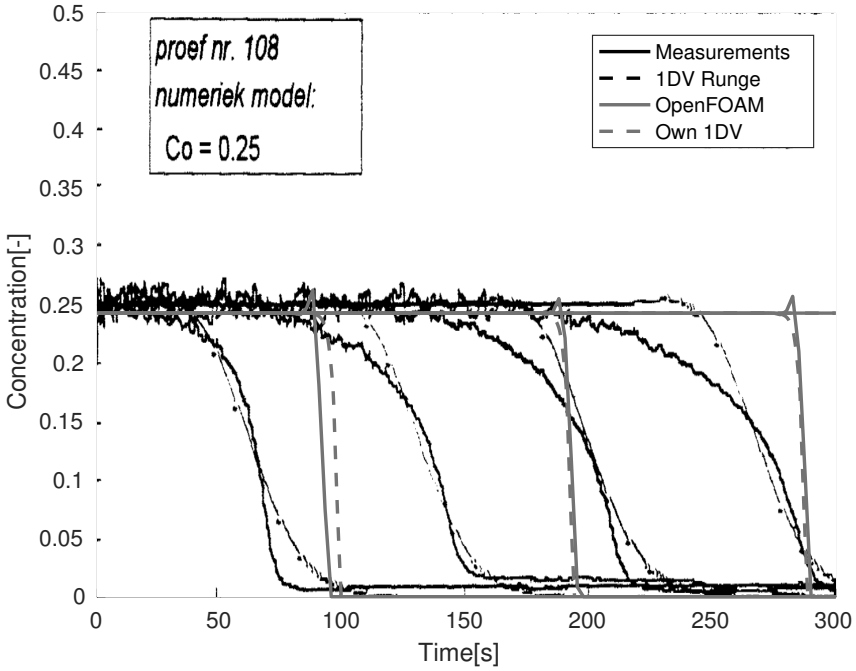

Figure F.5: Experiment 108 of Runge, sensors at z = 0.9 m, z = 1.05 m, z = 1.20 m and z = 1.35 m are used, $D_{50} = 80\ \mu m$

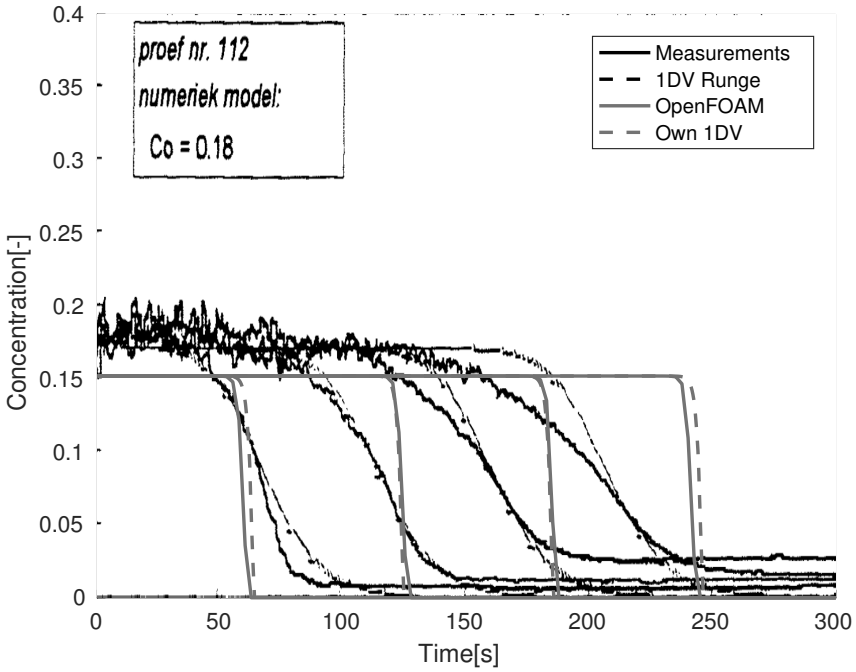

Figure F.6: Experiment 112 of Runge, sensors at z = 0.9 m, z = 1.05 m, z = 1.20 m and z = 1.35 m are used, $D_{50} = 80\ \mu m$

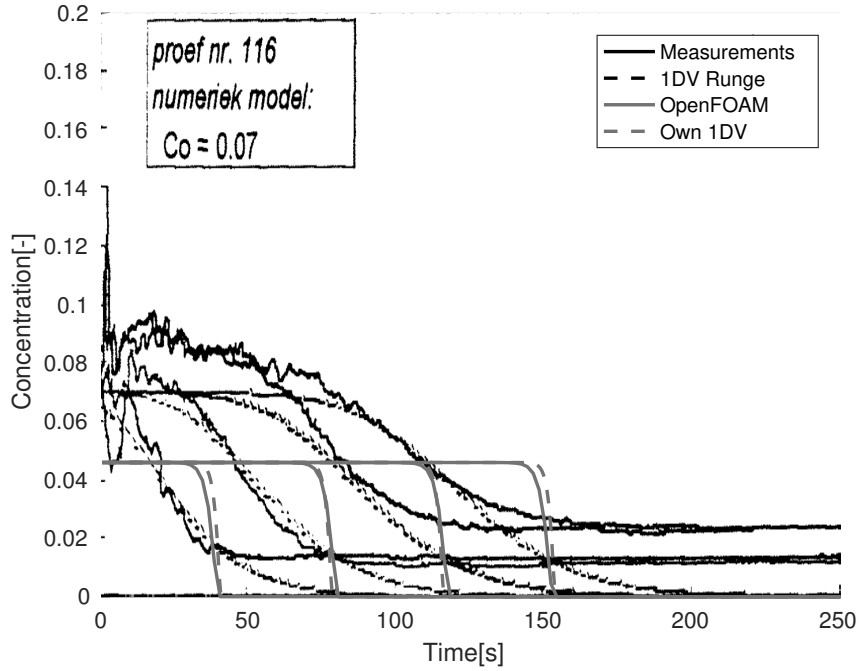

Figure F.7: Experiment 116 of Runge, sensors at z = 0.9 m, z = 1.05 m, z = 1.20 m and z = 1.35 m are used, $D_{50} = 80\ \mu m$

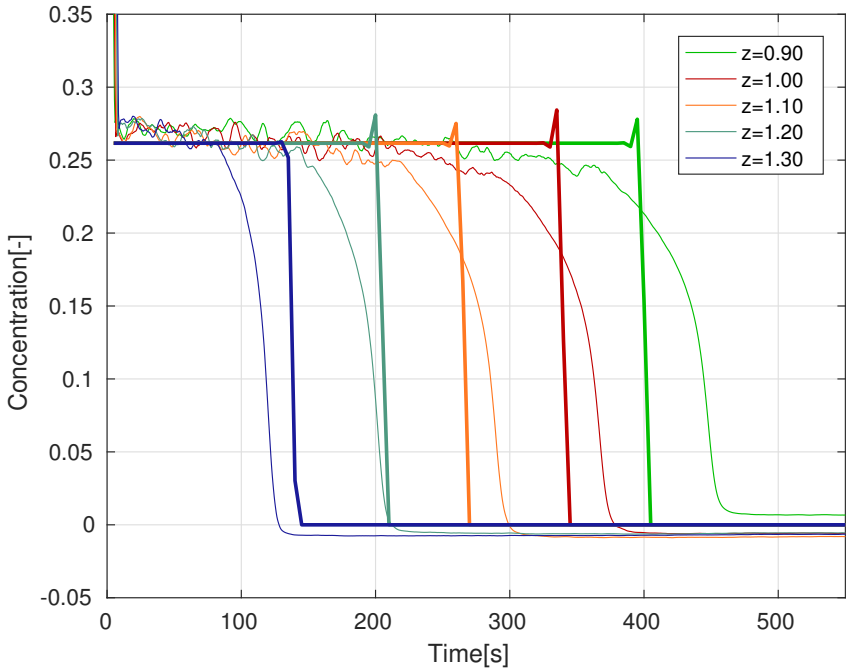

Figure F.8: Experiment 1 of Van Rhee (thin lines) compared with OpenFOAM (thick lines), $D_{50} = 80\ \mu m$

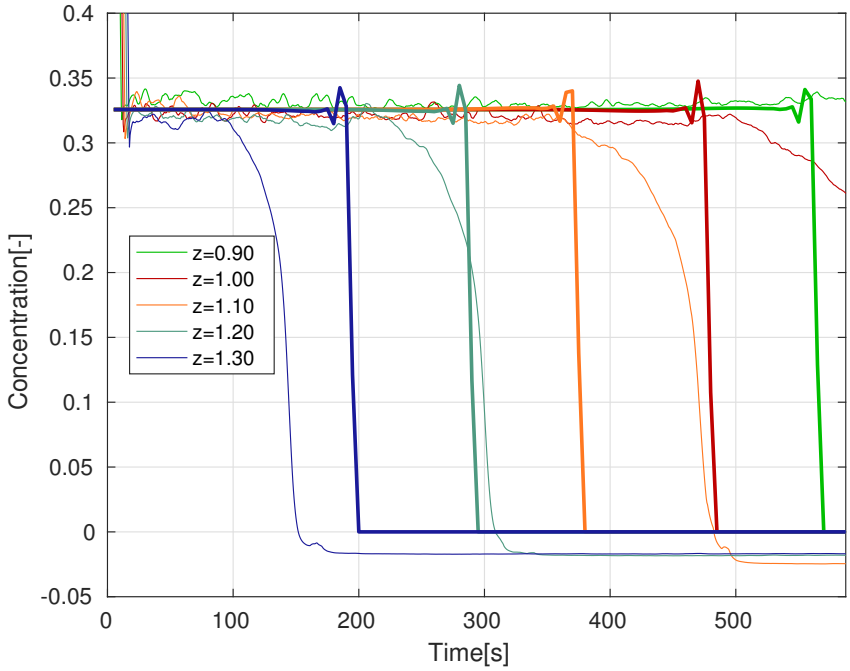

Figure F.9: Experiment 2 of Van Rhee (thin lines) compared with OpenFOAM (thick lines), $D_{50} = 80\ \mu m$

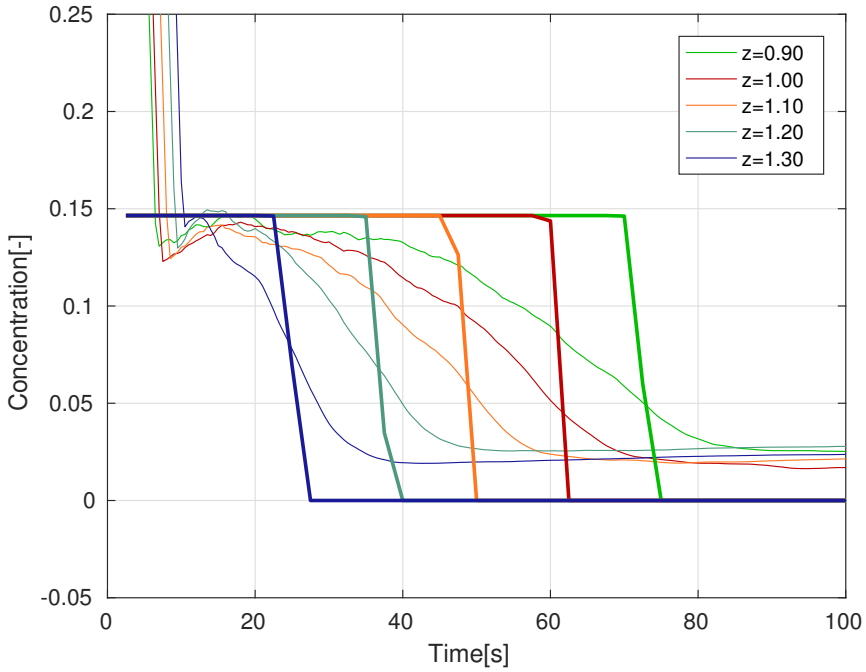

Figure F.10: Experiment 3 of Van Rhee (thin lines) compared with OpenFOAM (thick lines), $D_{50} = 160\ \mu m$

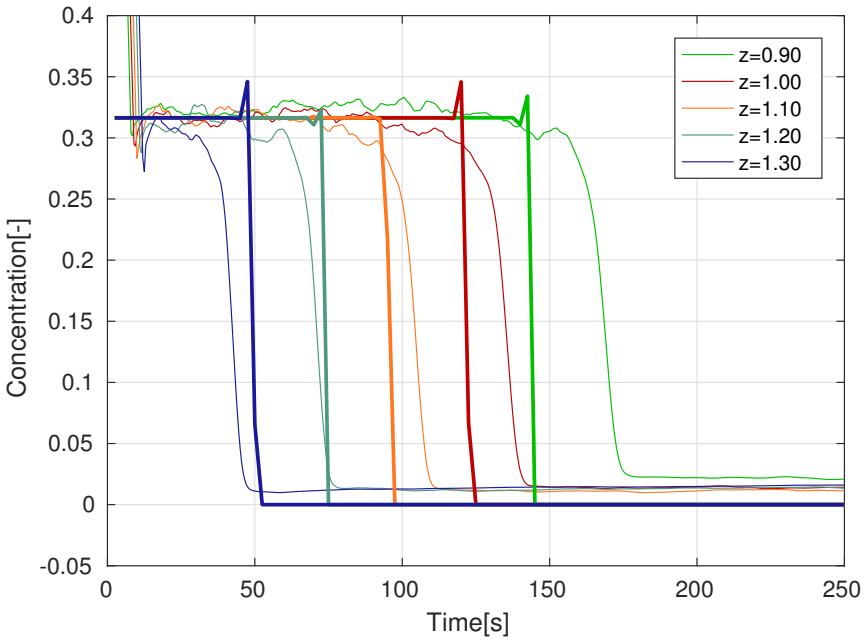

Figure F.11: Experiment 4 of Van Rhee (thin lines) compared with OpenFOAM (thick lines), $D_{50} = 160\ \mu m$

G

Numerical Error Analysis Sedimentation Simulations

In Chapter 6.2, the closed flume experiments of Van Rhee[49] were used to validate the sedimentation of the 2DV model. To do this validation, it was first needed to investigate the numerical error. That analysis is shown in this appendix.

In Appendix E, a numerical error analysis was done for the settling simulations. The same approach is used in this appendix.

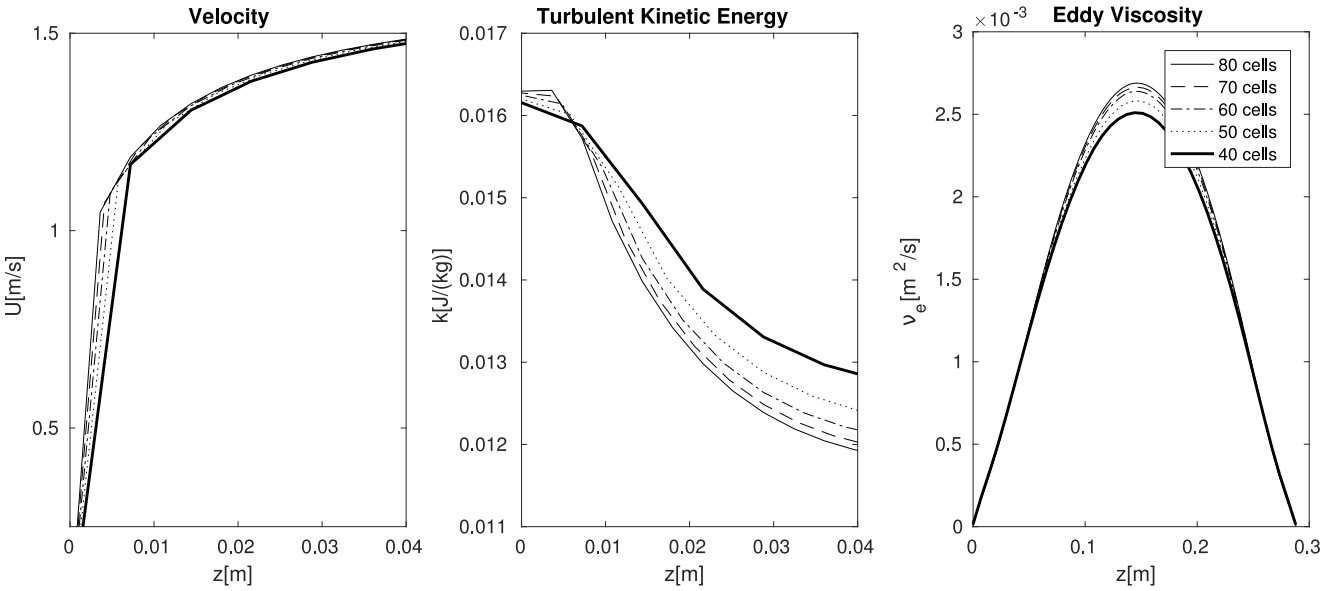

Figure G.1: Influence of the number of cells in vertical direction

First, the influence of the mesh, or in other words Δx, was investigated (Figure G.1). Next to the velocity, the k and ν_e were also observed, since these are important parameters for diffusion and erosion. It was chosen to use 80 cells in vertical direction.

Secondly, the influence of the tolerance for p_{rgh} on the sedimentation velocity is investigated. Next to the tolerance, the number of inner and outer correctors can be specified in `OpenFOAM`. Figure G.2 shows the influence of the tolerance with only one outer corrector. The simulations were instable with one **inner** corrector. Whether two or three inner correctors are used doesn't matter; it gives the same result.

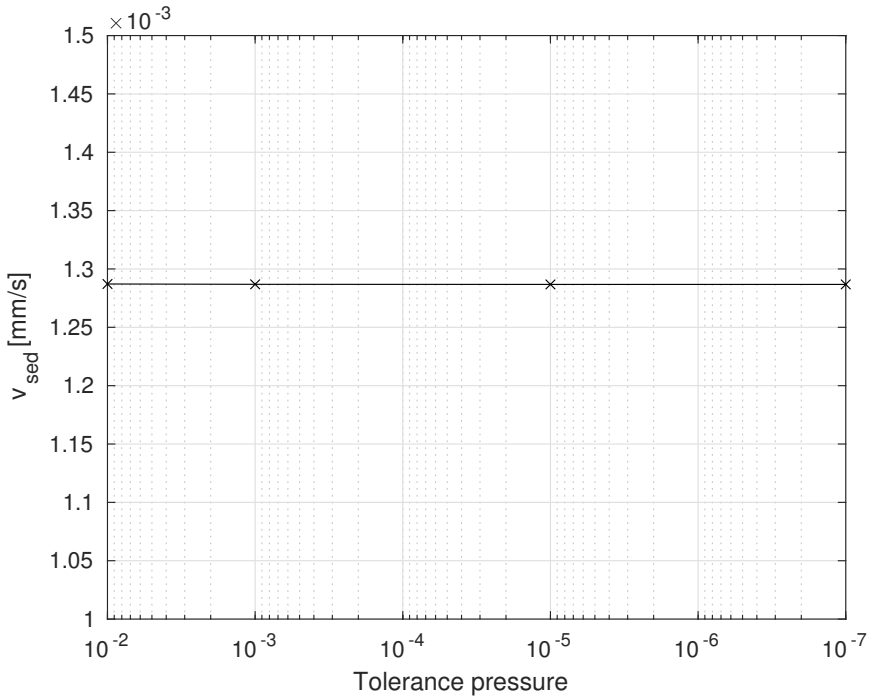

Figure G.2: Experiment 18: influence of the tolerance of p_{rgh} for three inner correctors and one outer corrector (dt = 10^{-3} s)

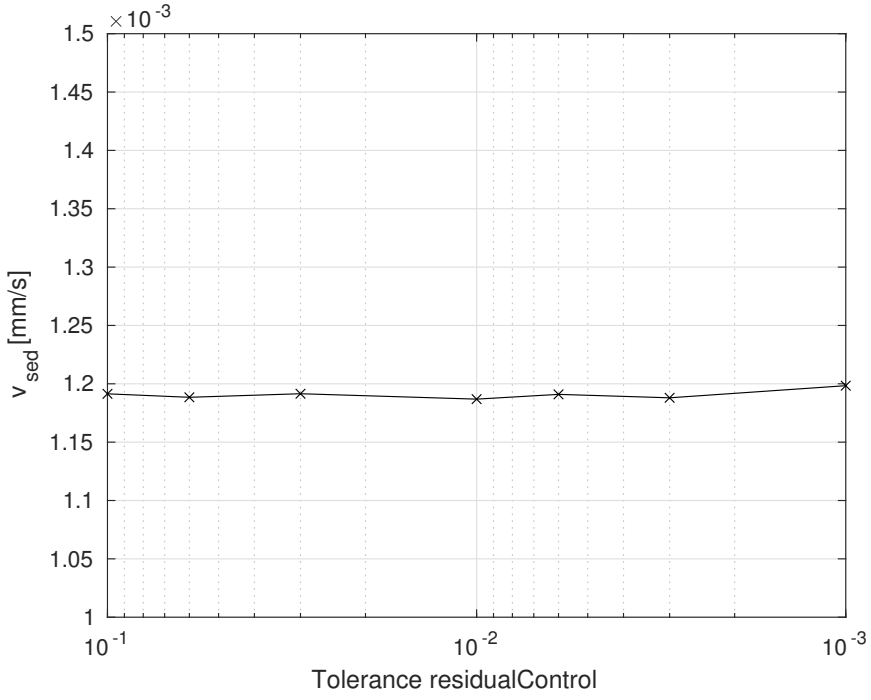

Figure G.3: Experiment 18: influence of the tolerance of p_{rgh} for three inner correctors and multiple outer correctors (tolerance final iteration = 10^{-7}, dt = 10^{-3} s)

With only one outer corrector it is, however, uncertain if convergence is reached. Figure G.3 shows the influence of the outer correctors. The x-axis shows the tolerance of the residualControl. The solver keeps iterating until the *initial residual* of an iteration comes under the tolerance of the residualControl; then a new time step is started. No convergence was reached with one or two inner correctors; three inner correctors were needed. Comparing Figures G.2 and G.3, it can be concluded that only one outer corrector is not enough. With one outer corrector the sedimentation velocity is 1.28 mm/s. With multiple outer correctors the sedimentation velocity is approximately 1.19 mm/s.

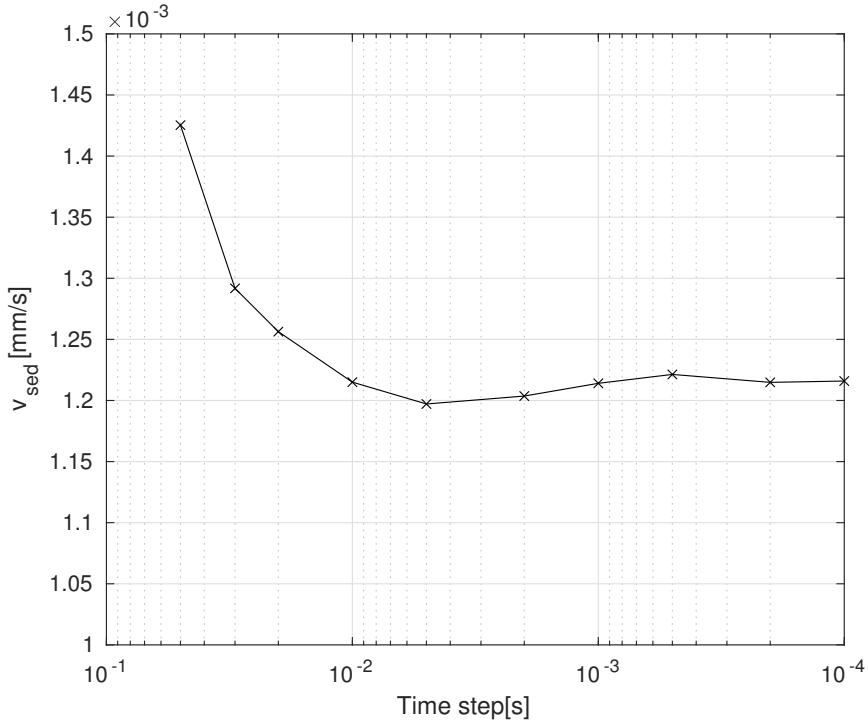

Figure G.4: Experiment 18: influence of the time step (three inner correctors, tolerance final iteration = 10^{-7}, residualControl: 10^{-3})

In addition, the influence of the time step is investigated. The results are shown in Figure G.4. Ideally, the time step should be made 10^{-3} s or even lower. This would cause huge calculations times, though. It was decided to use a time step of 10^{-2} s. This still lies within the expected accuracy.

At last also the influence of the tolerance for the concentration was investigated. It appeared that for smaller tolerances mass disappeared. To reach mass convergence at least a tolerance of 10^{-7} was needed.

Table G.1: Overview of the advised settings

Setting	**Value**
dt	10^{-2} s
dx	80 cells over the height
tolerance p_{rgh}	10^{-7}
inner correctors	3
outer correctors	residualControl: tolerance 10^{-3}
tolerance α	10^{-8}

H

Sedimentation Experiments

These experiments were executed in the closed flume of figures 2.4 and 2.5 by Van Rhee. Experiments 57 to 62 were not executed by Van Rhee, but only simulated in `OpenFOAM`.

Experiment	$\alpha_{in}[-]$	$U_{start}[-]$	$U[-]$	$V_{sed,1-3}[m/s]$	$V_{sed,2-4}[m/s]$
1	0.053333	2.6384	-0.0000555	0.00096154	0.00075758
2	0.051515	2.6384	0.39143	0.0010526	0.00083333
3	0.054545	2.6496	0.69964	0.0010309	0.0009009
4	0.055152	2.683	0.85561	0.00077519	0.00069444
5	0.053939	2.644	1.0841	0.00056818	0.00054645
6	0.05697	2.6551	1.1854	0.00028736	0.00026455
7	0.05697	2.6551	1.2741	0	0
8	0.053939	3.6146	-0.00030527	0.00095238	0.00077519
9	0.055758	3.5811	0.289	0.0011111	0.00096154
10	0.056364	3.6257	0.44397	0.0010204	0.0009901
11	0.056364	3.5755	0.61514	0.0012658	0.0010989
12	0.056364	3.6146	0.85244	0.00096154	0.00084034
13	0.058788	3.6034	1.0724	0.00013908	0.00011976
14	0.058788	3.6034	1.186	0	0
15	0.15273	2.7332	0.0007493	0.0025641	0.0025
16	0.15152	2.6886	0.48612	0.0025641	0.0021277
17	0.15394	2.7277	0.76464	0.0017241	0.0015873
18	0.15636	2.6998	0.99605	0.0010638	0.00087719
19	0.15879	2.7053	1.1998	0.00097087	0.00097087
20	0.16061	2.7053	1.3089	0.00065789	0.00039683
21	0.16061	2.7053	1.3762	0	0
22	0.1497	3.6759	0.00088805	0.0027778	0.0026316
23	0.14909	3.6146	0.42354	0.0018182	0.0021739
24	0.1503	3.6871	0.59538	0.0021277	0.0019608
25	0.15455	3.6982	0.99475	0.0013333	0.0012195
26	0.15758	3.6815	0.98484	0.0010101	0.0010989
27	0.15879	3.6871	1.0979	0.0004329	0.00028011
28	0.15879	3.6871	1.2947	0	0
29	0.2497	2.6886	0.0016651	0.0021739	0.0023256
30	0.24303	2.6329	0.41854	0.0022222	0.0023256
31	0.24667	2.6161	0.71255	0.0015873	0.0017544
32	0.24364	2.6551	1.0408	0.0011628	0.0011236

33	0.24121	2.7053	1.2014	0.001	0.00087719
34	0.24182	2.6942	1.3362	0.00028902	0.00017921
35	0.24182	2.6942	1.4411	0	0
36	0.23758	3.6146	0.0062441	0.0025641	0.0029412
37	0.24788	3.6146	0.39235	0.0023256	0.0025
38	0.25758	3.6703	0.71937	0.0021277	0.0020408
39	0.25818	3.6592	0.91813	0.0013889	0.0012346
40	0.25818	3.6536	1.1261	0.00040161	0.00025189
41	0.25576	3.6703	1.1991	0.00026316	0.00034247
42	0.25576	3.6703	1.1816	0	0
43	0.33333	2.6998	0.0037187	0.0023256	0.0022727
44	0.33333	2.6998	0.54115	0.0020833	0.0018868
45	0.3303	2.75	0.86854	0.0013889	0.0013699
46	0.32606	2.7444	1.0175	0.00081967	0.00077519
47	0.32061	2.7165	1.2735	0.00053191	0.0003876
48	0.32061	2.75	1.4239	0.00010482	0.0001032
49	0.32061	2.75	1.5245	0	0
50	0.32606	3.6201	0.0076039	0.0028571	0.0026316
51	0.32727	3.6425	0.27285	0.002381	0.0027027
52	0.32848	3.6536	0.68236	0.0022222	0.0025641
53	0.32606	3.6536	1.0176	0.0013514	0.0011905
54	0.3297	3.6034	1.2587	0.00056497	0.00036765
55	0.32848	3.6982	1.3681	0.00027855	0.00019231
56	0.32848	3.6982	1.4831	0	0
57	0.05697	2.6551	1.35	0	0
58	0.058788	3.6034	1.35	0	0
59	0.05697	2.6551	1.4	0	0
60	0.058788	3.6034	1.4	0	0
61	0.16061	2.7053	1.45	0	0
62	0.15879	3.6871	1.45	0	0

Table H.1: Measurements of Van Rhee

I

Numerical Error Analysis Hopper Simulations

In Appendix E, a numerical error analysis was done for the settling simulations. In this appendix, the same is done for the hopper simulations.
Again, first the mesh is analyzed. Both at the beginning and the end, the mesh is finer. Especially, near the inlet a fine mesh is needed. It is investigated how many cells are needed in the refined section near the inlet: 8, 12, 16 or 20. Half of these cells are under the inlet, and the other half next to it. The dimensions of the mesh are 12 x 2.25 m (L x H). Over the height, 60 cells are used.

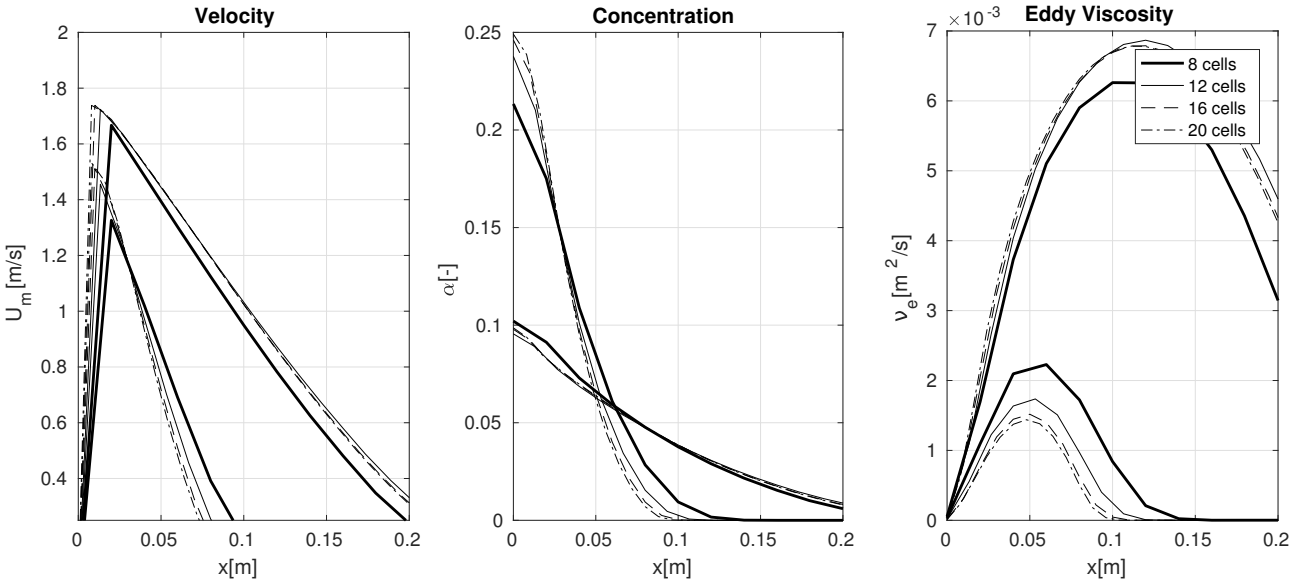

Figure I.1: Influence of the mesh at z=1.8m and z=0.5m.

In Figure I.1, it can be observed that 16 cells in the refined section gives sufficient accuracy. However, after some simulations it appeared that 16 cells could give instabilities, so it was chosen to use 20 cells in the refined section.
Van Rhee[49] concluded that for the middle section, cells with a width of 0.42 m still gave sufficient accuracy. He also concluded that over the height 60 cells were needed. For this analysis, the reader is directed to page 187 of Van Rhee[49]. In this thesis, also 60 cells over the height are used. For reasons of stability cells of 0.25 cm instead of 0.42 cm were used in the middle sections. This gives the mesh of Figure 6.5.

Next, the time step is investigated. From Figures I.2 and I.3, it can be concluded that a time step of 0.01 s is needed.

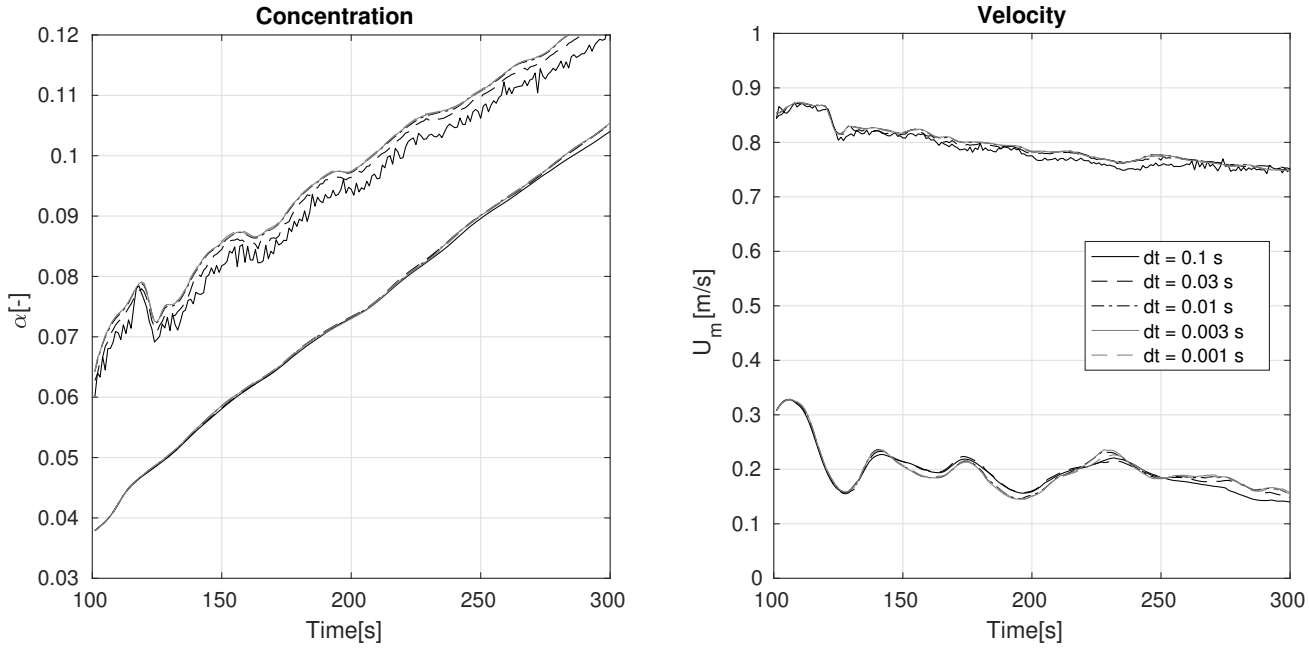

Figure I.2: Influence of the time step on the concentration and velocity in the points (0.08,1) and (3,0.2). Tolerances: three inner correctors, tolerance final iteration = 10^{-7}, residualControl: 10^{-3}.

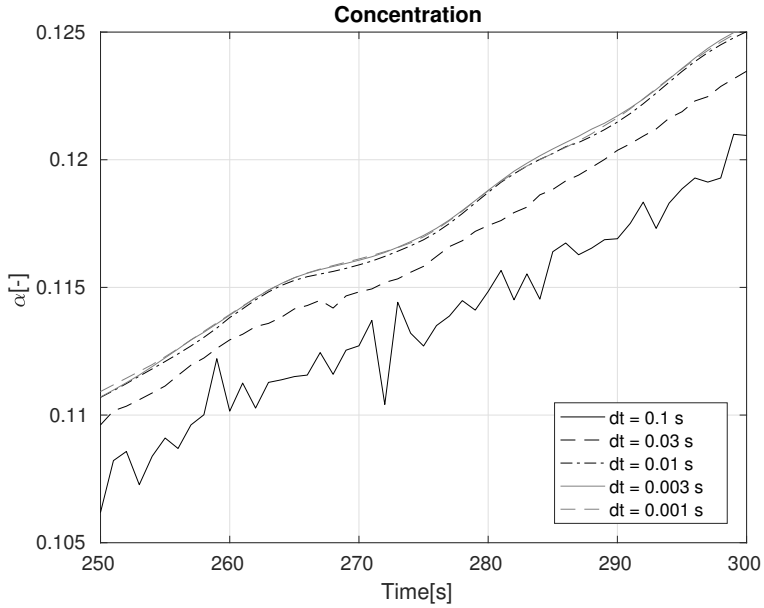

Figure I.3: Close-up of figure I.2

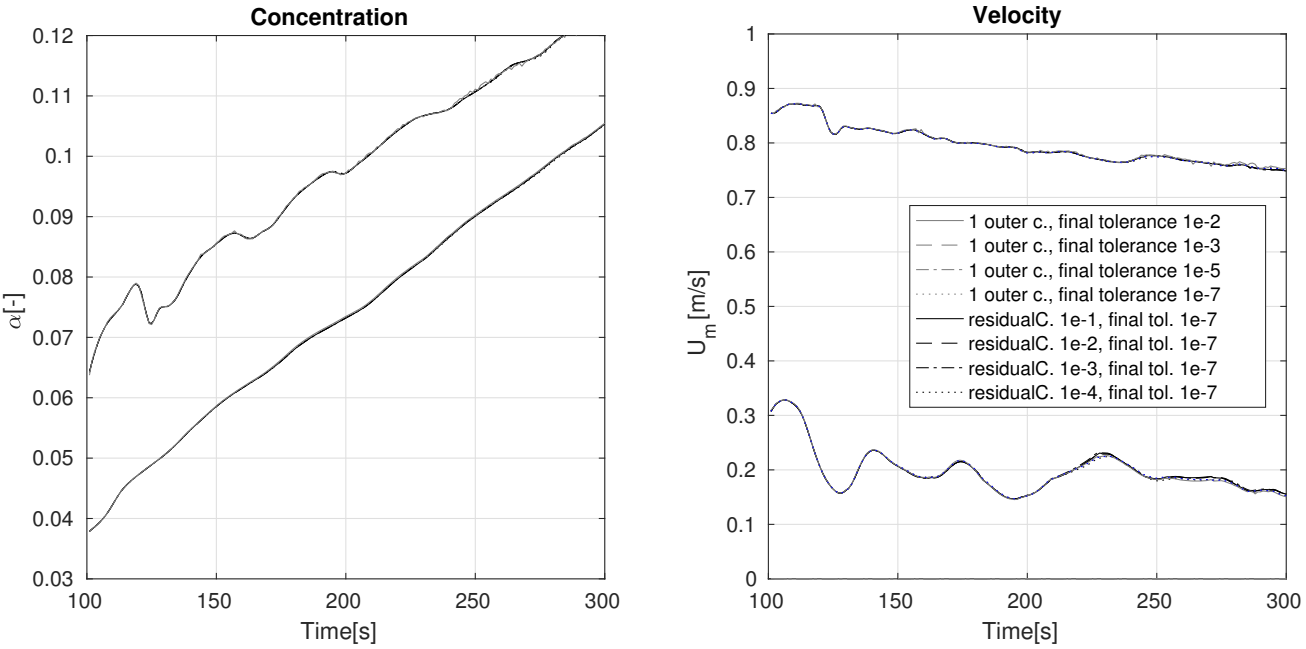

Figure I.4: Influence of the pressure tolerance. Settings: dt=0.01 s, three inner correctors.

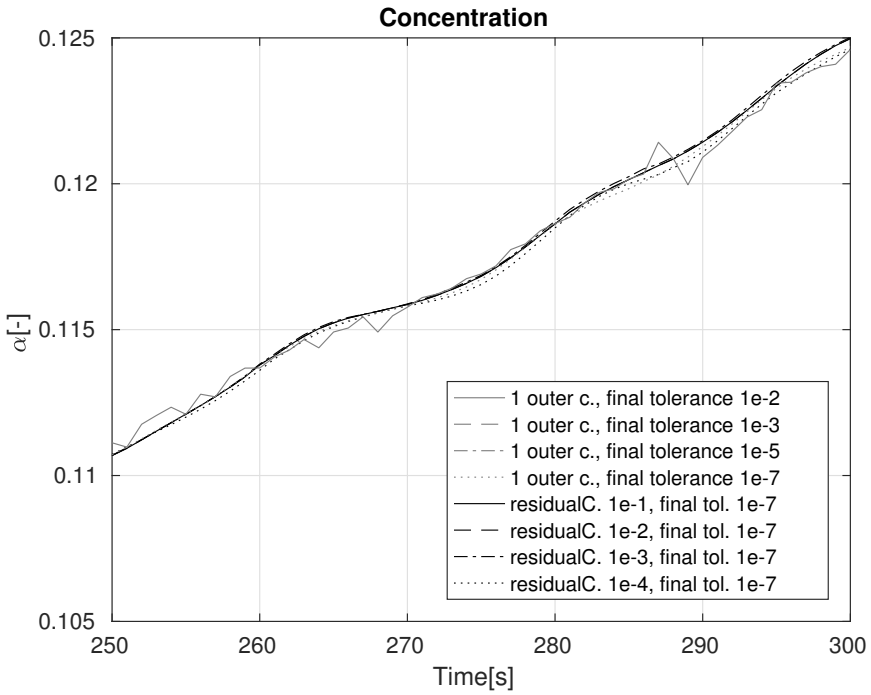

Figure I.5: Close-up of Figure I.4

In Figures I.4 and I.5, the influence of the pressure tolerance is shown. It can be seen that not a very strict tolerance is needed. When only one outer corrector is used a pressure tolerance of 10^{-3} is already sufficient. The usage of only one outer correcter can be risky, since it is unknown if convergence is reached. However, using one outer correcter reduces the calculation by more than a factor two compared to multiple outer correctors. It is therefore advised to use only one outer corrector. Using a high final tolerance doesn't add that much time, so it is advised to use a high final tolerance.

In Figure I.6 an extra analysis of the time step and pressure tolerance is shown. This corresponds to the findings in Figures I.4 and I.5: a time step of 0.01 s and only one outer corrector are sufficient.

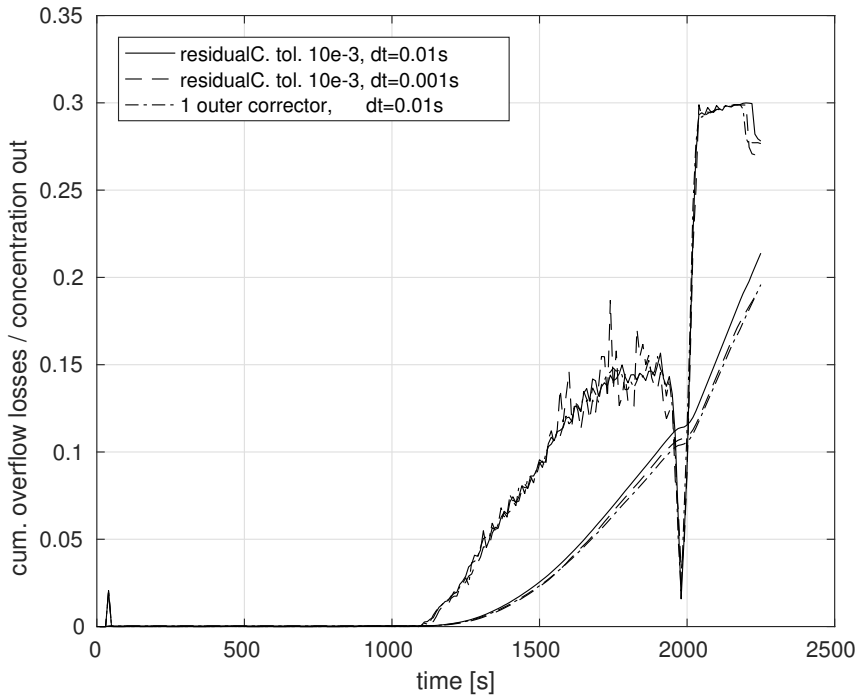

Figure I.6: Influence of time step and pressure tolerance on the overflow losses of Test 8 (three inner correctors, final tolerance = 10^{-7})

Until so far, an inlet of 8 cm consisting of 8 cells is used. For Test 8 (Q=0.075 m^3/s) this gives an inlet velocity of 0.30 m/s. The inlet velocity is unknown, but 0.30 m/s sounds as a low inlet velocity. In Figure I.7 it was analyzed if this low inlet velocity influences the overflow losses. Two extremes are simulated: a rather narrow inlet with a width of 2cm (1,21 m/s) and the big inlet with a width of 8 cm (0.30 m/s). Preferably, the inlet with a width of 8 cm is used, because then the simulation is more stable. It could be questioned whether or not the usage of a rather big inlet influences the overflow losses. As can be seen Figure I.7, it does. Using an inlet of 8 cm influences the outcomes too much. It is safer to use an inlet of 4 cm (0.61 m/s). A velocity of 0.61 m/s still sounds a bit low, but for most of the test the flow rate was higher, which gives realistic inlet velocities with an inlet of 4 cm.

In Table I.1 an overview of the advised settings can be seen:

Table I.1: Overview of the advised settings

Setting	**Value**
dt	10^{-2} s
tolerance p_{rgh}	10^{-7}
inner correctors	3
outer correctors	1
tolerance α	10^{-8}

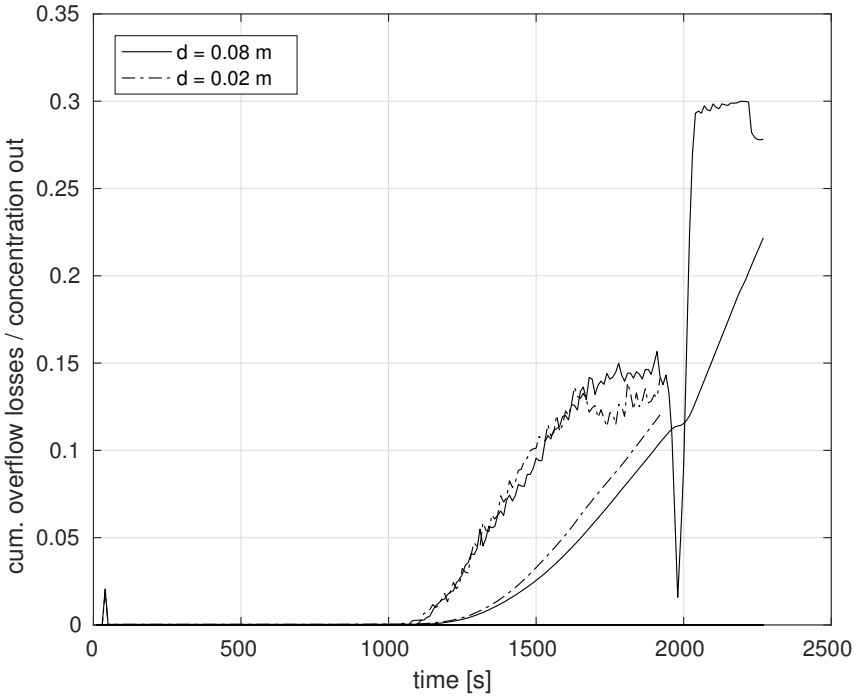

Figure I.7: Influence of the width of the inlet (test 8)

Acknowledgements

First and foremost, I would like to thank God for giving me the strength, knowledge, ability and opportunity to undertake this master thesis and to persevere and complete it satisfactorily. Without His blessings, this achievement would not have been possible.

I would like to use this opportunity to express my gratitude towards Damen Dredging Equipment and especially my supervisor Mark Winkelman. I am grateful for his guidance, supervision and willingness to drive to Delft numerous times.

I would like to express my sincere gratitude towards Geert Keetels. This thesis would not have been possible without his supervision, suggestions, knowledge and stimulating discussions. Next to Geert, I want to thank my colleagues at the Delft University of Technology. I want to thank Dave Weij, Joep Goeree, Bas Nieuwboer, Frans van Grunsven and others for their help with OpenFOAM.

I would like to thank my graduation committee. It is my honour that you agreed to be part of my defence.

Last but not least, I would like to thank my friends and family for their support throughout the years. Ann Elise, I want to thank you for your love, support and patience.

Ben Sloof
Delft, November 2017